UCRL-53868-02

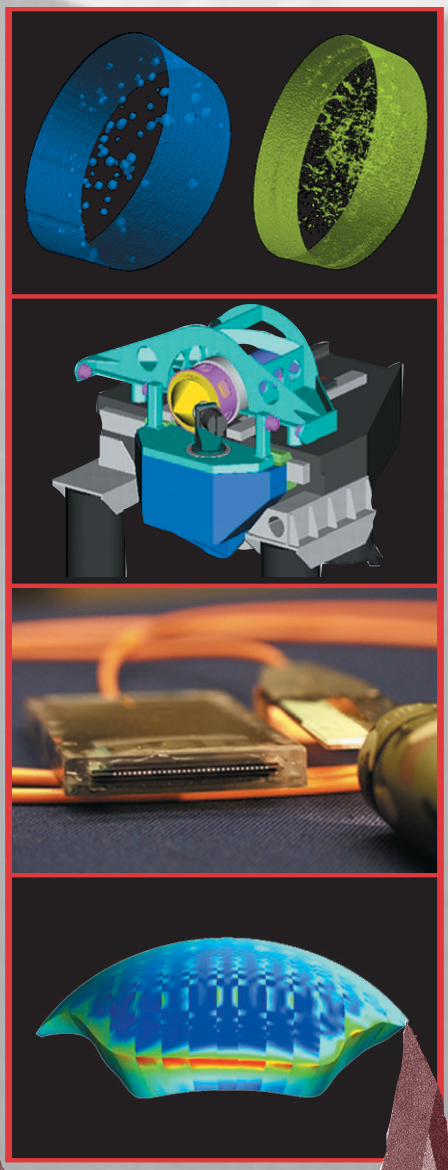

FY02 ENGINEERING TECHNOLOGY REPORTS

Volume 1:

Technology Base

MARCH 2003

ENGINEERING

Pushing engineering science to the Xtreme

Acknowledgments

Scientific Editing
Camille Minichino

Graphic Design
Irene J. Chan

Art Production/Layout
Jeffrey Bonivert
Debbie A. Marsh
Kathy J. McCullough

Cover:
Graphics representing technology-base projects from Engineering's five Centers and other technologies.

UCRL-53868-02

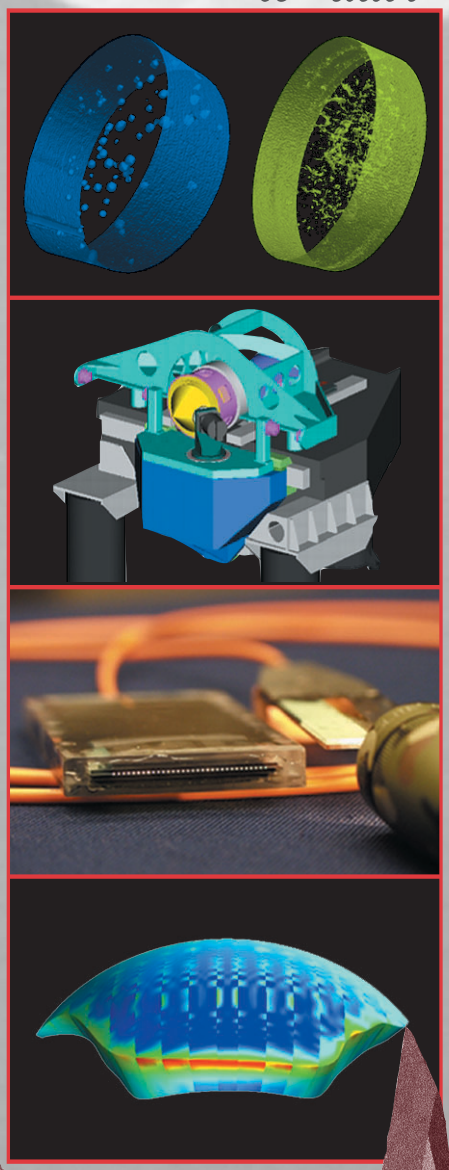

FY02 ENGINEERING TECHNOLOGY REPORTS

Volume 1:

Technology Base

MARCH 2003

Introduction

Center for Complex Distributed Systems

Center for Computational Engineering

Center for Microtechnology

Center for Nondestructive Characterization

Center for Precision Engineering

Other Technologies

Author Index

Introduction

Jens Mahler, Acting Associate Director for Engineering

Engineering has touched on every challenge, every accomplishment, and every endeavor of Lawrence Livermore National Laboratory during its fifty-year history.

In this time of transition to new leadership, Engineering continues to be central to the mission of the Laboratory, returning to the tradition and core values of E. O. Lawrence: science-based engineering—turning scientific concepts into reality.

This volume of Engineering Technical Reports summarizes progress on the projects funded for technology-base efforts. Technology-base projects effect the natural transition to reduction-to-practice of scientific or engineering methods that are well understood and established. They represent discipline-oriented, core competency activities that are multi-programmatic in application, nature, and scope.

Objectives of technology-base funding include:

- the development and enhancement of tools and processes to provide Engineering support capability, such as code maintenance and improved fabrication methods;
- the support of Engineering science and technology infrastructure, such as the installation or integration of a new capability;
- support for technical and administrative leadership through our technology Centers;
- the initial scoping and exploration of selected technology areas with high strategic potential, such as assessment of university, laboratory, and industrial partnerships.

Five Centers focus and guide longer-term investments within Engineering. The Centers attract and retain top staff, develop and maintain critical core technologies, and enable programs. Through their technology-base projects, they oversee the application of known engineering approaches and techniques to scientific and technical problems. The Centers and their leaders are as follows:

- Center for Complex Distributed Systems: Donald J. Meeker, Acting Center Leader
- Center for Computational Engineering: Robert M. Sharpe
- Center for Microtechnology: Raymond P. Mariella, Jr.
- Center for Nondestructive Characterization: Harry E. Martz, Jr.
- Center for Precision Engineering: Keith Carlisle

FY2002 Center Highlights

The **Center for Complex Distributed Systems** exploits emerging information technologies to develop unique communications related to data gathering, advanced signal processing, and new methodologies for assimilating measured data with computational models in data-constrained simulations of large systems.

Current Center technology-base activities include: vibration-signature-based modeling and simulation; extending the capabilities of wireless network on demand and of NTON; time-reversal resolution imaging; sensor-based weather and regional modeling technology; wideband antenna arrays for countermeasure; radar vision; an acoustic transmitter/receiver system; high-resolution video surveillance; scene-based wavefront sensing; and contact algorithm improvements.

These technology-base projects are delivering application-ready tools into the hands of engineers supporting programs, and thus serve a critical link in transitioning from research to practice.

The **Center for Computational Engineering** orchestrates the research, development and deployment of software technologies to aid in many facets of LLNL's engineering mission. Computational engineering has become a ubiquitous component throughout the engineering discipline. Current activities range from tools to design the next generation of mixed-signal chips (systems on a chip) to full-scale analysis of key DOE and DoD systems.

Highlights of the Center's technology-base projects for FY2002 include enhancements of engineering simulation tools and capabilities; progress in visualization and data management tools; and updates in parallel interface algorithms. The Center has offered a real-world computing capability that opens the door to solving a wide variety of fluid/solid interaction problems in transportation, aerospace, and infrastructure settings.

The mission of the **Center for Microtechnology** is to invent, develop, and apply microtechnologies to support LLNL missions in Stockpile Stewardship, Homeland Security, Nonproliferation, and other programs. The capabilities of Microtechnology cover materials, devices, instruments, and systems that require microfabricated components, including microelectromechanical systems (MEMS), electronics, photonics, microstructures, and microactuators. Center staff have achieved considerable national recognition for the successes demonstrated in Chem-Bio National Security Program instrumentation, supported by the DOE and

the Defense Intelligence Agency. Our FY02 projects include the technology issues associated with high-voltage photovoltaics; microaccelerometers and microactuators; sample collectors, sample preparation modules, and fluidic systems for water security; and the fabrication of practical x-ray imaging systems. One project dealt with the upgrading of the manipulation stage for our laser pantography system (laser-based, 3-D, direct-write technology).

The **Center for Nondestructive Characterization** advances, develops and applies nondestructive characterization (NDC) measurement technology to significantly impact the manner in which LLNL inspects, and through this, designs and refurbishes systems and components. The Center plays a strategic and vital role in the reduction-to-practice of scientific and engineering NDC technologies, such as acoustic, infrared, microwave, ultrasonic, visible and x-ray imaging, to allow Engineering in the near-term to incorporate these technologies into LLNL and DOE programs. This year's technology-base projects include distributed processing algorithms for x-ray CT image reconstruction; enhancements in infrared techniques; a new synchrotron microtomography capability; investigation of a CMOS-based x-ray detector; advanced applications of ultrasonics time reversal and image rendering; and ceramic NDC.

The **Center for Precision Engineering** advances LLNL's high-precision capabilities in manufacturing, dimensional metrology and assembly, to meet the future needs of LLNL and DOE programs. Precision engineering is a multi-disciplinary systems approach to achieve an order of magnitude greater accuracy than currently achievable. Essential to the Center's success are its core technologies, which are the building blocks for the future machines, systems, and processes that will be required for future programs. The Center's core technologies are essential to the Lab's future because they will reduce the amount of research and development required to build the next generation of instruments and machine tools; the risk, by using proven technology; the lead and design times, and the time to complete. By using the existing core technologies fully, we were able to build and supply on time, a complete manufacturing facility for a commercial vendor to supply optics to the Laboratory. Highlights for FY02 technology-base projects include the evaluation of a newly developed porous ceramic bearing material that has the potential to greatly improve the rotational accuracy over that of traditional bearings.

Science-Based Engineering

Our five Centers develop the key technologies that make Laboratory programs successful. They provide the mechanism by which Engineering can help programs attract funding, while pioneering the technologies that will sustain long-term investment.

Our Centers, with staff who are full partners in Laboratory programs, integrate the best of mechanical and electronics engineering, creating a synergy that helps turn the impossible into the doable.

Center for Complex Distributed Systems

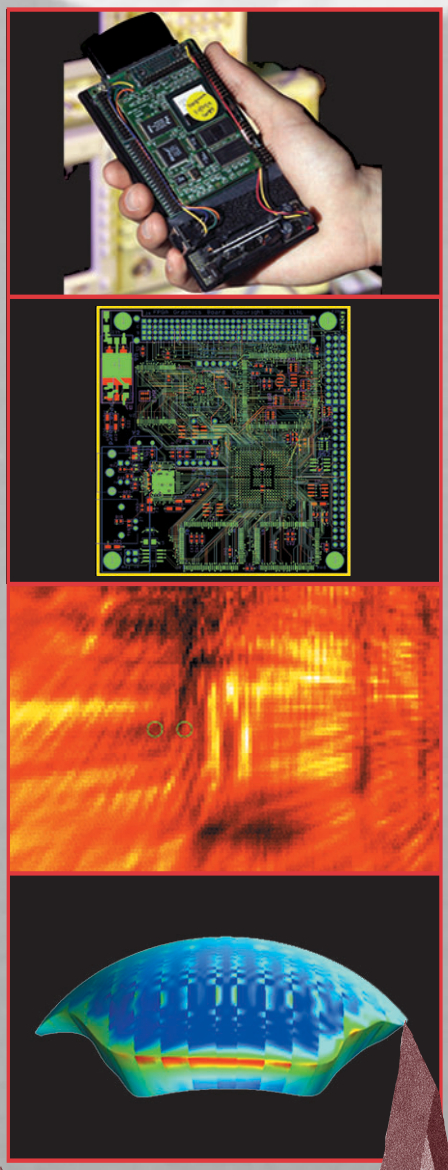

Vibration-Signature-Based Modeling and Simulation

R. E. Glaser, C. L. Lee, W. G. Hanley

The goal of this project is to create a system identification methodology that can be used for new finite-element-based numerical simulations of mechanical and structural systems, and validate existing ones.

In our approach, measured vibration data from the real structure is combined with an initial-representation simulation model to create an improved or "updated" simulation model. Model parameters are estimated from a posterior probability distribution. This project is an implementation of the algorithms created through LLNL's Stochastic Engine (SE) project.

The SE is a Bayesian inference procedure that uses a Markov Chain Monte Carlo sampling process formulated by a version of the Metropolis algorithm. It was originally developed for geophysical applications, but is finding many applications within LLNL.

In FY02, we successfully demonstrated that the SE methodology can be applied to a mechanical finite-element model. Starting with a uniform, linearly elastic, fixed-free cantilever beam example, the SE algorithms were used to identify the configuration of the beam in terms of its stiffness matrix. In "virtual experiments" (simulation data instead of measured data) of applied force (input) and static nodal displacement measurements (output), we investigated the following issues: 1) accuracy in sampling the posterior distribution; 2) robustness under degraded conditions, including noisy data, missing data, model misspecification, and an incorrect prior distribution; 3) characteristic behavior under state-space misspecification; and 4) sensitivity and accuracy in using spatial domain or frequency domain data.

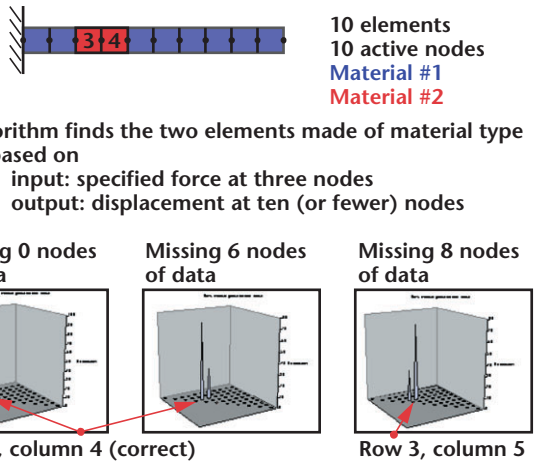

Vibration-signature-based modeling and simulation.

The following representative result demonstrates that this method can be used to find the location of a damaged section of a structure. Consider a beam that has n=10 equal, homogeneous beam elements where each element has an elastic modulus that corresponds to one of the three types. Here we take the first type (Material #1) to be the nominal or "undamaged" material and the other two types (Material #2 and Material #3) to be "damaged" materials.

Assuming the presence of at most two flawed elements, there are $2n^2 + 1 = 201$ possible configurations. The data is degraded in two ways: noisy output measurements (in this case, nodal displacements) and loss of output data. For this example, there is a 1% noise to signal ratio. The number of missing output data (at specific nodes) ranges from 0 to 8, out of a possible 10. The posterior distribution is summarized via a 3-D representation (see figure).

The figure shows 56 coordinates, one of which represents the zero-flaw case, 10 of which represent the different flaw locations for the one-flaw case, and 45 of which represent the different flaw location pairs for the two-flaw case. The height of the spike at each location indicates the posterior probability of the corresponding flaw configuration. For this example, the true state of nature was taken to have two flawed elements located in positions 3 and 4. Note that when there is no missing data the posterior probability of the flaws being in positions 3 and 4 is virtually 1.0. In fact, there is negligible loss of precision when 4 or fewer of the 10 available output nodal displacements are not measured. Only when 8 output nodal displacements are missing data is the flawed state (3, 4) not the most probable configuration, but the most likely state (3, 5) is nearby. In spite of this, the analysis of the posterior distribution reduces the space of potential location configurations from 56 to 2.

In FY03, we will expand the sophistication of the structural/mechanical model to handle problems of significantly increased size and complexity and address the issue of scalability to very large size models (millions of degrees of freedom). The numerical simulations will be generated directly from NIKE3D or DYNA3D, allowing 3-D, nonlinear dynamics models to be used in the SE. Along with "virtual experiments," we will validate the results on a laboratory test-frame with accelerometer measurement data.

Extending the Wireless Network on Demand

B. Henderer

The Wireless Network on Demand (WNOD) is based on the open source software known as Mobilemesh. Originally, the software was installed on embedded 486 computers, and demonstrated. In this project, the system advanced in several ways, including ease of integration, deployment, and universal operability.

The first advancement in the WNOD software was in ease of integration. Software was developed to allow external devices to use the wireless node with either an Ethernet interface or a serial interface. Serial data is encapsulated in User Datagram Protocol, and sent via wireless Ethernet to another node where it is returned to serial or can be read out directly with software. In Ethernet mode, the wireless device behaves exactly like a router and is transparent to the user. Software was developed to allow an analog-to-digital converter (ADC) card to be used in a second PCMCIA slot of the system. Data accumulated by the ADC software is sent by Transmission Control Protocol to a remote node using the wireless Ethernet.

The second advancement was in a prototype deployable unit. This included the design of a power conversion board to allow 9- to 18-V input to be used (*e.g.*, a 12-V battery), water tight enclosures, and antennas. This provides for nodes that are truly ready to deploy. The parts are mostly off-the-shelf parts that can be quickly obtained.

The last advancement is the most significant. The code base has been ported to multiple platforms. This will allow for truly universal operability. The code was first ported to Windows 2000. This is mostly a direct port with some library calls needing to be converted from Linux calls to Windows calls. This port provided great insight into the Mobilemesh code. The code was then ported to Java. This is a complete re-write of the software. Any machine that can execute Java can now run Mobilemesh. LLNL is in the process of releasing this code as open source. The Mobilemesh code is now available on the original Linux, Windows 2000, and any platform capable of Java.

This software has been shown to work on several different platforms. Embedded PCs, PC laptops, and a Macintosh PC operated the Java version of the code. The original embedded 486 is no longer available, but the code has been demonstrated on the replacement 586 processor.

WNOD nodes (see figure) are being used on the BASIS project, in a prototype ground sensing/vehicle tracking demonstration, for vibration sensing in NIF, and for a portion of the wireless networking involved in a defense technology project.

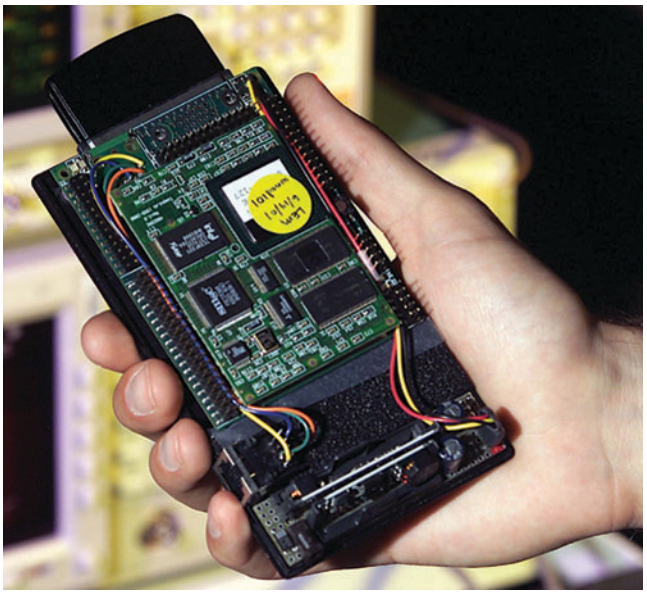

Wireless networking node.

Time-Reversal Resolution Imaging Experiment in Glass

S. K. Lehman, B. L. Guidry, K. A. Fisher

The goal of this project was to collect experimental ultrasonic data under controlled laboratory conditions, to which can be applied a new time-reversal (T/R) imaging algorithm. The T/R algorithm is applied mathematically after the data have been collected, as opposed to real-time pitch/catch of the measured field.

We used a 32-element ultrasonic T/R mirror (TRM) machine to perform three wave-probing experiments. We wished to apply a new T/R algorithm to the data to form images of the internal structure of the material under evaluation.

Using an existing rectangular glass bar with targets of opportunity, we performed three experiments: a reflection mode from the top of the bar; a reflection mode from the side of the bar; and a transmission mode from the side to the top of the bar.

For the reflection mode experiments, the TRM was used without modification. For the transmission mode experiments, we purchased a separate 64-element ultrasonic array to be used as the source array. To achieve accurate timing, the TRM was modified to drive the second array by disconnecting the input of one of its transducer elements and using it to drive each of the source array's elements in succession. We collected fully bi-static data from each of the transmitters to each of the receivers.

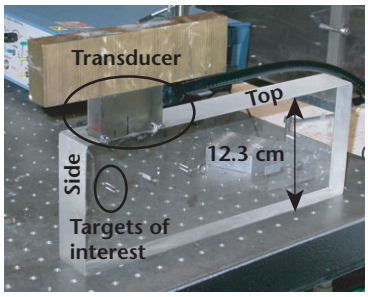

Figure 1. *Experimental set-up.*

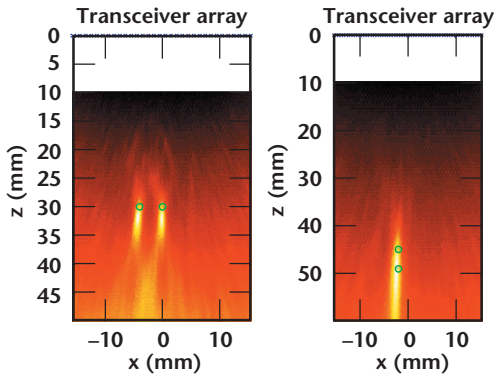

Figure 2. *Reflection mode reconstructions: (a) side; (b) top.*

Figure 1 is a photograph of the glass bar instrumented for the side reflection mode experiment. The bar is homogeneous with the exception of pairs of drilled holes 1 mm in diameter. We used the left-most set of holes as our targets, using time gating to eliminate the scattering from the other hole pairs. The separation between the target holes is 4 mm.

We were successful in forming images using the new T/R algorithm from all the sets. The reflection mode results are presented in Fig. 2. The green circles superposed on the images show the actual location of the hole targets. The reconstruction for the top reflection mode experiment shows the shadowing of one hole by the other as expected.

Figure 3 shows the transmission mode reconstruction. Figure 3(a) presents the reconstructed area with respect to the transmitting and receiving arrays. The green circles superposed on the images show the actual location of the hole targets. The reconstruction shows the targets shifted with respect to their true locations. We have not been able to determine the source of the error. Figure 3(b) shows a slice through the reconstruction. The two peaks of the slice are separated by 6 mm rather than 4 mm.

We have validated with experimental data the new transmission mode algorithm.

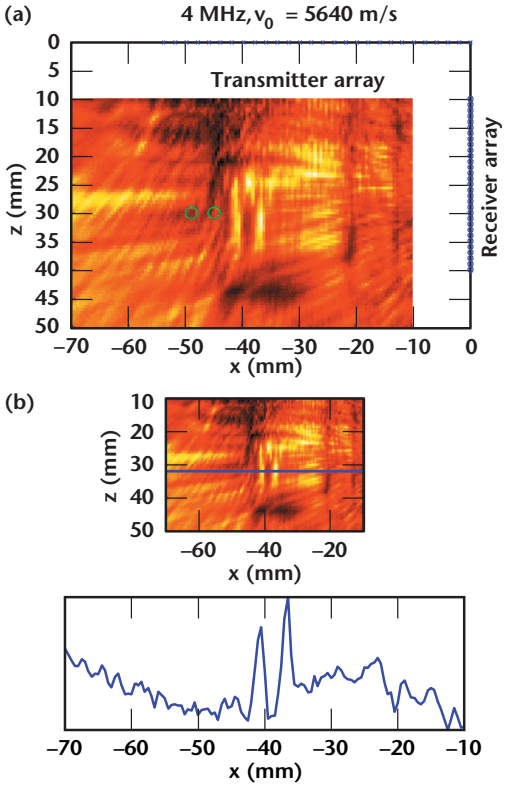

Figure 3. *(a)Transmission mode reconstruction; (b) slice through reconstruction.*

Wireless Communications for Large-Scale Structures

B. Henderer

The goal of this project was to leverage the achievements of the Wireless Network on Demand (WNOD) technology-base efforts and create useable wireless nodes.

We used the majority of the money for purchasing hardware and assembling the actual nodes, since most of the software and testing has already been accomplished.

Five sets of hardware were purchased. This included 486 embedded processors, 802.11-b wireless Ethernet cards (PC card format), watertight cases, power-conversion boards, and high-gain antennas.

All of this equipment was packaged and assembled into five operational nodes (see figure for example). Due to the limited time schedule, the nodes were not deployed, but are ready for use.

Some software testing was completed to verify that the nodes would actually connect to the sensors involved, and move data from the sensor to the command post.

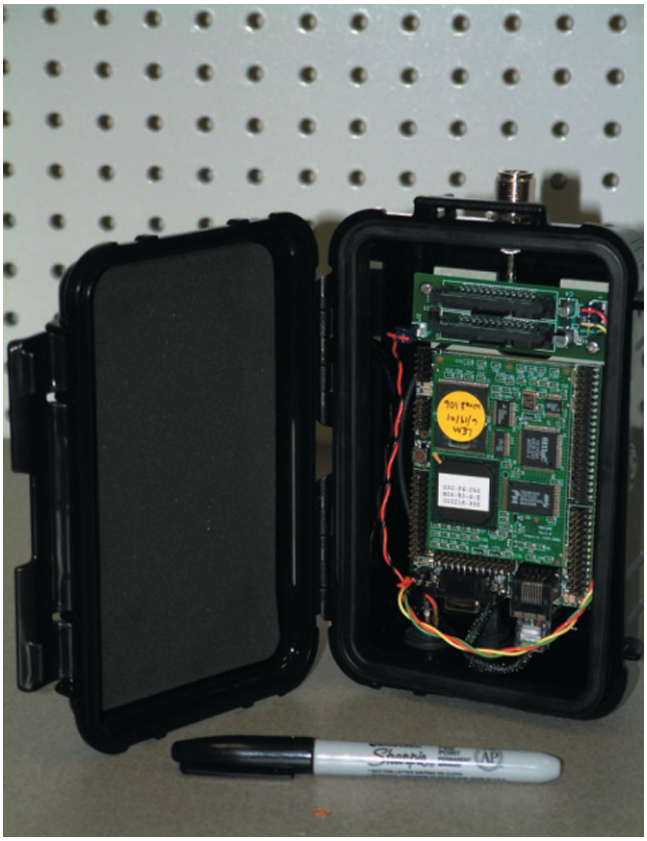

WNOD weather-tight operational node.

Automated Sentinel

V. Kohlhepp, M. Linderman

Our original proposal was divided into two separate tasks of equal complexity: 1) design and build a PC104-format PCI board based on a XILINX Virtex II one-million-gate field programmable gate array (FPGA) with integrated video capture circuitry; and 2) verify board operation and write basic test and interface software to allow it to operate attached to the LLNL Smart Camera development platform. Phase one has been completed; an FPGA-based video accelerator board was specified, designed and built.

The Smart Camera project seeks to mate innovative video processing algorithms and specialized processing hardware with Internet connectivity and existing camera technology to provide an autonomous surveillance and security system far more capable than anything currently available. To meet this goal a powerful, yet flexible, processing architecture is needed that can both meet the computation specifications and also be adapted in real time to a particular situation or stimulus.

A FPGA-based solution is optimal as the system can exploit parallelization to outperform current processors, but also be easily reconfigured to implement multiple algorithms. A PC-104 compliant Xilinx FPGA-based video processing board has been designed to meet the needs of the Smart Camera project and other users. The board serves as a video capture and co-processor board for off-the-shelf PC-104 single-board computers.

The XILINX Virtex II series of FPGAs was selected due to several factors:

1) SRAM-based reprogrammability provides the flexibility for dynamic reconfiguration and quick development cycles.
2) The Virtex II series of FPGAs offer high I/O pin counts and internal architectures optimized for signal and image processing.
3) The XILINX Foundation ISE FPGA development system software was already in use by the development team.
4) The "Handel-C" language parallel compiler, bought under other funding sources, has been demonstrated and is being used by the development team and others at LLNL.

Due to the requirement to process real-time video sequences, the external RAM was maximized in the design and split into two completely independent blocks. These 18-Mb blocks are independently addressable and can operate in different clock domains.

The video ADC selected was a Phillips Saa711 series, due to the commonality of the part and the fact that both reference designs and existing Smart Camera subsystems use similar parts.

The board form factor was required to be PC104 to integrate into the existing development system.

The FPGA accelerator board (see figure) was completed on schedule and on budget. The test plan outline is complete and the required mixed-signal test equipment has been purchased. A preliminary software driver has been written, and application algorithms have been targeted for the initial operational tests. Several government entities (SO-21, Secret Service, LLNL/SAT, LANL) have expressed interest in using the FPGA accelerator in their own programs.

Given the success of the first phase of this project, we expect that additional resources will be made available to facilitate the completion of the hardware test and software integration of the Automated Sentinel reconfigurable image processing accelerator.

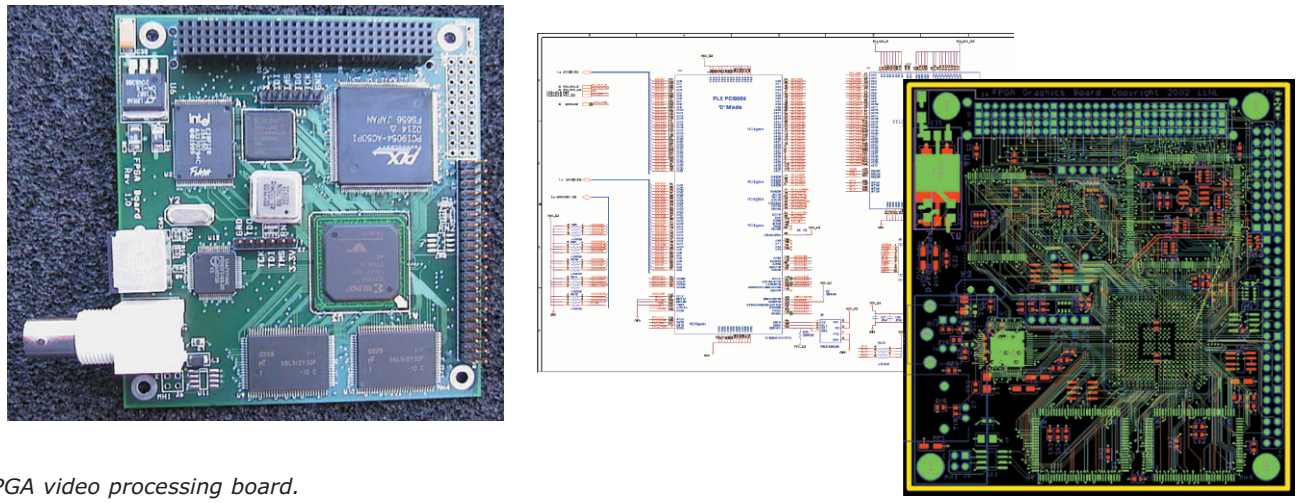

FPGA video processing board.

Extending NTON High Performance Capabilities

W. J. Lennon

We are using the technology and capabilities LLNL developed initially for the National Transparent Optical Network (NTON) to define the information and communications technology infrastructure needed to monitor large-scale water systems

The proposed system will deploy fixed, networked sensors throughout waterways. Real-time measurements would be input to advanced simulation models used to characterize and predict complex environmental processes. Timely collection and insertion of sensor data into "live" simulation models will enable models to "learn" about the details of environmental media, to adapt and reconfigure for rapidly-changing conditions, and to "train" dynamic mobile sensor configurations to optimize the quality and utility of information.

Through data fusion with related information such as rainfall and satellite observations this modeling oriented "monitor" system would detect anomalies, predict consequences and outline detailed measurement scenarios. Typically, a large number of floating, wireless network sensors with position tracking capabilities would be deployed upstream of any sensors detecting an anomaly (Fig. 1). This self-organizing network would report enough additional information to compute the plume profile and predict the likely contamination source.

This problem can now be addressed because of a confluence of developments. Computing power continues to double and cost reduction to be cut in half every 18 months. Wireless communication systems are becoming smaller, cheaper, adaptive, and more seamlessly connected with the Internet and other ubiquitous communication channels. Similarly, environmental sensors, including those developed at LLNL, are becoming smaller, smarter, cheaper, less invasive, and lower power. Finally, ClearStream Communications, Inc. has developed and is installing a diversely routed national "fully optical" fiber-optic communications network throughout various riverine and coastal waterways of the US and neighboring countries.

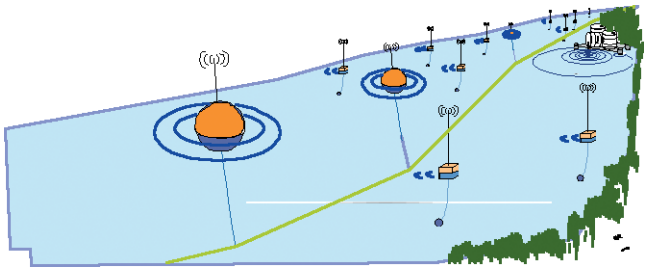

Figure 1. *Depiction of floating, wireless network sensors with position tracking capabilities.*

The network (Fig. 2) has been designed to allow concurrent deployment of both a commercially viable, advanced optical network (>1 Gb/s end user access) and a network foundation for a national riverine and coastal monitoring system.

The first phase is the deployment of a test-bed to demonstrate the waterway emplacement technology, to test the sensor and data network architecture, and to build a regional test platform connected to US research networks. The resultant network will field-test new sensor and optical network technology; provide connectivity to the national R&D network backbone; and prototype environmental, water integrity, and waterway security applications. The initial applications will require simple sensors for environmental monitoring and video to demonstrate security capability. The initial optical technology will be Optical Code Division Multi-Access transport of Ethernet.

Preliminary high-level designs and initial interactions with the applications scientists and potential users led to the initial deployment plan. First, the test-bed will be deployed at LLNL with a leg to San Francisco Bay. Second, a longer water deployment will take place in Chesapeake Bay. Finally, a full Chesapeake Bay deployment will link Baltimore, Washington, Norfolk, and intervening sites to each other, and also to the national network backbone.

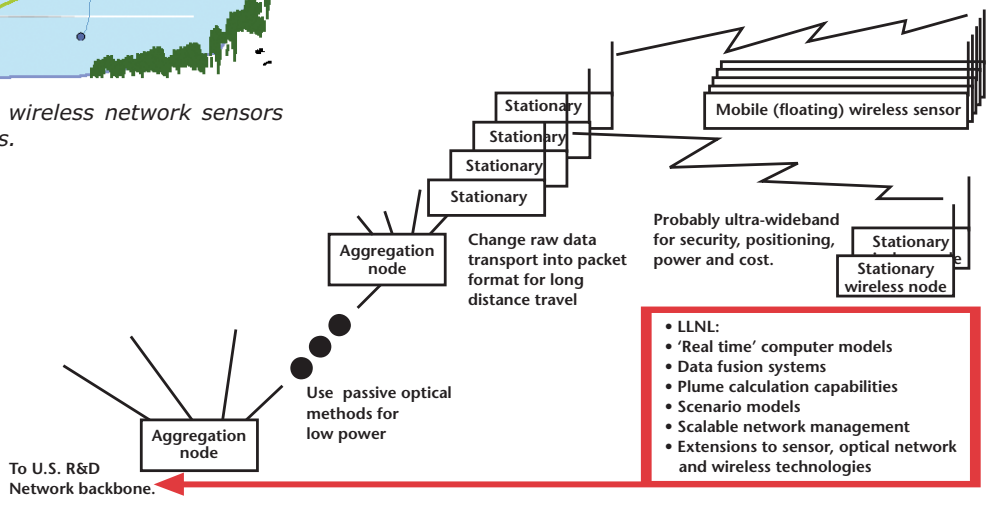

Figure 2. *Proposed system to deploy fixed, networked sensors throughout waterways.*

Sensor-Based Weather and Regional Modeling Technology (SWARM)

S. Azevedo

The objective of this project was to define systems issues and identify key technologies required for a novel concept to deploy a "swarm" of micro-sensors for measurement of weather parameters. The technologies that were identified are broad-based and are now being applied to several areas, including the cargo container security problem.

There are both military and civilian interests in improved prediction of weather. The DoD requires accurate three-to five-day knowledge of weather conditions in regional battlefields or surveillance areas. However, much of climate research has focused on satellite surveillance, which does not provide altitude profiles of data that is needed for most models.

Based on a concept proposed by E. Teller, deployment of thousands, or millions, of micro-balloons containing low-power sensors, intelligence, and communications distributed in a constellation of free-floating, neutrally-buoyant transponders would provide atmospheric data that can be used to initialize future high-resolution numerical weather-prediction models. This concept can be made feasible by microtechnology research at LLNL and U. C. Berkeley, but there are formidable systems issues to address.

For weather forecasting, the required spatial resolution (globally) is on the order of 10 km, and vertical resolutions on the order of 0.5 km. The concept involves deploying small (10-cm-diameter nominal) balloons equipped with advanced sensors, on-board GPS, communications, and simple networking capability—balloons that can be placed at various altitudes (up to 20 km) and locations (see figure). The observed quantities we are measuring are wind (vector), temperature, pressure, humidity, and, later, water content (phase) and chemical concentrations. For every group of (say, 100) sensors deployed, there would be a somewhat larger package to relay data to a satellite or ground station for forecast/analysis processing. Simple integrated sensor and line-of-sight communications packages of this size have already been demonstrated.

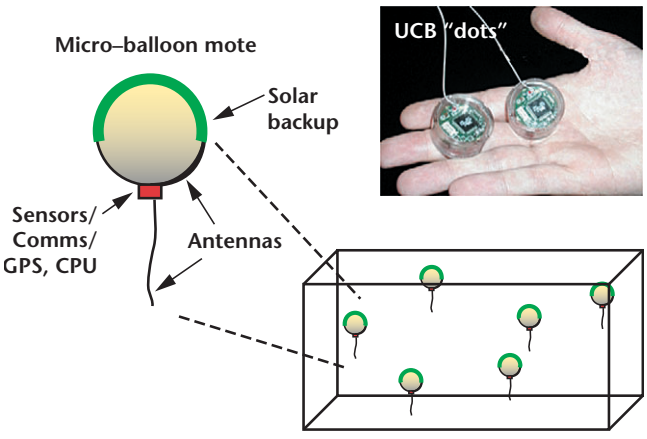

Micro-balloon sensor package.

Several engineering issues associated with the design of the balloon package were addressed. One is the communications link, which must have extremely long range (preferably tens to hundreds of kilometers). A possible solution is active reflectance with a thin metal dipole antenna that acts as a "tail" for keeping the balloon upright. A higher-power ground station senses the on-board switching capacitor that would modulate the return signals (see table for communications options). Simulations show that these systems could be deployed from hundreds of kilometers and require very low on-board power (μA).

Another issue is the inclusion of GPS in a small package along with the sensors and the processing element. On-board power that meets the needs of all subsystems is critical; currently we are using an integrated battery or fuel cell, coupled with solar backup power on top of the balloon. Finally, a means of attaining neutral buoyancy at various altitudes, and providing simple altitude control, will be a requirement.

Small sensor packages for detection of nuclear, chemical, or biological threats (as well as rudimentary imaging) are also under development using similar networking and communications scenarios.

Comparison of Communications Options for Micro-Balloons.

Option	BW[1] (bps)	Range (km)	Power[2] (W)	Weight[3] (g)	GPS[4] req'd?	Relative cost[5]
Cell phone	1000	10	.3	20	Y	Med.
Satellite phone	1000	400	.8-1	100	Y	High
Two-way pager	10	20	.05	15	Y	Med.
JSTARS/tags	1000	250	10^{-4}	1	N	Low
Dedicated radar & tags	10,000	500	10^{-4}	1	N	Low

1. Bandwidth (BW) is "uplink" speed from sensor to base station. Downlink (sensor data transfer) speeds must be faster than uplink (control) speeds.

2. Power is the estimated power draw for the full communications system from antenna through to microprocessor, while communicating at the maximum bit rate. All handshaking protocols are handled by this subsystem. Any of these systems could be controlled to only communicate at specific intervals, thereby reducing power requirements.

3. Weight is estimated for the communications subsystem alone, not including power supply or other subsystem.

4. GPS is required for systems that have no other means of localizing the individual balloons. Radar-based systems will determine location of each platform, but at lower resolution than GPS.

5. Relative cost estimates are for the sensor communications only. Base station costs will be considered separately.

Wideband Antenna Arrays for Electronic Countermeasure

A. Spiridon, F. Dowla

The objective of this project is to design antenna arrays for electronic countermeasure for the detection and intercept of adversarial wideband communication and radar systems. There is a concern that current collection systems are unable to detect ultra-wideband (UWB) systems. Further, UWB arrays could easily defeat narrowband collection. We are studying a new approach based on searching the 2-D space to defeat wideband arrays. More specifically, we are studying how arrays can be designed in conjunction with time-domain signal processing to implement data collection systems.

The performance of an array depends on the link environment, *e.g.*, multi-path; the volume of space the array occupies; and the support hardware to implement it. First, a fixed array must achieve its optimal parameter settings within a given fidelity. Primary focus of the effort will then be on how the array improves link margin at desired locations. The interplay of spatial processing introduced by the array, and the temporal processing as used by our communication link design, will be addressed.

Most of the effort this past year has been on analysis and computer numeric simulation of the field signal emitted by the arrays, properly augmented with experimental data to reflect noise effects. Key issues addressed in the effort are: identification of the architectures of arrays, including topology; and theoretic bounds on beam focusing to a point communication link.

We have also collected a limited amount of data on the background interference to assess its impact on data collection.

In FY02 we have demonstrated with computer simulations that UWB arrays can be designed to focus the beam at a point in space. We have used both linear and distributed arrays for beam focusing. Our main conclusions are: 1) UWB is capable of bringing into a focal point the beam for points in the near-field of legacy antenna systems (as shown in the figure); and 2) in the far-field the focal point is elongated along the range away from the antenna, but the grating lobes are suppressed.

In FY02 we have also studied the receiver operating characteristics of UWB pulse detection using radio metric models for collection systems. The main conclusions are: 1) low-voltage pulse links require integration of a large number of pulses per bits; 2) the coherent processing gain, relative to non-coherent, for such links is the (time × bandwidth) product. Both lead to the conclusion that lower data rates will have a better advantage.

The effort to date was for nominal waveform, fixed nodes, in an ideal environment with no multi-path, and with no consideration of hardware complexity and processing limitation. Future effort will address the impact of UWB signal burst waveform and timing. Next year we intend to perform limited experiments using two-element arrays to check on obtained results. We will select candidate temporal processing systems and plan to compare the arrays in these settings. Work will focus on identifying critical hardware required for the array system and the limitation it might impose on performance and array configurations, including scanned vs. fixed beam capability.

We also need to do a first order assessment of mobility impact on performance and fold in more detail of the dynamics of the UWB signaling and data collection system, taking into consideration the errors induced by the hardware, the multi-path, and the uncertainty in the UWB operating parameters. Finally, we plan to quantify search parameters and seek times. The results will be aimed at assessing the effectiveness of data collection and identifying means to reduce the vulnerability of friendly UWB systems.

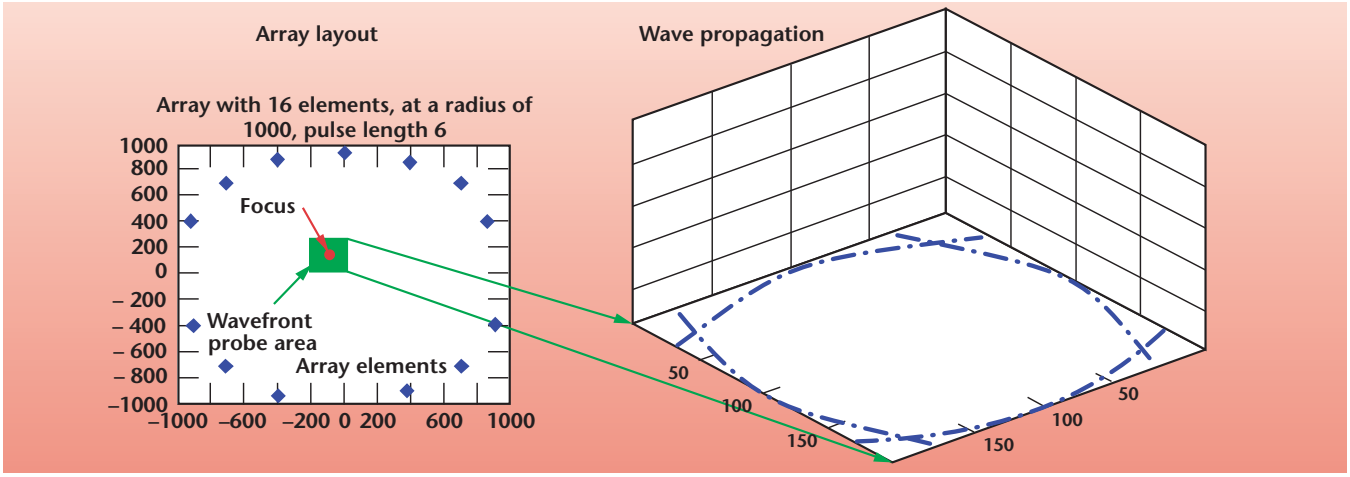

Circular array capable of focusing beam to a point at its center.

Ontologies for Representing Automatic System Analysis

T. Canales, R. R. Johnson

Our computer project provides a bridge between the Analysis, Collection, and Exploitation Support (ACES) tool-set, an automated intelligence analysis system, and "Nebraska," a system being developed to store and retrieve information to support intelligence analysis tasks. The ontology supports a formalized definition of automated analysis quality.

In general terms, an intelligence analyst's job is to be presented with a system, such as a computer network, international monetary system, or physical processing plant, and produce an analysis of that system. Increasingly, intelligence analysts are finding it necessary to use systems that automate all or some of the aspects of the process.

Information systems depend on an ontology to formalize the organization of the data used for, and produced by, the analysis of a system of interest. To date, ontological research for intelligence analysis applications has focused almost exclusively on the organization of data that can potentially be used to analyze systems of interest. This work focuses on ontological issues arising from the need to capture, store, and retrieve information that describes how a particular system of interest has been analyzed by an automated system. Towards this end, an ontology has been developed that represents aspects that are unique to automated analysis.

Automated analysis provides for capabilities that are not possible with the conventional analysis methodologies. For example, it is often the case that new data, or better analysis strategies, will become available after a system has been analyzed. The ontology should provide the support to determine which analyses could benefit from the new data or analysis strategy. These analyses can then be updated to reflect the new data and strategies.

In a similar vein, previous analyses dependent on data and/or analysis strategies that are found to be faulty could also be updated.

Evaluating the quality of an analysis is crucial when it is to be used for subsequent analysis tasks, for planning purposes, or to form policy. Determining the quality of a conventional analysis (*i.e.*, wholly the result of an analyst's judgment) requires a manual approach that is often labor intensive, and/or imprecise. In contrast, it should be possible to formalize the notion of the quality of an automated analysis. The ontology developed here supports a formalized definition of automated analysis quality.

This work is being performed by designing a computer system that provides a bridge between the ACES tool-set, an automated intelligence analysis system, and Nebraska, a system being developed to store and retrieve information to support intelligence analysis tasks.

In general terms, ACES provides an archive of models that describe physical processes and has the capability to evaluate how well a particular model matches a given set of observations by determining a numerical score. Automatic analysis of a system of interest is achieved by directing the system to determine which model has the highest score for the observations of the system of interest.

The figure is a screen shot of the tool that was used to develop the ontology.

There are many aspects of the ontology that are unique to automated analysis, and, at first glance, are counterintuitive. For example, a model is a description of a process potentially including specifications of inputs and outputs, and a mathematical formula relating the inputs and outputs. In contrast, a commodity is completely specified by its name (*e.g.*, CO_2, KiloWattHour). However, the ontology treats model and commodity as equivalent in that they are both subtypes of observables. This organization is non-intuitive to a human analyst, but is necessary in the case of an automated analysis system.

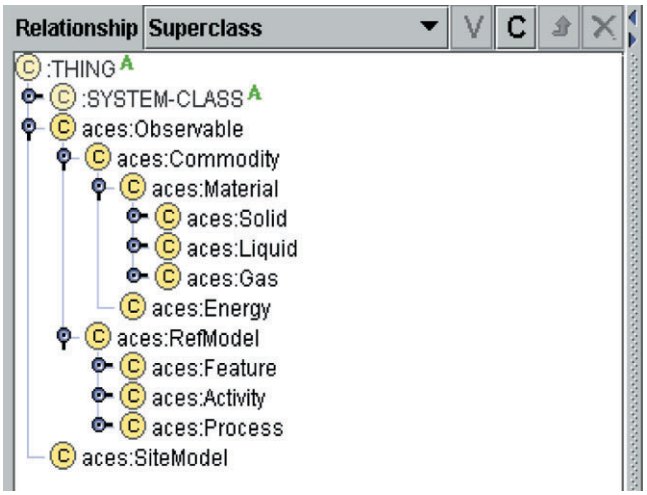

Sample screen of tool used for the ontology for representing automatic system analysis.

Radar Vision

K. Romero, G. Dallum, J. E. Hernandez, J. Zumstein

Our low-power, compact, high-resolution radars could be well-suited for a lightweight, portable Synthetic Aperture Radar (SAR) imaging system for "through wall" and smoke imaging applications

Special Forces, DARPA, DOE, and the intelligence community need the capability to "see" through walls and smoke. Law enforcement first responders, such as SWAT teams, require a portable, affordable device that will provide them real-time, full motion images of a crime scene through exterior and interior building walls, and through smoke.

The ability to differentiate between perpetrators and victims, and to locate weapons is highly desired. Ultrasound and ground penetrating radar (GPR) devices could be used to detect moving people behind certain types of indoor and outdoor walls. However, some type of imaging system is needed to generate a 2- or 3-D map of the interior of a room to locate and discriminate multiple people, especially if they are not moving. Infrared cameras could be used to image people through smoke, but they are not always useful for detecting obstacles for the purpose of navigating safely and quickly through smoke.

To get a good quality image useful for shape recognition, an ultra-wideband scanning radar system or an array of radars, with suitable imaging algorithms, is needed to obtain a high resolution SAR image of the scene.

LLNL is a world leader in developing high-resolution SAR imaging systems for NDE applications such as the inspection of bridge decks. We have pioneered the use of low-power ultra-wideband impulse radar scanning systems and arrays for high-resolution imaging of materials. Our low-power, compact, high-resolution radars could be well-suited for application in a lightweight, portable SAR imaging system for through wall and smoke imaging situations.

In our second year of funding, we have designed the control boards (Fig. 1a) necessary to perform beam-steering with an array of MIR radars (Fig. 1b). Through FPGAs and digital delay circuitry, we can now scan any volume in space by delaying each transmitter so that all their energies focus on one point in space at the same instant in time (Fig. 2a). By then delaying each receiver so that they cohesively add up the energy returned from that point in space, we can interrogate the volume (Fig. 2b).

With the flexibility provided by the test-bed, multiple scanning patterns have been tested, due to the ability of the system to arbitrarily scan any volume, plane, or line. Additionally, experimentation has been carried out on radar placement and array configuration (transmitters, receivers).

During the third year, signal attenuation will be addressed by the design and implementation of variable gain control boards. This, coupled with data acquisition onto a computer, should permit 3-D visualization of data and provide insight into the best approach for a portable SAR imaging system for imaging objects from a distance through air and a variety of wall materials.

Based on FY01, FY02, and expected FY03 accomplishments, the results of our work will provide the groundwork for attracting follow-up funding for a complete portable imaging system prototype for intelligence applications.

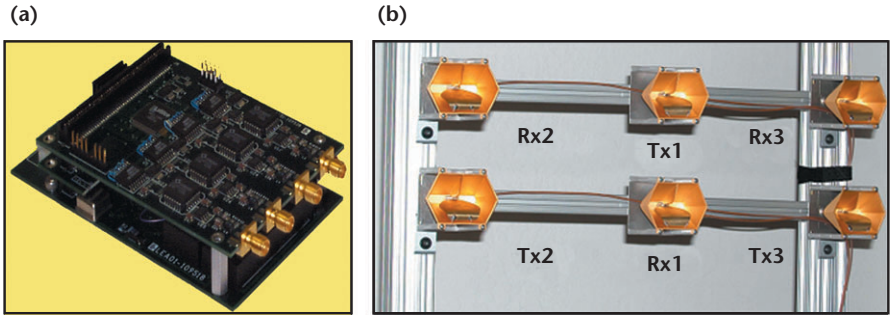

Figure 1. *(a) Control boards; (b) MIR radar array.*

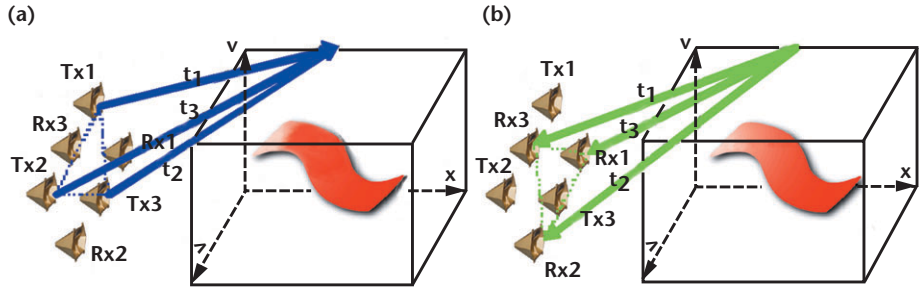

Figure 2. *(a) Illustration of how impulses from transmitters are delayed so that the energy from each transmitter reaches the same point in space at the same instant in time. (b) Illustration of how receivers are gated so that they cohesively add up the energy returned from the queried point in space.*

Acoustic Transmitter/Receiver System Based on Time-Reversal Signal Processing

A. J. Poggio, A. W. Meyer, J. V. Candy, B. L. Guidry

A feasibility study in FY01 demonstrated that time-reversal signal processing (TRSP) could enable intelligible communications in a reverberant channel, such as encountered in multi-path environments. This project was directed toward the confirmation of a prototype design for the digital transmitter-receiver system.

An acoustic-propagation experiment was conceived where the propagation channel would be inside an enclosed structure, giving rise to reverberation. We selected LLNL's NIF Target Chamber Assembly Building (Fig. 1a) before the building was dismantled. The building was a large, cylindrical, but not smooth, steel structure with randomly located internal features. This structure was essentially empty, containing a distribution transformer generating harmonics of line voltage and acoustic humming. This environment was also contaminated by external traffic noise. Thus, propagation took place in a noisy, reverberant environment.

A bi-phase modulated code (200-Hz symbol rate) representing the information sequence on an acoustic carrier (800 Hz), and a white-noise pilot sequence were separately transmitted from a loud speaker to a single microphone receiver some 40 ft away (Fig. 1b). The acquisition system consisted of a mixing board, amplifiers, a sampling oscilloscope with a digitization rate of 4 kHz, and a computer.

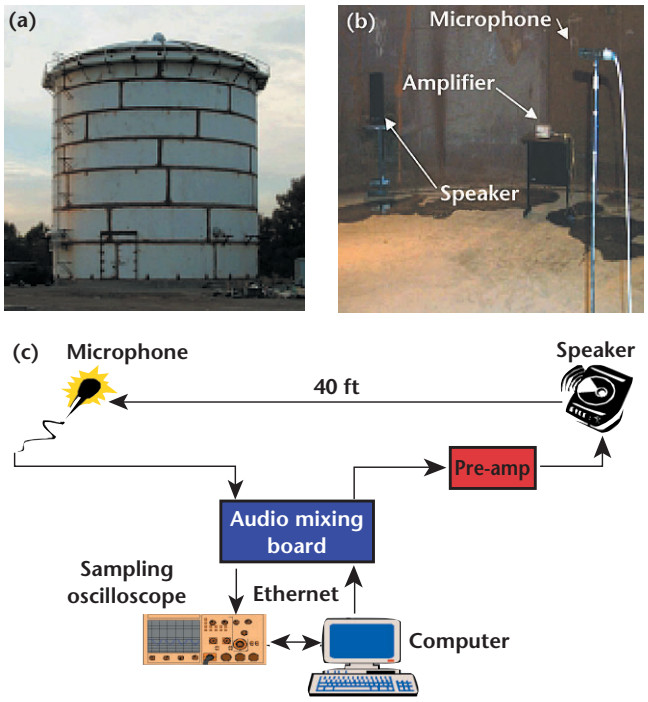

***Figure 1**. Experimental environment and setup for T/R communications: (a) steel cylindrical structure (60 ft H × 60 ft D); (b) experimental setup showing speaker and microphone; (c) experimental system.*

The basic approach was:

1. *transmit* the pilot signal through the reverberant medium;
2. similarly *transmit* the modulated information signal;
3. *receive* both noisy, reverberant sequences; record and digitize;
4. *process* the raw data with the time-reversal (T/R) (software) based on TRSP;
5. *post-process* the T/R receiver data to *detect* and locate the transmitted *signal*, and to *extract* the signal for performance analysis.

We evaluated our T/R system by post-processing the output signal and comparing it to the original information sequence (Fig. 2). We first demodulated the receiver output to get to base-band. The matched filter detection clearly indicated that the transmitted code was detected, but some additional processing was required to extract it from the noisy measurement data, namely, band-pass filtering to achieve shaping of the waveform, and quantization to obtain a binary data stream. Our use of a "very broadband" white-noise pilot sequence rather than a "sufficiently" broadband pilot signal may have contributed to some difficulties.

We also performed some steps in an order that, while technically correct, was sub-optimal when applied to real data. Nonetheless, after post-processing we regularly achieved sample error rates of ~5%, but symbol error rates very close to 0% — an indication of a very robust T/R system.

Further tests of our prototype T/R system were performed in a follow-on campaign in a stairwell. The experiment was similar in nature except that the pilot signal was a chirp of ~2-kHz bandwidth. The results confirmed our confidence in the system performance.

The results, only touched upon above, will be presented at the CASSIS conference in November 2002.

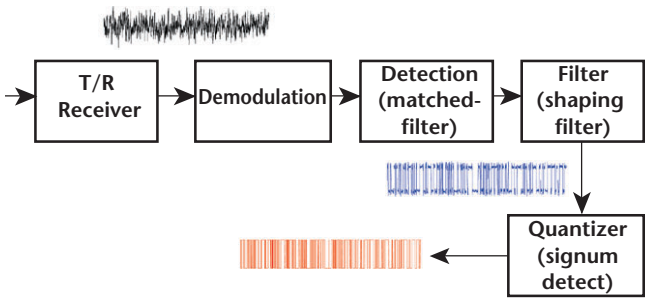

***Figure 2.** Signal processing of experimental data.*

High-Resolution Video Surveillance

C. Carrano

Atmospheric and optical aberrations reduce the resolution and contrast in surveillance images recorded over long (>0.5 km) horizontal or slant paths. A capability of improving such images is of great interest to the DoD/Intelligence communities. We proposed to demonstrate a prototype remote surveillance system that corrects these aberrations and improves resolution in such scenes using speckle imaging techniques.

Speckle imaging techniques require multiple frame acquisition of short-exposure imagery to recover the high-resolution information that is lost in a typical blurred long-exposure image. In FY01 we delivered a prototype remote video surveillance system consisting of both hardware and software, and initial experimental results.

In FY02 we accomplished a number of important tasks, including dramatic improvements to the image processing; many more experiments from a hillside location; demonstration of long-range face recognition with speckle-processed imagery; and quantification of imaging performance.

Image processing

After obtaining the raw camera images, we account for bad pixels due to any dust that may be on the camera CCD by replacing them with the average of the surrounding good pixels. The frames are then registered to each other, from applying the shifts calculated from frame-to-frame cross-correlation. The large image data cube is next split up into subfields, which are overlapped by 50%. The subfields are then apodized or windowed, and then speckle-processed. Finally, the processed tiles are reassembled to form the full-sized image.

The improvement over last year is the subfield processing capability, which allows the reconstruction of high-resolution images even when the atmosphere is unfavorable. Figure 1 demonstrates the effect.

Face recognition

To test the feasibility of long-range face recognition, we tried to match our face imagery at 1 km, both unprocessed and speckle-processed, to a database of photographs. Using Visionics FaceIt DB commercial face recognition software, we added a close-up photograph of our subject to their database of 685 people. We then asked the program to find a match for our long-range imagery. With the unprocessed imagery, it could not make a match, but with the speckle-processed imagery, our subject was the number one match.

Image quality

We constructed a resolution target with sine wave patterns at varying frequencies. By measuring the modulation in the resulting images for each of the frequencies, we are able to construct a curve and compare it to the curve for an ideal telescope. In Fig. 2 we compare the ideal modulation transfer function (MTF) curve at 1.3 km range for our telescope with that from the shift-and-add image and the speckle-processed image. It is clear both in the image and in the MTF plot that the speckle processing improves the image resolution to nearly the diffraction limit.

In FY03 we will work on a near-real-time imaging capability.

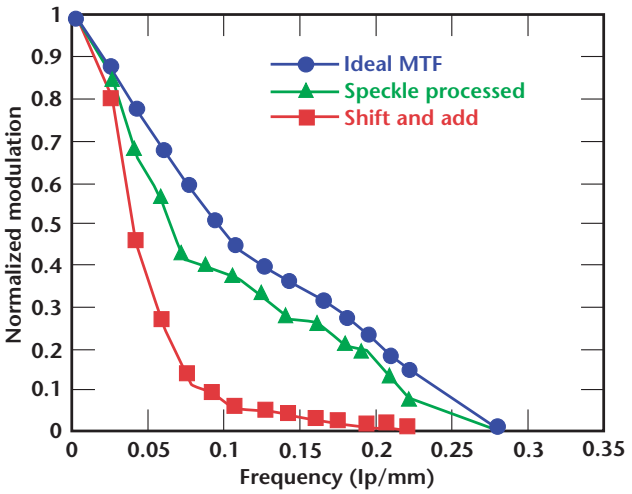

Figure 2. *Comparison of MTFs for the shift-and-add image and the speckle-processed image with the ideal curve for the telescope.*

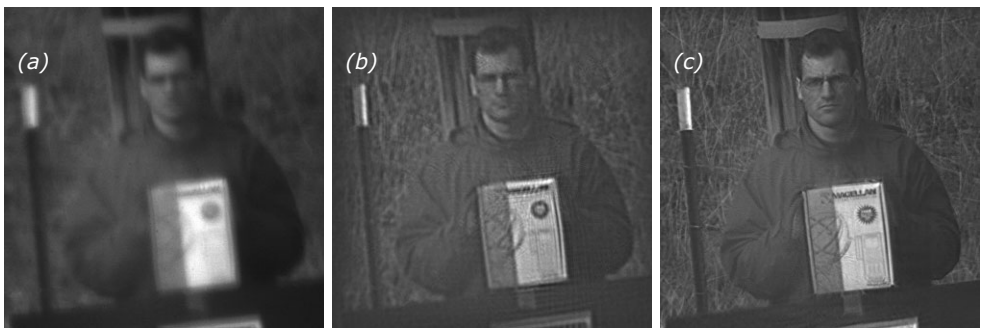

Figure 1. *(a) Raw unprocessed frame of a person imaged from 1.3 km away; (b) full-field speckle-processed image; (c) subfield speckle-processed using 256-x-256 pixel tiles.*

Distributed Control System

L. Flath, C. Thompson, E. Johansson

The purpose of this initiative was to extend the current object-oriented framework and demonstrate a compact distributed controller using off-the-shelf CPUs interconnected with high-speed Ethernet. This goal was achieved, and preliminary testing on a multiprocessing PC was performed.

Prior to this project, an object-oriented framework for control systems was designed and implemented as a Windows dynamic link library. The objects encapsulate functionality common to adaptive control systems, and process data in a pipeline fashion. Data flows between connected objects, each one processing that data in a custom fashion according to its configuration.

As shown in Fig. 1a, the class hierarchy consists of a base class DCDataProcessor from which all others derive. DCDataprocesors each own a thread that processes data from the object's input port to its output port (see example in Fig. 1b). Objects are configured either directly in code or via XML configuration files. DCCamera objects hide all of the hardware (camera, cables, frame grabber) and software (device drivers, frame-grabber APIs) required to operate a camera. DCSensor objects implement algorithms that convert raw input data (such as images) to a measured quantity. Control loop algorithms are realized in DCLoopControllers, and means for manipulating external physical quantities (such as voltages) via digital I/O hardware are embodied by DCModulator objects.

Internal to the DCDataProcessor, a thread performed math operations on data from the object's input port to its output port. Once this pipeline processing is completed, the thread goes to sleep until new data arrives at the object's input port. To construct a system, the output ports of sink objects are connected to the output ports of source objects, as shown in the example adaptive optics system of Fig. 1c. Camera objects have no input port, as they collect data from external hardware. The output of the camera is fed to a sensor object, which takes wavefront sensor image data and converts it to wavefront slopes using a Shack-Hartmann methodology (tracks spot positions relative to a reference input). A loop controller object uses this sensor data to exercise its control law (usually via a vector matrix multiplication and a compensator). The modulator then implements the control response by writing to hardware (in this case a MEMS-based optical phase modulator).

The first step in augmenting the DistCtrl.dll framework for inter-object communication was to implement a messaging architecture. A concise message data structure (32 b) is sent over the network medium (TCP/IP-based Ethernet) for every communication. The message field of this structure is information used by the receiver. Testing of the messaging framework occurred in two phases: acquisition of the computational hardware, and testing of the software on that platform. This permits each half of a system to communicate with the other without any bandwidth interaction. Each segment contains a dual 1.4-GHz Pentium III PICMG PC with full peripherals, including 100 Base-T Ethernet (see Fig. 2).

Tests with this setup were successful, with systems configured to run over both a cross-over cable and Ethernet hubs. To reduce the latency of the messaging, Gigabit Ethernet cards were installed in both segments. A major finding was that current hardware / software implementations of this technology consume up to one-half of the CPU's processing, thus eliminating any possible advantage of the increased bandwidth. All further experiments will use the built-in 100 Mb/s networking found in almost all current PC hardware.

In FY03 we will extend the architecture further by moving the code base onto the Linux platform, and attempting to seamlessly add FPGA hardware processing.

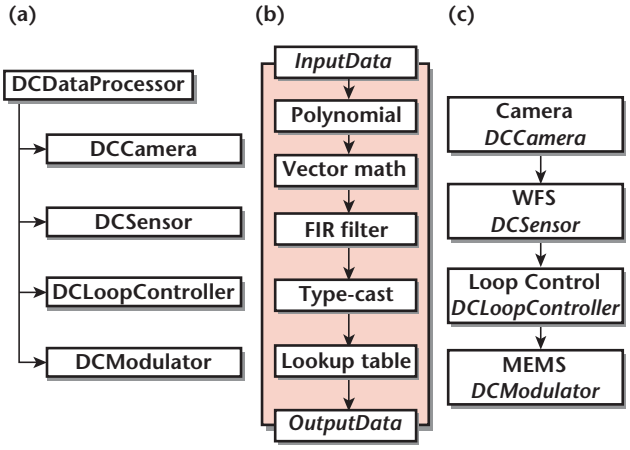

Figure 1. *Distributed control framework: (a) class hierarchy; (b) internal data processing of the root class DCDataProcessor; (c) example control system.*

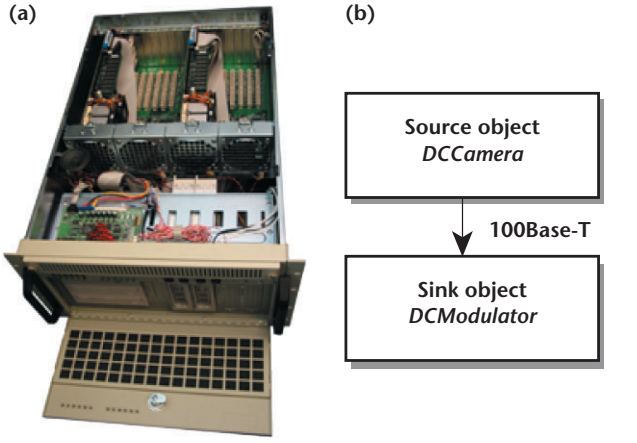

Figure 2. *Server computer: (a) with two dual 1.4-GHz PIII PCs in separate 64-bit/66-MHz PCI segments, and (b) connection of objects using 100 Base-T Ethernet.*

Scene-Based Wavefront Sensing for Optical Correction of Large Space Optics

L. Poyneer, K. LaFortune, E. Johansson

In this project, we analyzed and demonstrated the key technology advances required to design and implement a wavefront control system that will produce high-resolution imagery using a large-aperture, lightweight, space-based optical system. We developed a point design, produced an end-to-end simulation demonstrating its performance, and demonstrated the key technical advances in wavefront sensing required to field such a system.

The capability to provide on-demand, real-time video imagery of any selected location on Earth would revolutionize intelligence and reconnaissance. Although implementation using current technologies is prohibitively expensive, new technologies have emerged that make this a real possibility. Systems based on lightweight diffractive and refractive optics, which minimize deployment costs, are being evaluated. In general these optics can have large aberrations due to lightweight mounting structures, thermal cycling, and deployment errors. To produce acceptable image quality these aberrations must be corrected with an adaptive optics (AO) system that is lightweight, low power, and inexpensive.

The design we chose is a Cassegrain-type telescope using a large gossamer optic made from carbon-fiber-reinforced polymer for the primary mirror, with a conventional secondary. The gossamer optic is extremely lightweight and capable of being rolled up into a reasonably compact package. Both qualities are requirements for space deployment.

The AO system and instrumentation are mounted in a small package behind the primary. The AO system uses a standard Shack-Hartmann sensor for wavefront sensing, coupled with a very small deformable mirror based on MEMS technology for wavefront correction. The design details of the AO system are based on the desired optical system resolution and the scale of the aberrations on the primary mirror. These are both dependent on the size of the primary, which may range from 1 to 10 m in diameter.

A diagram of the proposed optical system is shown in Fig. 1, in both the deployment and the operational configurations. Based on an analysis of the material of the gossamer optic, its aberrations were simulated using a superposition of time-harmonic Bessel functions of random relative phase, which produce a disturbance that is similar to the vibrating surface of a drum.

Traditionally, the aberrations corrected by an AO system are measured using a precision reference point source. Unfortunately, this is not feasible when imaging an uncooperative target, as will typically be the case with our space-based optical system. We must somehow estimate the wavefront errors using information from the scene being imaged.

This "scene-based wavefront sensing" has been the major emphasis of the project. Based on similar work done by solar astronomers, we have successfully generated a robust scene-based wavefront sensing technique capable of real-time implementation. It has been thoroughly tested by detailed end-to-end simulation of the entire AO control loop and optical system, and yields excellent results. Results for a sample simulation are shown in Fig. 2.

Also, we have analyzed the accuracy and performance of the wavefront sensing technique based on image content (*e. g.*, contrast and noise) with the goal of being able to predict performance. Finally, we have analyzed the computational complexity of the algorithm to determine the CPU requirements for implementation.

Future work will include extending the technique to horizontal-path imaging through the turbulent atmosphere, improving performance for low-contrast scenes, automated scene selection for optimum performance, and evaluation of transmissive diffractive optics.

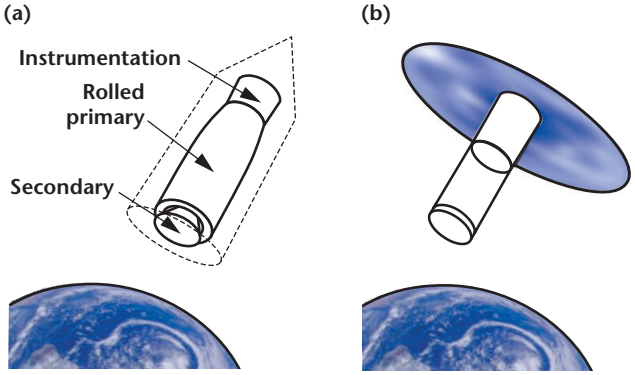

Figure 1. *Lightweight space-based optical system shown in both (a) deployment and (b) operational configurations.*

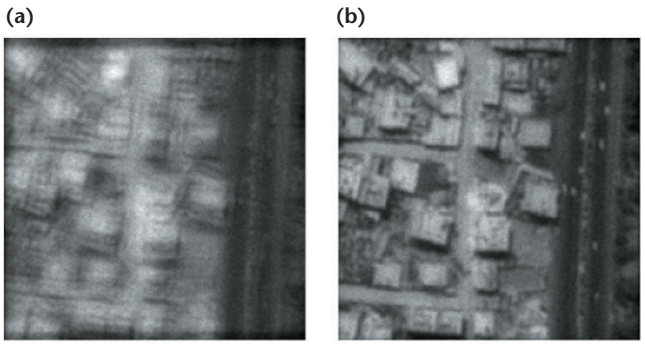

Figure 2. *Results of end-to-end simulations of the scene-based wavefront sensing algorithm, showing (a) uncorrected and (b) corrected images.*

Contact Constitutive Relationships for Interface Surface Features

C. Noble, J. Solberg

The objectives of this project include: 1) to determine a constitutive law that accounts for interface surface features; 2) to validate the algorithm with experimental data; 3) to implement the algorithm into finite-element (FEM) codes; and 4) to develop university collaborations.

Before this study, contact algorithms lacked the sophistication to accurately model the local topology of a structure's contact interfaces, where load is often transferred between components through the use of geometrical discontinuities. The presence of discontinuities is a common feature in many mechanical systems, such as rock interfaces, weapons components, concrete dams, and concrete bridges.

One example is the modeling of concrete arch dams. Concrete dam structures may consist of 30 or more contact interfaces that include shear keys, which result in unique directionality effects along the concrete interfaces, similar to those in rock interfaces. This year we added the capability of modeling these shear keys to both the implicit (NIKE3D) and explicit (DYNA3D) FEM codes at LLNL. The new contact algorithm is able to correctly account for the shear keys along separate slide surfaces that are located on user-defined planes (Fig. (a) and (b)).

We validated the algorithm with simple test problems. The first test was sliding one block past another in NIKE3D. These blocks are of the same size as those seen in a typical arch dam. The slide surface between the blocks was given the parameters necessary to replicate the shear keys in Fig. (b). The plot (Fig. (c)) shows the transverse displacement vs. the upstream-downstream displacement.

The contact algorithm does a good job of accurately modeling the behavior of these shear keys. Another test problem consisted of using the new contact algorithm in the FEM during static (gravity and hydrostatic loading) initialization of the dam, and comparing the results to the original FEM that used a proven method with discrete springs (Fig. (d)). The tensile stresses were very similar, and the FEM that used the new contact algorithm had lower tensile stresses, which is more realistic for a double-curvature arch dam.

This technology-base project played an integral part in the success of the Nonlinear Seismic Analysis of Morrow Point Dam Project. The US Bureau of Reclamation will be funding LLNL for the third year in a row for future seismic analyses of Morrow Point Dam.

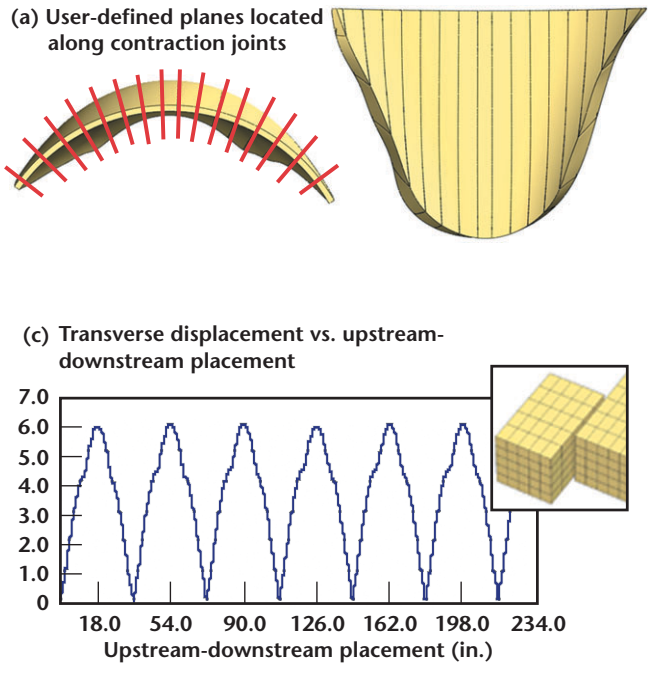

(a) FEM showing vertical contraction joints of Morrow Point Dam; (b) shear keys common to concrete arch dams; (c) NIKE3D sliding block test showing contact algorithm replicating the behavior of shear keys; (d) comparison between tensile stresses in arch dam, from a model using discrete springs and a model using new contact algorithm.

Center for Computational Engineering

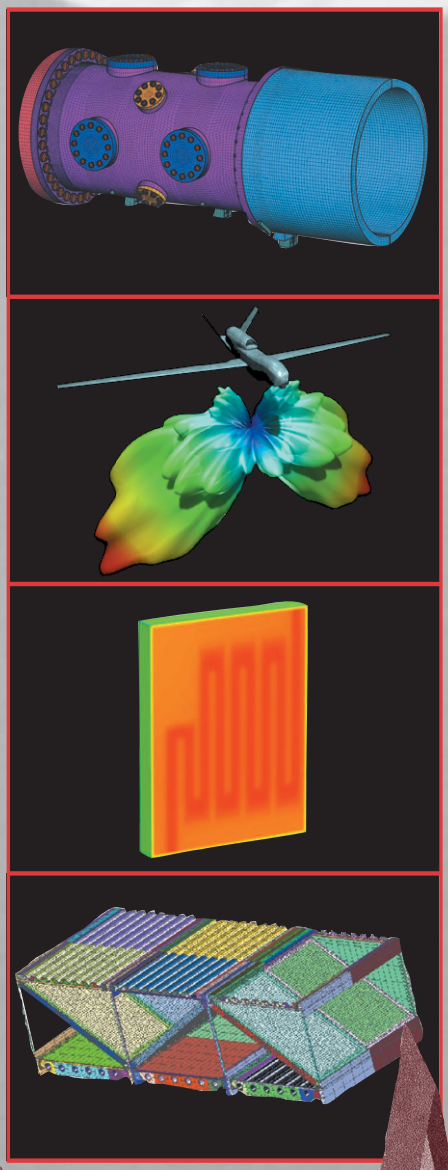

Engineering Visualization Laboratory

M. Loomis, R. Sharpe

The Engineering Visualization Lab (EVL) was recently established as a venue in which to highlight work being performed by LLNL engineering personnel. While the first year of the project focused primarily on construction of the physical facility and system integration, the emphasis in FY02 was on demonstrating the production capabilities of the facility.

As a presentation theater, the EVL facility integrates a large projection video screen and surround audio system with a number of media sources, including computer display output, digital disc recorder, VCR, DVD, and a video network feed from LLTN. Presenters can easily patch a laptop computer into the system or use the resident hardware to present their material on the large display. The room provides seating for 10 to 15 people, and provides an unclassified environment suitable for small-group collaborations, software demonstrations, or video presentations.

As a media production workshop, the facility also enables the development of high-quality visualizations to help engineers better communicate their ideas. High-end animation, compositing, and image processing software manned by knowledgeable operators provide the tools and expertise necessary to achieve this goal.

An engineering movie, "Sensor Network Scenario" (UCRL-MI-149948) was produced to help visualize a number of issues related to electronic signal propagation in topologically rugged environments. A still from the movie is shown in the figure. This movie was created with a number of goals in mind: 1) to fill a programmatic need; 2) to demonstrate a path for visualizing computational results by incorporating actual data; 3) to showcase various types of animation to illustrate the creative possibilities and techniques that are available for engineers to use in future animation productions; and 4) to demonstrate the EVL's capability.

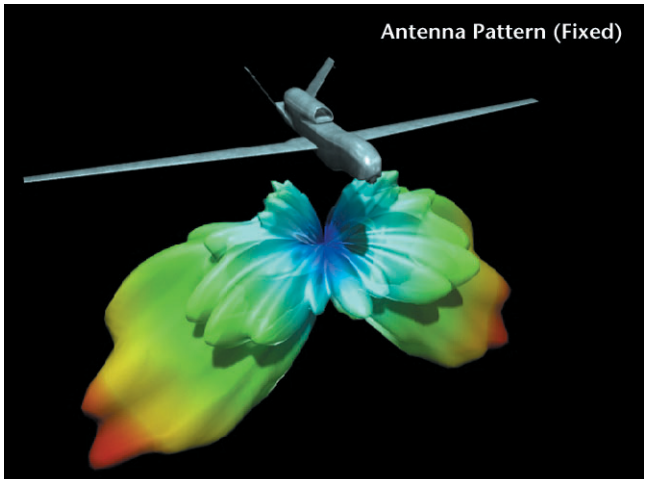

Still from movie created to demonstrate the EVL's animation production capability.

We addressed programmatic issues by consulting with LLNL engineers to create a storyboard that helped them communicate key concepts and issues directly related to their work. To demonstrate the fusion of actual data, the animation includes a visualization of an antenna pattern that was computed for an unmanned air vehicle. A number of animation techniques including soft-body motion, collision detection, particle systems, and explosion effects were used. The result was a movie that brought engineering ideas to life in a form that was both instructive and visually compelling.

The animation was previewed for several key engineering personnel on the large video screen in the EVL facility. By combining creative media production with the display capabilities inherent in the assembled hardware, we believe that the presentation demonstrates the potential for using the EVL as a tool to effectively communicate engineering concepts.

Another animation will explore signal propagation in an urban environment.

A list of components follows:

Hardware:

Computer 1	SGI Onyx 2
Computer 2	Macintosh G4
Large Screen Display	Clarity Visual Systems Lion
Digital disk recorder	Accom WSD 2-Xtreme
S-VHS video recorder	Panasonic AG-1980
Video Monitor	Panasonic DVD-A120
Surround sound speakers	Klipsch Synergy 6
AV Receiver	Denon VR-3300
Video switcher	

Software:

3-D Animation	Alias/Wavefront MAYA
Compositing, Image Processing	Alias/Wavefront Composer
Video Editing	Apple final Cut Pro
DVD Authoring	Apple DVD Studio Pro
Format Conversion	Equilibrium Debabblizer
Digital Video Compression	Terran Media Cleaner

Network Monitoring and Analysis Framework

R. Burleson, E. Quinnan, M. Casado, D. Crawford

There are numerous network monitoring and intrusion detection software products. However, these products are limited, and do not provide the complete functionality needed by US government organizations to monitor and protect their computer networks from reconnaissance and intrusion. The Network Mapping and Analysis Framework project builds on capabilities that have already been developed at LLNL and elsewhere to meet the requirements of the DOE, DoD, and the Intelligence Community (IC).

Our initial efforts focused on intrusion detection and log file analysis that can be used by DOE's Computer Incident Advisory Capability (CIAC), computer security organizations at LLNL, and other DOE laboratories and US government organizations.

The Information Operations and Assurance Center (IOAC) has generated many of the technological components required to maintain a dynamic network map that can display the network topology and characteristics, highlight vulnerabilities, display intrusion paths, and diagnose various suspicious activities. Some of these component technologies have not been integrated in the past, and this project has completed the first steps toward creating a framework and tying in some of the various capabilities. State-of-the-art commercial products and systems developed by other R&D organizations can be relatively easily integrated with this framework.

The Montana network mapping system creates a model of the network that can be built automatically. The Montana/Nevada tool suite allows the user to display the network topology and the characteristics of each computer system on that network, and identifies and highlights potential vulnerabilities.

We have now modified Montana to accept input from tools such as Logger (a CIAC-developed firewall log analysis system), SNORT (an open source intrusion detection system), and system and web logging capabilities. Data from these diverse sources can be either analyzed in isolation or integrated with the data from the other sources, as well as with the Montana network map. Entering this data into Montana's Network Management Data Base allows the user to manipulate and analyze the data in a graphical format.

A simple example is the Bad IP List data in Fig. 1. This data shows IP addresses of computers from which scans or intrusions are launched against the protected sites shown in the picture. The data from multiple sites is integrated in this view, allowing the user to easily pinpoint computer systems launching attacks or scans against multiple sites.

Our goal is to provide a real-time network display as conceptualized in Fig. 2, showing the actual current state of the network, updating the display as characteristics and topology of the network change. We will be able to display the path of an intrusion into the network, identify various types of intrusions, identify access patterns by particular off-site individuals or groups, and screen for unusual traffic patterns. This project has provided the basic system which can be easily built upon and expanded for future network analysis capabilities.

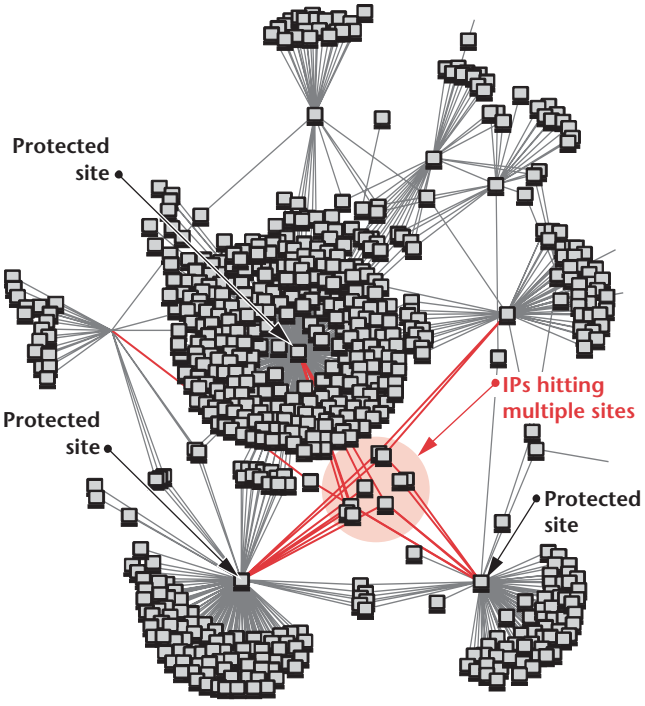

Figure 1. *Visualization of Bad IP List.*

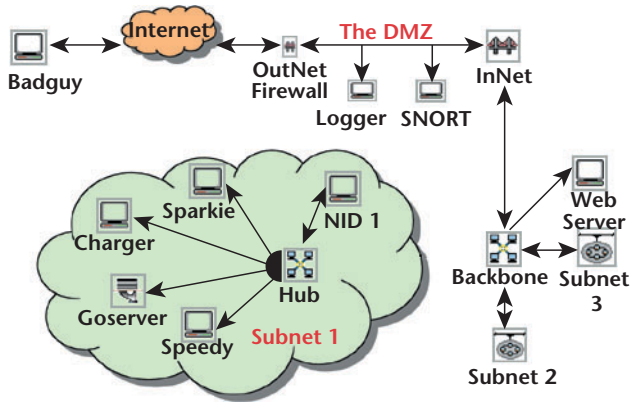

Figure 2. *Conceptual picture of a real-time display of an organizational network.*

MEMS Models for Miniaturized Power Sources

M. A. Havstad, J. D. Morse

The availability of portable power sources is critical for many aspects of the military and intelligence communities. Microreactors driven by small or microscale fuel reformers may fill this need. Our thermal models of microscale reformers have good agreement with experiment for a range of flow rates approximating that required for producing an integrated microreactor package with electrical output in the 1- to 10-W range. These models are now being used to estimate the power needed for start-up and steady-state operation.

In reactor design for microscale power sources, thermal management is key, for three reasons: the high temperature of the fuel-reforming reaction must be isolated from human users for safety reasons; efficiency and useful life can be strongly influenced by the waste and start-up heat required; and it is desirable to minimize the thermal signature of any power source (particularly for NAI applications). Modeling, rather than repeated fabrication and test, is the preferred approach to working, cost-effective solutions to these thermal management issues.

Our approach is to etch a microchannel reactor for steam-reforming of methanol in a glass or silicon wafer. The microchannel is filled with a catalyst and connected to a fuel reservoir by microfluidic interconnections. Resistive heaters are positioned on the wafer along the reaction zone, allowing the catalyst to be heated as fuel flows through the microchannel. With a steam and methanol mixture, a fuel-reforming reaction occurs at temperatures (*e.g.*, 300 °C) greatly below those found in traditional bulk solid oxide fuel cells. The reaction produces H_2, CO, and CO_2, and consumes much of the steam and methanol.

Surface chemical kinetic and plug flow reactor models of this steam-reforming process were implemented in TOPAZ3D and exercised on several reactor-on-a-chip concepts. A model of a device in test at LLNL's Microtechnology Center was also built and used to predict performance (fuel-conversion efficiency and hydrogen output), thermal profile, and heating requirements. We obtained excellent agreement between modeling and tests (Fig. 1) for a simple reactor geometry. The good agreement for the CO concentration is particularly valuable because of the tendency of very low levels of CO to degrade the performance of many types of fuel cells. We have begun to work start-up, heat recovery, and 3-D heat loss issues (Fig. 2).

Challenges for the coming year, as we create a workable prototype, include reducing heat loss to the ambient, and isolating a relatively low-temperature (~60 °C) proton-exchange membrane fuel cell from the fuel reformer.

Our consistent and computationally efficient treatment of reformer and heat exchange effects enables screening of device concepts prior to fabrication; optimization and intelligent thermal management of promising devices; and determination of transient thermal stress effects on start-up and shut-down. To date our "plug flow reactor" model has been an effective tool and design aid.

A more detailed analysis that couples multi-component diffusion, solid conduction, and chemically reacting surfaces will be useful for complete validation. We have developed an unstructured grid finite-volume approach that has successfully solved a simple flow problem and requires very little extending to treat a multi-component diffusing flow configuration, the key fluid aspect of a thin-film catalytic microreactor.

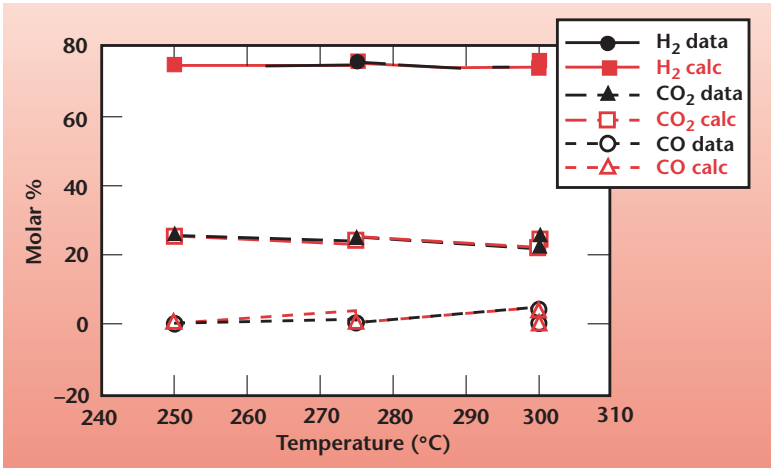

Figure 1. *Fuel reformer products: predictions vs. measurements.*

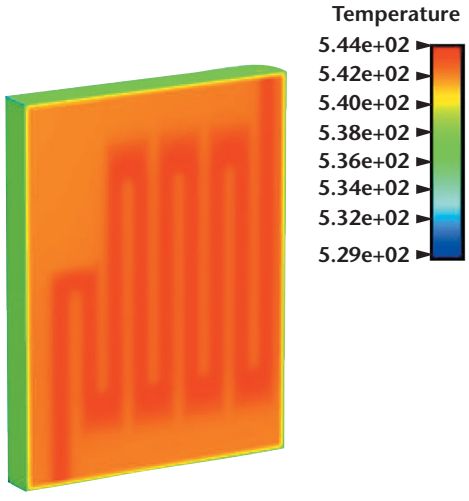

Figure 2. *Thermal profile (K) of microreactor on a wafer with the back side insulated.*

Multi-Phase Flow Modeling Capability with Chemical Kinetics

T. Dunn, J. Ortega, D. Flowers, T. Piggott, K. Wittaker, R. Couch

The purpose of this project was to enhance LLNL's fluid dynamics capability in the area of multi-phase and chemically reacting flow. This was accomplished by building upon the current tools available in the ALE3D multi-physics hydrocode. The project focused on discrete particulate transport, free-surface flows, and chemical kinetics. Verification and validation were emphasized to provide confidence in the accuracy of the methods.

The particle-tracking module was developed to simulate problems involving particulate transport within a carrier fluid. Dilute particle flow is assumed where local aerodynamic forces control the particle's motion and particle-particle interactions are neglected. Momentum is transferred from the particle to the fluid through the fluid's continuum equations. Each particle is individually tracked in a Lagrangian reference frame using an equation of motion derived from Newton's second law. The equation accounts for the steady-state aerodynamic and gravity/buoyancy forces acting on the particle, as well as pressure and shear gradients within the flow-field. A random-walk model was developed to predict turbulent dispersion of the particles (Fig. 1). An inelastic hard-sphere bounce model is used for particle-wall interaction. Additional physics may be easily added to the model by adding additional terms to the particle's equation of motion.

Droplet dynamics has been the main thrust of the free-surface modeling effort. The deformation and breakup of droplets involve complex coupling between aerodynamic forces and the droplet response. The Arbitrary-Lagrangian-Eulerian (ALE) formulation in ALE3D is ideally suited to model the droplet motion. A surface-tension model was added to ALE3D to simulate the intermolecular forces within the droplet. In addition, a mesh-relaxation scheme was added such that the computational grid surrounding the droplet is mapped to the droplet motion and a constant level of grid refinement near the surface is obtained throughout the simulation. Another method consisted of an interface-tracking algorithm for fluid/droplet interfaces that do not conform to mesh boundaries.

Another aspect of this project was to explore ALE3D's capability to handle coupled fluid mechanics and chemically reacting flow by modeling hydrogen-oxygen detonation in a shocktube. This involves complex interaction between shock waves, contact discontinuities and expansion waves, and the chemistry of combustion. First, a 1-D model was used to quantify the capabilities and limitations of ALE3D. The calculations showed a large temperature overshoot at the contact discontinuity, as well as temperature oscillations after the shock (Fig. 2). Additional 2-D simulations including the reaction of an H_2-O_2 mixture were also performed.

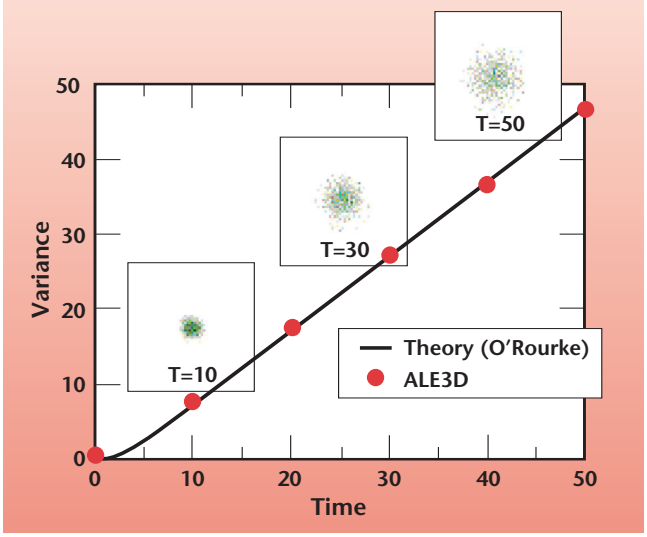

Figure 1. *Theoretical and calculated variances in the distributions of drop position. The calculations used 1000 particles released from a point source.*

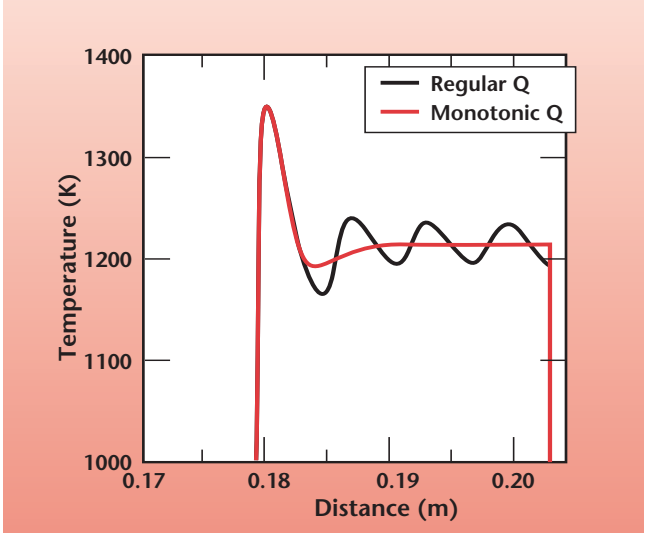

Figure 2. *Calculations of a hydrogen-oxygen detonation in a shocktube, showing the effect of artificial viscosity (Q) on the temperature prediction.*

Model-Based Manufacturing

R. N. Frank, M. Prokosch

The goal of the FY02 Model-Based Manufacturing (MBM) Project was to improve skills and procedures for "paperless" manufacturing within the Manufacturing and Materials Engineering Division at LLNL. The primary focus was to establish Pro/Engineer as a business tool within the Main Bay facility.

We purchased a modern workstation for the Main Bay Planner and another for the Programmer. We acquired Pro/E licenses for those workstations, and an ICAM post-processor license. The post-processor is required to translate generic numerical control (NC) code into machine specific code. The software was installed and configured.

We obtained Pro/E training for the Main Bay personnel as well as one Inspector (funded independently). Once the basic Pro/E skills were established, we contracted with a recognized expert in NC programming from Sandia National Laboratory to give a one week, hands-on class at LLNL. All the participants felt this was an outstanding session and we hope to repeat it at a more advanced level this year.

The bulk of this project did not occur in a laboratory environment, but rather on the program-driven shop floor. Scheduling difficulties and programmatic work delayed the completion of the Pro/E training until early May. Post-processor development is done in-house and a heavy workload in the NC Shop also impeded development until late in the fiscal year. In spite of these factors, we were able to develop a functional expertise with the technology by the end of the year.

Early in the project we received MBM projects from Laboratory programs. The increase in our skills, knowledge, and ability were highly evident. We were unable to exactly account for the time required to manufacture a part at each phase, but the part took well less than half as long to complete the second time we did it. Past experience dictates that this efficiency will continue to increase as MBM becomes a routine business method.

The MBM project also had a larger scope. Laboratory personnel concerned with Computer Integrated Manufacturing met to discuss MBM issues during the life of the project. Since MBM uses relatively raw data from designers, a common interface needs to be forged between design and manufacturing. In traditional methods, the formal drawing is that interface. In MBM, the model fills that role and must satisfy both groups.

Through these discussions and practical experience we began a MBM specification for LLNL. This document will serve as a guideline for designers and manufacturers to incorporate design for manufacturability techniques into a model. This will reduce the cost of detail drawing, yet provide sufficient information for accurate and efficient fabrication. We expect to have a draft ready for review and submission in the near future.

This project gave us the opportunity to purchase the tools and training we needed to incorporate an important technology into our main manufacturing facility. We enhanced the MBM capabilities in the NC Shop and are looking forward to developing Model-Based Inspection.

Furthermore, the project brought several very talented people from different organizations together. This combination of technology, training, and collaboration laid a solid foundation for a technology that promises to deliver critical products for our customers faster, better, and cheaper than before.

Computational Mechanical Engineering Tools

C. Hoover, R. Ferencz

Current code-enhancement activities include adding and improving models for elements and materials to more adequately describe the behavior of foam, rubber, viscoelastic explosives, and layered composite materials. Contact algorithm development for improving the treatment of material interfaces is an ongoing activity.

Sophisticated computational mechanics tools are an essential part of a mechanical engineer's analysis and problem solving strategy. LLNL's Methods Development Group and Thermal Fluids Group develop nonlinear finite-element codes (NIKE3D, DYNA3D, TOPAZ3D, ParaDyn, Diablo) for solid, structural, and thermal/fluid analysis. In addition, the two groups support the analysts' activities with individual consulting, up-to-date online documentation, and training classes.

Progress in FY02 is described in part in articles by Lin, Puso, Speck, and Shapiro, elsewhere in this Volume.

New capabilities in the visualization software are based on a flexible binary database format generated by the Mili I/O library and supported with the GRIZ4 visualization tool. The latest database development and enhancements provide the ability to visualize time-history results and coupled results from analysis programs, and conveniently add new results to the databases.

A new anisotropic fracture mechanics material model used for rock mechanics and other fracture mechanics applications benefited from the design flexibility of the database.

A frequent requirement of high-fidelity simulation is combining the effects of relatively slow processes, *e.g.*, assembly loads from bolts, or gravity load, with the effects from rapid events that characterize the service life or possible accident scenarios such as rapid pressurization or earthquake loading.

The figure shows a representative analysis of a containment vessel that couples pre-load results calculated in NIKE3D with a time-dependent analysis using DYNA3D. The purpose of these calculations was to measure the stress on the bolts for different types of loads and for an envelope of expected load levels for each type of load. To include the detail needed in the analysis, the size of this mesh was 300,000 elements. The next calculation of a containment vessel is expected to be twice as large, suggesting the need for a coupled parallel analysis using the NIKE3D program with a parallel linear solver coupled to ParaDyn.

Early in FY02 we sponsored a four-day class to meet the training needs of newly-hired analysts and to keep our experienced analysts up-to-date. The class included a one-and-a-half-hour lecture for each software product, an introductory lecture on the theoretical background for finite-element analysis, and an overview of the Diablo code development.

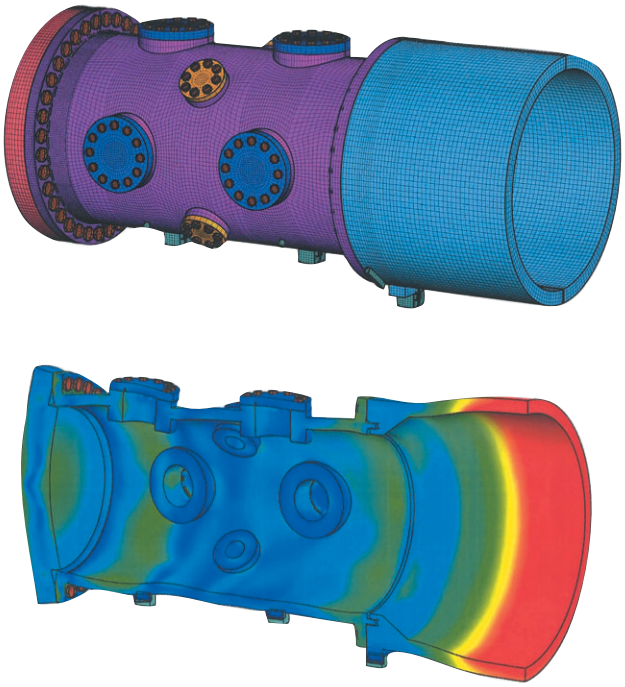

Representative analysis of a containment vessel. The containment vessel for the Piano sub-critical test apparatus required detailed examination of the effects of both bolt pre-loads and subsequent rapid internal pressurization. Both the detail of the mesh and the stresses created by internal pressurization are highlighted. Deformations are magnified in the lower image.

Capability Enhancements in NIKE3D

M. A. Puso

In FY02, we added features and efficiency improvement to NIKE3D, in support of multiple applications. This report highlights new plasticity models and algorithmic enhancements that led to large performance increases.

Two new hyper-elasto-plastic material models were implemented. These models are derived from strain energy functions and thus guarantee proper thermodynamic behavior in large strains. This improves upon the older, common hypo-elasto-plastic models that can display anomalous behavior, especially in cyclic loading and unloading. Exact linearizations were derived and implemented and provide more rapid convergence for nonlinear problems.

The figure illustrates this improved performance for a model problem of a copper bar undergoing large deformation due to impact.

An important issue in implicit finite-element technology for nonlinear problems is the inclusion of the so-called geometric stiffness arising from the internal state of stress in a body. That a violin string takes on a higher pitch as it is tightened is a common manifestation of this effect, but it can be important in many situations. Buckling is another phenomenon related to this effect.

Unfortunately, always including the geometric stiffness can slow convergence or even algorithmically destabilize some nonlinear analyses. In support of modeling an x-ray columnator, a thin-walled structure, new logic was implemented for activation of the geometric stiffness in NIKE3D. This logic delays inclusion of the geometric stiffness until the energy norm reaches a prescribed threshold. For the columnator analysis, this reduced the number of time steps from 200 to 8, reducing the execution time by a factor of 15.

Two new enhancements were motivated by on-going efforts (reported elsewhere in this volume) to model a concrete, segmented arch dam. A special contact algorithm to mimic the effect of an interlocking "key joint" was prototyped to establish feasibility, then fully implemented with project funds. This capability will permit the modeling of key ratchet without using many small elements to capture the detail of the joint geometry. The dam/reservoir/canyon model involved contact facets and initialization of the model was slow. To avoid the N^2 search previously required to identify elements, and thus a material stiffness, for each contact facet, an inverse node-to-element map is now computed. This was found to speed up the contact initialization by roughly a factor of 100.

Clearly, all large models will benefit from this improvement.

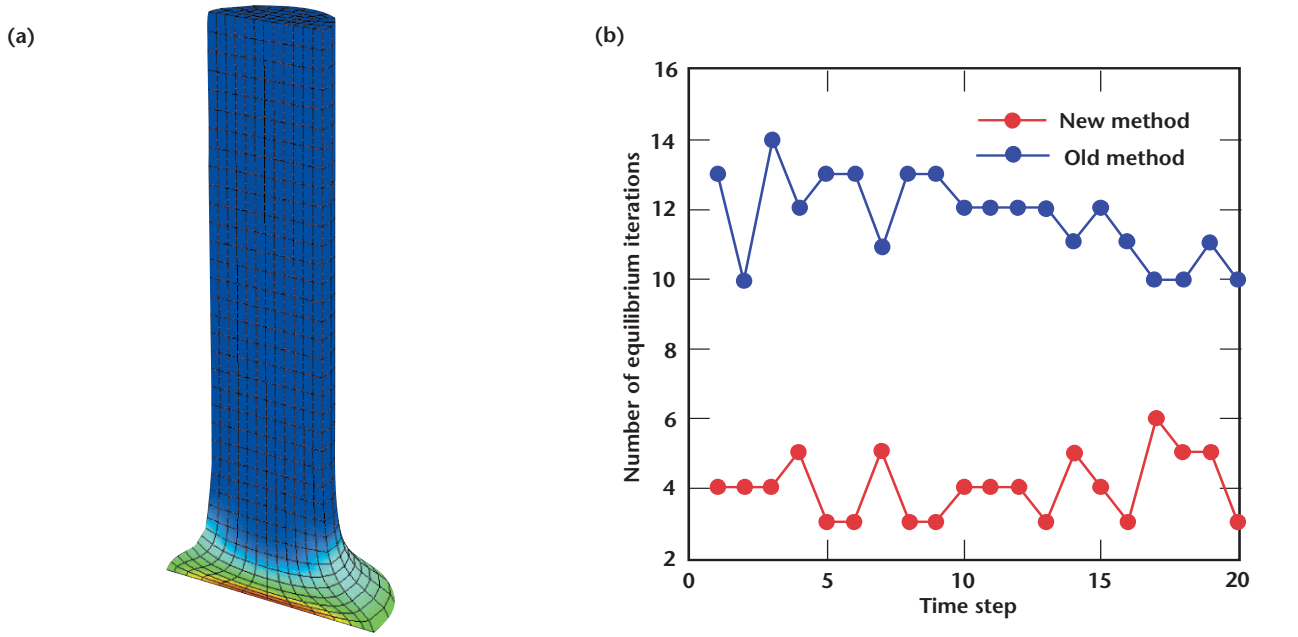

(a) NIKE3D Taylor bar simulation. (b) Number of equilibrium iterations per time step with old and new plasticity algorithms for the simulation. The new algorithm requires far fewer iterations, and is therefore much more efficient and robust.

Heat Transfer and Fluid Code Enhancement

A. Shapiro

We have extended the capabilities of Topaz2d, TEXSTAN, and Topaz3d.

Topaz2d

A major effort, started in FY01, was the addition of a new slide-line algorithm in Topaz2d. This was driven by the needs of a defense program activity. The existing algorithm was intended for master and slave surfaces that start and end at the same spatial location. This condition is not overly restrictive for heat transfer problems since no motion is taking place due to applied forces.

However, for the W80, a mechanical mesh was created consisting of 83 slide surfaces, for which many slave-master pairs did not meet the condition of identical starting and ending points. This high-fidelity mechanical model was also to be used as a thermal model. A new slide-surface algorithm was implemented in which the slave and master surfaces could start and end at arbitrary locations.

The method is a surface-to-surface algorithm, as opposed to the simpler node-to-surface algorithm currently in Topaz2d. The algorithm maps (*i.e.*, finds the shadow of) the smaller surface area of the slave-to-master pair onto the larger surface. This shadow area is called the contact area, A_c. The heat transfer between the surfaces is then calculated by $\dot{q} = hA_c(T_m - T_s)$ where T_m and T_s are the temperature of the master and slave surfaces, respectively. The heat transfer coefficient, h, can be defined as a convection conductance, a radiation conductance, or a combination of both.

TEXSTAN

TEXSTAN is a code that calculates the momentum and energy boundary layer for slab and axi-symmetric geometries. The code was obtained several years ago from the University of Texas. The code is used by the Mercury Laser Project to determine convection heat transfer coefficients and predict flow separation in the gas-cooled amplifier units. Several bugs were fixed in the code during porting of the code to SGI UNIX. Verification and validation were performed on the code by comparing calculated results for the various turbulence models to analytical solutions.

Topaz3d

Input file formats for integer variables have been set to I5 (*i.e.*, five integer digits are to be read). This places an upper bound on the finite-element model size of no more than 99,999 elements and 99,999 nodes. Recent models, such as the amplifier end-effects thermal-recovery unit (shown in the figure) required more than 120,000 elements. The entire input structure of Topaz3d was modified such that integers would be read in I8 (*i.e.*, eight integer digits) format. This will allow up to 99,999,999 elements and nodes in a model.

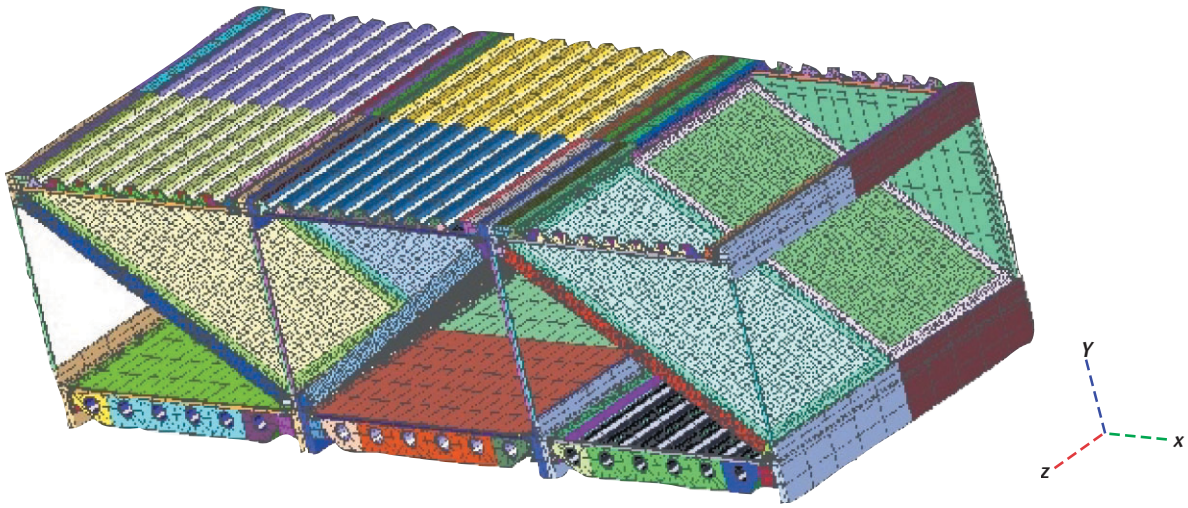

Model of laser amplifier end-effects recovery unit.

Post-Processing and Data Management Activities

D. Speck

An important improvement in FY02 was the creation of an initial Mili version of the TAURUS time-history database, which is paving the way to have a single tool (GRIZ) post-process both plot and time-history databases.

This year's trend to 64-bit computing impacted graphics and data management software in multiple ways. Both the GRIZ finite-element post-processor and the Mili I/O library were updated to have 64-bit "clean" source code. GRIZ was further enhanced with an initial capability to accommodate double-precision simulation data from Mili databases, with the addition of code to convert such data to single-precision as it is read in. This will enable GRIZ to visualize the analysis code link files used to communicate simulation data between analysis applications.

One desirable capability that has been identified since the initial implementation of Mili and version 4 of GRIZ is the ability to define and write data associated with surfaces. The surfaces of interest might be boundary condition surfaces, contact surfaces, or rigid walls. These are data managed in the analysis, but heretofore they have lacked a natural form of expression in Mili or logic for post-processing in GRIZ.

One of the major accomplishments in FY02 was the implementation of a surface "superclass" in Mili, plus initial supporting logic in GRIZ, to load and manage surfaces and the simulation data associated with them. This new code is being tested and integrated with the production source.

Experience to date with Mili version 1.0 has demonstrated areas where additional new capability is required, as well as areas where the existing design can be improved in terms of its generality, correctness, or efficiency. These new and improved capabilities have been collected and documented to define the requirements for Mili version 2.0.

In FY02, we developed a Mili 2.0 requirements and design document. A version 2.0 development branch was created in the Mili source code repository and implementation of Mili 2.0 was initiated.

An important aspect of the Mili 2.0 effort is a move to improve the overall quality of the code and limit debugging time in later development stages by instituting proven software quality assurance practices. One practice, already described, is the explicit documentation and review of both requirements and design for the new Mili version.

Another new practice is the integration of application code and unit-testing modules so that new code can be tested throughout its lifetime. A third practice planned is that of code reviews in which new code is circulated among cognizant developers for critical feedback.

One software engineering practice that supports improved quality is formal change control. We have used SCRTrack for several years to manage software change requests (SCRs). Most of the use of SCRTrack has been devoted to GRIZ and Mili activities. In FY02, 41 SCRs were resolved: 29 for GRIZ and 12 for Mili. Of these, 11 originated with GRIZ/Mili developers, 12 originated with other code developers, and 18 originated with engineering analysts. There were 31 new SCR's defined in FY02 that went unresolved, but of these, only eight were bug reports (the rest were enhancement requests), and none of the eight was critical.

In FY02, two trends can be identified among the forces driving post-processing and data management code development activities at LLNL. One is a more thorough exercising of GRIZ (and implicitly, Mili) by the new engineering analysts. These users have no preconceptions about how the codes should behave, nor have they established patterns of use that might limit their exploration of new features in the code. These characteristics lead to valuable new insights and perspectives on code behavior, as well as the discovery of both new and long-hidden bugs.

Another trend has been analysis using Mili, which affects Mili directly and GRIZ indirectly. As the new implicit analysis code, Diablo, matures and an expanding set of material-model-specific simulation data from ParaDyn/DYNA3D are expressed in the Mili database, features planned for years ago are finally being exercised. At the same time, equally important (and unanticipated) new requirements are being generated that will increase Mili's utility and value in the years to come.

Gas-Induced Pressure Loads in DYNA3D

J. Lin

We have added new features to DYNA3D for structural analysis of gas-induced pressure loads.

In structural analysis of mechanical systems, one often encounters the modeling of gas-filled chamber-like structures. The pressure load imposed on the structure by the enclosed gas will change because of the addition of more gas into the chamber or the change of the chamber volume. The obvious examples for the former are the gun barrel and the vehicle airbag, and for the latter, the piston chambers in an engine.

In computer simulations, the structure surfaces enclosing the gas are usually discretized into triangular or quadrilateral patches. During an analysis, either a pre-defined function of time or a pressure/volume gas law usually determines the gas pressures exerted on these patches. The pre-defined function approach involves predicting the chamber volume change *a priori,* and often does not reflect the interaction between the structure and the gas. The gas law option is usually a more desirable approach, since it updates the current chamber volume continuously, and thus takes the evolving structural deformation into account.

In an explicit finite-element code like DYNA3D, because of its inherent limitation on time-integration step size, efficient algorithms for updating the chamber volume are essential to the gas law approach.

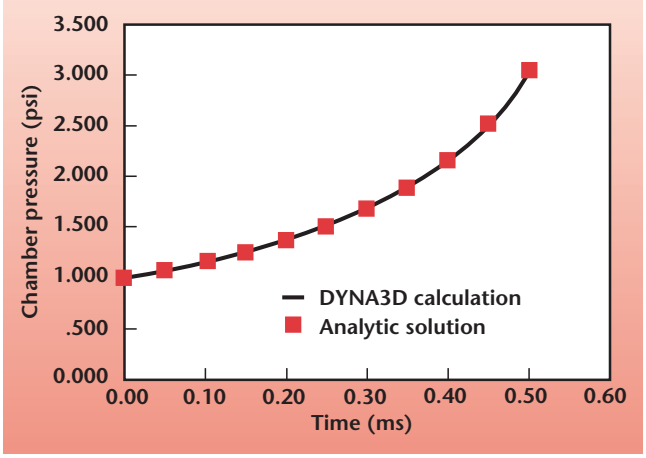

Pressure-time history of a rigid piston suppressing a rigid chamber.

The use of the Divergence Theorem of Gauss with properly selected projection plane attains this goal. The new algorithm hinges on the quick calculation of the volumes of truncated triangular prisms formed by the triangular patches that define the closed chamber and their projections on a common plane. The common projection plane is chosen such that the volume calculation for the truncated prisms is trivial. By orienting the triangular patches so that their normal vectors all point outward from the closed chamber, the chamber volume can be quickly obtained by summing the volumes of all truncated prisms.

In structural analysis, symmetry conditions are often used to reduce the size of the model. The plane of symmetry may cut through a closed chamber in which the gas pressure is present. In this situation, the chamber would appear open because of the lack of discretized patches on the plane of symmetry to close it. The new feature takes this into consideration and overcomes it by selecting a projection plane coincident or perpendicular to the plane of symmetry.

The closed chamber, such as an airbag, is defined by the same set of patches, whereas a piston chamber can be defined by different sets of patches depending upon the position of the piston. When the piston motion suppresses the piston chamber, the chamber will be enclosed by fewer patches, since some of the patches originally in the list will be entirely covered by the piston.

These piston-covered patches may later become active again as the piston moves away. A technique of adaptively tracking the patches defining the piston chamber is accomplished by the use of a reference plane moving in the direction of the piston motion.

A rigid piston suppressing a rigid chamber filled with ideal gas at a constant velocity is used as a benchmark problem because of the available analytical solution. The plot in the figure demonstrates the effectiveness of this new feature in DYNA3D.

Theoretical Model for the EM Effects Induced by High-Energy Photons in Dielectric Materials and Electronic Systems

J. H. Yee, D. J. Mayhall, M. F. Bland

We constructed a model that includes the equations that describe the physics of the recombination and generation of electron-hole pairs by the high-energy photons in the dielectric materials, Compton electron generation rates, and Maxwell's equations.

When a beam of gamma photons penetrates a transmission line or cables, energetic electrons and holes (carriers) are created in the metals and dielectrics of the system by the Compton and photoelectric effects. Through the interaction of the high-energy electrons with the atoms in the solids, many low-energy holes and electrons are created. Since the density of the solids is very high, the mean free path of the high-energy electrons is very short (yielding a time constant of picoseconds or less).

Since electronic systems typically do not respond in such a short time, we can make the approximation that the number of low-energy carriers can be determined by energy deposition by the gamma photons, with the use of a Monte Carlo code. We then divide the deposited energy by the average amount of energy necessary to create an electron-hole pair. To investigate how the EM wave is created by the gamma photons and its behavior as it propagates through the electronic system, we have considered the various recombination and trapping processes of the electrons and holes in the dielectric material.

We modified an implicit, 2-D, finite-difference, time-domain, EM, electron fluid computer code for the propagation of transverse EM (TEM) and transverse magnetic (TM) modes in a parallel plate transmission line in a rectangular geometry, with pressure-variable air as the dielectric material.

To model a coaxial cable to first order in two dimensions, we have also implemented a radial geometry code with two different solid dielectrics between a cylindrical center conductor and an annular outer shield conductor. Both conductors are presently considered to be perfectly electrically conducting.

The first problem that we considered for the gamma radiation effects is for a coaxial cable. We obtained EM wave propagation for gamma ray illumination about the axial mid-point of a two-dielectric coaxial cable model with a step pulse in time, with a strong Gaussian distribution in the axial direction and gamma attenuation in the negative radial direction.

Figure 1 is a surface plot of the E-field generated by the gamma near the axial midpoint of the two-dielectric coaxial cable at 1 x 10^{-16} s. The cable is 0.531 m long and 0.0568 cm at the outer dielectric radius. The discontinuity in the peak E_r indicates the radial discontinuity in the dielectric constant. Figure 2 is a surface plot of E_r at 1.5 x 10^{-9} s. Two wave peaks at r = 0.0346 cm are seen moving toward the ends of the coaxial cable at z = 0 and z = 0.531 m. The peak E_r occurs near dielectric interface at the axial midpoint.

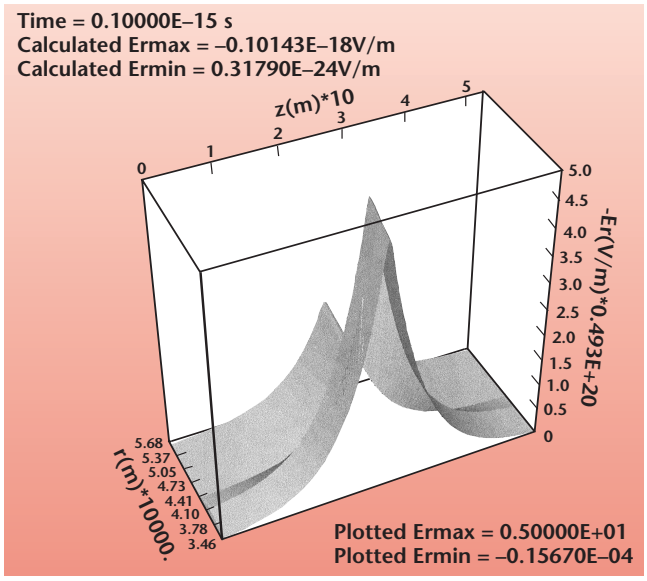

Figure 1. *Surface plot of the E_r field generated by the gamma near the axial midpoint of the two-dielectric coaxial cable at 1 x 10^{-16} s.*

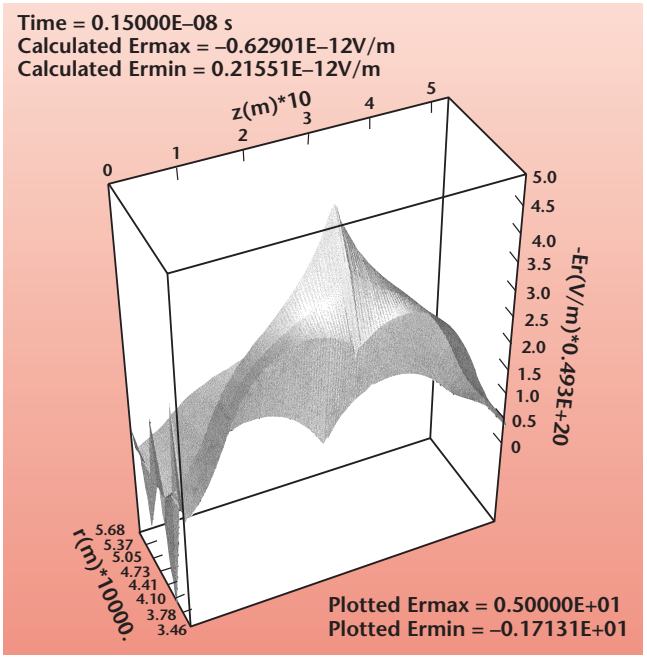

Figure 2. *Surface plot of the E_r of the two-dielectric coaxial cable at 1.5 x 10^{-9} s.*

Center for Microtechnology

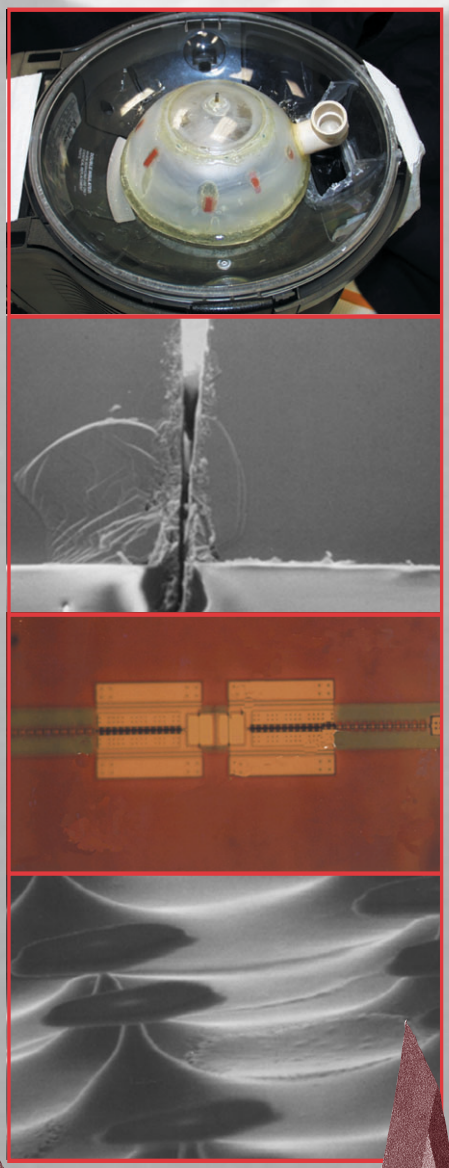

Detector for High-Energy-Density and Inertial Confinement Fusion Diagnostics

J. D. Morse, M. Pocha, J. Kotovsky, E. Behymer, C. Yu, T. Perry; K. Lui (Bechtel, Nevada)

Advanced diagnostics for HED and ICF applications will require detectors sensitive to the 10- to 20-KeV x-ray spectrum. These detectors will make up an imaging array, which is then coupled to a streak camera. We are using the concept of a solid-state x-ray detector, with a field-emission cathode to convert electron-hole pairs generated by the absorbed x rays into electrons emitted into vacuum. Our focus this year has been the suitable detector design and material, demonstration of field emission on the basic platform, and process integration of the field-emission cathode and x-ray detector into this common platform.

A GaAs PIN photodiode has been identified as the nominal solid-state device to achieve both high sensitivity to x-ray photons in the 10- to 20-KeV range, and the temporal resolution requirements for monitoring the time response with acceptable signal-to-noise ratio.

The initial detectors fabricated were PIN photodiodes having a low-doped p layer approximately 4 µm thick. This thickness represents about 8% internal quantum efficiency for the x-ray photon energy of interest for HED and ICF applications. The final design would increase the thickness to match the desired time response (~10 ps/µm): ~50 µm. Additional designs will lead toward gated FEAs for further control of linearity and dynamic range.

One key element in the x-ray cathode design is a high-voltage PIN diode design having low leakage current under reverse bias with no photon signal. For effective photodiode and photon-to-electron conversion, a high electric field must be sustained in the depletion region of the GaAs diode between the N+ and P+ contact electrodes. This is critically dependent on diode fabrication design, to maintain uniform electric field distribution as the charge is depleted in the P-region. In the first run, a planar diode design was fabricated, with the result of very low reverse-breakdown voltage, and high dark current under reverse bias. The subsequent design incorporated a mesa design in the n+ electrode, as illustrated in Fig. 1.

To characterize the electron emission, devices having 200-nm N+ electrode layers were mounted in an ultra-high-vacuum test system at Bechtel, Nevada. A first set of FEA tips formed in an N+ GaAs surface is being tested with a high voltage anode probe. Further tests are underway.

GaAs field-emission cathodes are also being developed to provide another means to convert x-ray photon current into an electron source that can be coupled to an imaging streak camera. Controlled isotropic etching of GaAs is being developed to form uniform arrays of nm-diameter tips (Fig. 2). Subsequent testing in a high-vacuum probe station exhibits >10 µA of field-emission current at 3-kV anode voltage.

These results are a first for LLNL's Microtechnology Center, and further process development will improve the uniformity of the FEAs, and possibly explore low-work-function coatings to improve the emission current.

Next-generation device designs will integrate a gate structure with the field-emission cathode. This will provide an independent electrode to bias the cathode in the linear regime of the field-emission curve, which will, in effect, provide higher linearity and dynamic range.

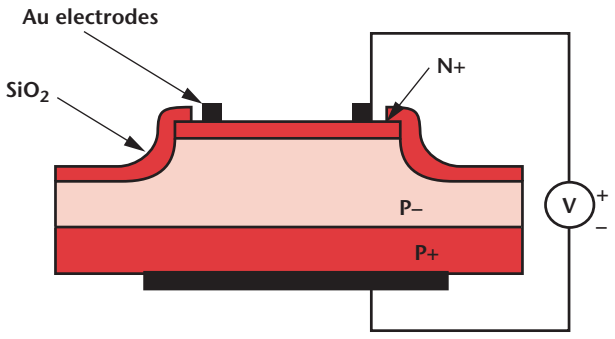

Figure 1. *Cross-sectional schematic of GaAs PIN diode structure with N+ mesa fabrication design.*

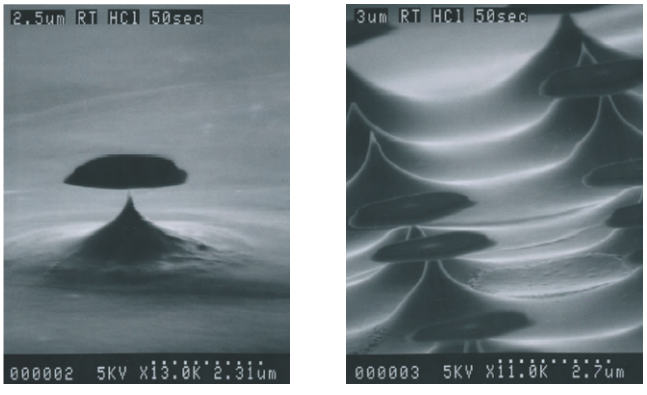

Figure 2. *Ungated GaAs field-emission cathode arrays.*

Fiber Optic Accelerometer

S. Swierkowski, J. Trevino, G. Jacobson, C. McConaghy, A. Throop, C. L. Lee

Miniature accelerometers are broadly useful instrumentation sensors for mechanical systems. Weapons testing needs very small, preferably passive, accelerometers. We have built a 200-g accelerometer, with a footprint of just 4.5 mm x 7 mm, using a fiber optic interferometer readout of proof mass position.

Most commercial devices are large and have electrical power and signal readout; often this is a small signal and the electrical wiring is a hazard in explosive environments.

We have built a 3.5-kHz resonant frequency, 200-g MEMS sensor, using bulk wafer RIE machining, and epoxy packaging. A wafer yield is about 100 parts. The proof mass moves laterally and forms the moving mirror of a Fabry-Perot cavity. The fixed mirror is provided by an optical fiber that is packaged into the 150-µm-square groove in a 400-µm-thick wafer, shown on the right in Fig. 1.

Figure 2 shows the silicon part, epoxy bonded between two glass plates.

The heart of any accelerometer is the proof mass and spring combination (Fig. 3); the resonant frequency determines the bandwidth and the sensitivity of the accelerometer. By adjusting the tether spring thickness a few micrometers with processing, the response of this device can be tuned from about 10 g to 1000 g. Initial testing shows the DC response to be 37 nm/g with 23-µm tethers. A more robust fusion bonded package is desirable for temperature range and stability.

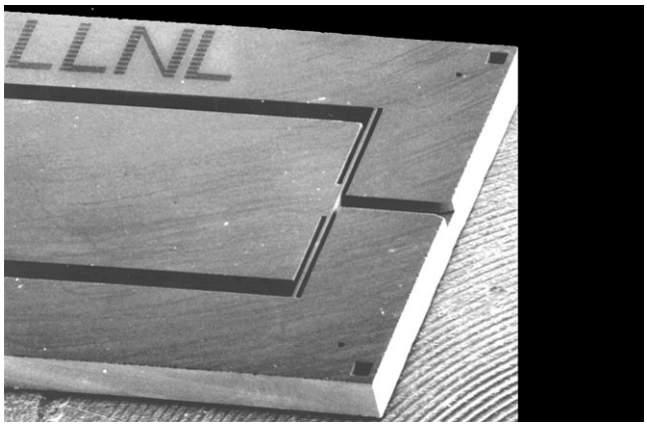

Figure 1. *Key component: the silicon proof mass, with 2 of 4 tethers, 1 mm long, in the frame shown.*

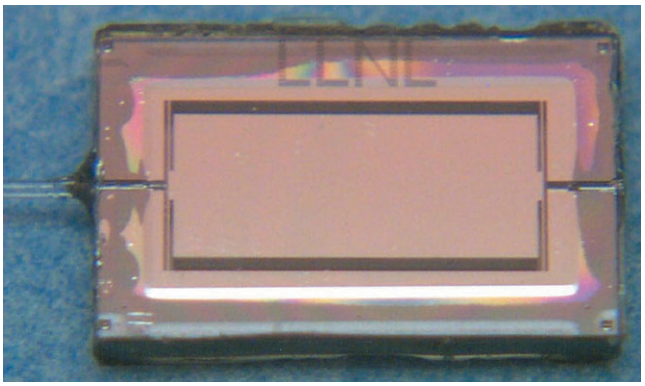

Figure 2. *Silicon part, epoxy bonded between two glass plases, with a multimode optical fiber, to complete the 200-g, 4.5-mm-x-7-mm MEMS accelerometer sensor.*

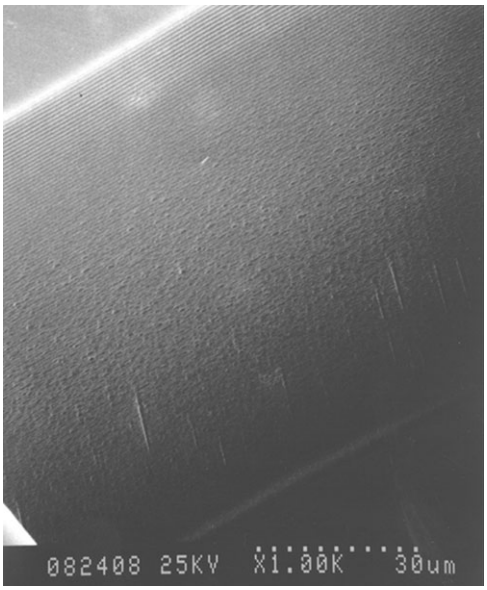

Figure 3. *Silicon proof mass mirror, RIE etched sidewall, smooth enough for the white light interferometer and multimode fiber readout.*

Fiber-Optic MEMS Interconnect and Mirror

S. Swierkowski, J. Kotovsky

During the past year, a 200-g accelerometer has been demonstrated that includes several design, processing, and packaging changes to improve the mechanical robustness, ease of fabrication, and temperature stability. Additionally, 45° mirrors for right-angle optical interconnects have been fabricated and are now in testing.

Significant effort has produced success in packaging the accelerometer in ananodically-bonded high-temperature fusion package. Previous generation sensors were packaged by gluing the three-part, glass-silicon-glass sandwich together. This technique was difficult to fabricate reliably and lacked mechanical robustness. The process was improved by replacing the glue with a fusion bond that hermetically sealed the MEMS device, while maintaining 50-µm alignment and minimizing stress in the proof mass beams. This seal and the internal MEMS components, without the fiber insert (see figure), have been immersion-tested successfully from –196 °C liquid nitrogen to +100 °C water.

Recent versions of the device have attached the optical fiber to the MEMS with a UV-curing adhesive. Control against the adhesive wicking into the sensitive MEMS cavity is achieved through overflow channels, designed for the purpose. Although successful, the fiber attachment process with glue is difficult and tedious because it requires delicate alignment and timing. More importantly, the final positional stability of the fiber is subject to small, slow variations caused by curing and temperature-dependent adhesive properties. To improve this process, a fiber attachment technique with solder has been designed into the next generation of sensors. The attachment technique also includes a self-limiting fiber stop for easier alignment. The new design will offer a more robust and thermally-stable junction of fiber and MEMS. Initial tests with a low-temperature (154 °C) 80 In/15 Pb/5 Ag solder show very strong adhesion to bare glass, polyimide coated fibers, and to Ti/Ni/Au contact pads on silicon.

Several geometry changes have been implemented in the MEMS to improve its performance and to accommodate a wider range of applications. Success of current prototypes has generated interest in versions of the device of varied sensitivity. Continued work optimizes design and processing of the device to improve its mechanical robustness. An improved two-stage plasma etch has been implemented to produce precise mass and spring geometries with much smoother sidewalls for improved mechanical and optical performance. The design has been improved to avoid breakage from shock loading.

Design work for 20-g, 200-g, and 2000-g devices has been completed and is currently in processing. Finally, the sensor size has been reduced by 50% to decrease the cost of manufacture of the device and to improve its function.

A right-angle optical bend has been designed and fabricated. The optical turn is accomplished with a 45° silicon mirror, formed with a plasma-etching process. A package similar to the accelerometer has been produced to pigtail fibers or alternate MOEMS devices to the part. The parts are currently being characterized to determine the coupling loss.

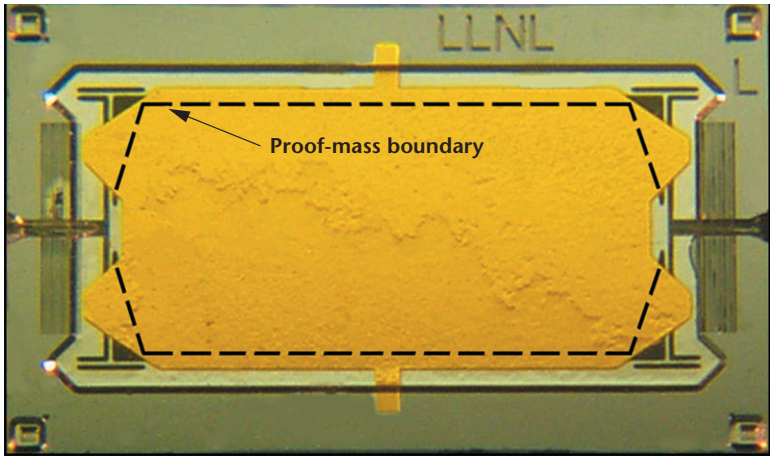

Fusion-bonded 200-g accelerometer with improved bonding, process yield, ruggedness, temperature range, and hermeticity.

Fast-Fiber Multiplexer

M. Pocha, C. McConaghy, T. Bond, T. Lavietes

High-fidelity flight tests required by the Stockpile Stewardship mission demand miniature, minimally invasive sensors to go inside weapons. We have established the Microsensors Program for miniature optical readout sensors. Several different sensors are being developed to measure variables such as acceleration, strain, displacement, pressure, and temperature at various locations within test assemblies.

Sensor measurement techniques are often interferometric, requiring maintenance of coherency of the analog signal between the measurement instrument and the sensor. Space constraints make it almost impossible to bring a bundle of fibers out of a high fidelity assembly. Multiplexing the measurement system is essential to the success of the Microsensor Program.

We have made significant progress, detailed elsewhere. This report summarizes our activities and results for FY02.

We learned that there are a number of applications for compact sensor systems with differing requirements and constraints, which complicates our problem. However, we have identified several potential solutions and are narrowing these down to one or two final candidates. We have also implemented a prototype of one measurement scheme — "In-Phase-and-Quadrature (I/Q)" — that is scalable to smaller size and also allows for multiplexing at least a few sensors in one measurement module.

It became clear that, to meet all requirements, the systems would have to operate within a very severe environment. For example, the full temperature range for weapons grade systems is –65°F to +165°F. Also, components used in many flight tests need to withstand accelerations up to 200 g. There are actually two kinds of measurements that need to be made — absolute and relative; and two ranges of data capture speeds — <100 Hz/channel for most of the parameters being measured (temperature, pressure, strain), and >5 kHz/channel for others (acceleration, and possibly some gap measurements). These demands, along with the multimode analog bandwidth requirement, place severe constraints on any multiplexing scheme.

We learned from our survey that most commercial effort is going into single-mode switching for the telecommunication industry and is not likely to produce components for our needs in the near future. Commercial multiplexers are lacking bi-directionality, or bandwidth, or the speed required for our applications. We continue to follow developments in this fast changing field, but will most likely have to develop our own multiplexing technology.

Of the several technologies that could be used for multiplexing, (MEMS mirrors, liquid crystal, bubble switches, electro-optics, thermo-optics, holographic switches, acousto-optics, spinning mirrors, source switching, interferometric switches), we have narrowed our attention to three areas that are most likely to work for our applications — thermo-optics, source switching, and rotating mirrors.

We have collected a large number of papers on thermo-optic and electro-optic switching, some of which discuss multimode operation. If we can design a scheme that allows us to achieve the switching speeds required with multimode operation, then this technology could make very compact switches that would be relatively easy to fabricate.

The prototype I/Q measurement system we designed this year is compatible with a limited degree of multiplexing, using source switching — a separate optical source (*e.g.*, LED) is connected to each sensor, and multiplexing is done by switching the sources on and off. The readout of the signals from all the sensors can be done in a common, single optical path. The required measurement speed can be achieved, and, although our prototype is a relative measurement system, absolute measurement capability is possible.

Spinning mirrors are multi-faceted mirrors that are mounted on high-speed motors and scan a reflected input beam across the face of several output fibers. High-speed, miniature motors are available that can achieve up to 100,000 rpm in about a 1-cm-long package. These are sufficiently fast to spin a multi-faceted mirror at the speeds needed for 5-kHz multiplexing, but further study is needed to see if a compact lens and optical path can be designed to confine the beams sufficiently for fiber-to-fiber free space multiplexing.

While continuing to follow commercial developments, we recommend that our efforts be focused on the three techniques we have identified as the most promising for the Weapons Program requirements. With further study we expect that one or two of these will clearly stand out as the optimal solution(s) to the multiplexing problem.

Fabrication and Testing of High-Stroke Adaptive Optics Actuator

A. Papavasiliou

The purpose of this project was to build and test a high stroke actuator for use in space telescopes. The unique scissors jack design converts small horizontal displacements into large vertical displacements. Our goal was to reduce this approach to practice.

The specific technology to be incorporated is a MEMS-based actuator for deformable mirrors (DMs) that can be used to correct for aberrations in lightweight space telescopes. These telescopes are under increasingly active investigation to substantially lower costs.

A serious concern with lightweight mirror technologies is how to control their optical quality during both fabrication and deployment, and how to maintain the surface quality on orbit with changing gravitational, centrifugal, and thermal loads. A potential method for correcting aberrations in lightweight space telescope optics is to use a DM to cancel the primary mirror aberrations. As on-orbit changes in the primary mirror occur, the shape of the DM can be readjusted to maintain the correction.

Conventional DMs have many drawbacks — they are expensive, heavy, use significant power, have limited stroke, have limitations on the number of actuators, and do not work in cryogenic environments. MEMS-based adaptive optics (AO) has the potential to address all of these issues.

The goal of achieving a high stroke actuator with 50 µm of vertical displacement was to be accomplished by designing beams that buckle out of the plane of the wafer when they are actuated parallel to the plane of the wafer. To do this, a basic design was worked out that was compatible with a conventional fabrication process.

The design included beams with crenellations engineered to force the beam to buckle in the right direction, electrostatic comb actuators, and stabilizing springs. Two different types of actuator were designed, a two-beam actuator and an eight-beam scissors jack-type actuator.

A computer model was created to describe the predicted performance of the devices. That computer model was then used to find optimal designs. The constraints on the optimal design were the specifications of the fabrication process on film thicknesses and minimum feature sizes and spacings. The optimal criterion was to make the displacement vs. voltage curve have as large a stable region as possible while reaching 50 µm at 100 V.

The optimal designs and a number of other variations were laid out and submitted to the foundry service. A post-processing method was developed to use a SU-8 photo-curable epoxy block as an insulating mechanical connector between the two high-potential sides of the actuator. Two different release processes were investigated to allow the fragile polysilicon parts to be released from the silicon dioxide in which they were fabricated without permanently sticking together. An existing critical point dryer was re-certified, and a process was implemented to coat the chips with a hydrophobic self-assembled monolayer, akin to coating the pieces with a monolayer of Teflon.

Our test results are as follows.

Probe actuation

The devices were pushed horizontally by mechanical probes and reliably translated the horizontal motion to a vertical motion. This showed that many aspects of the design do indeed work properly; the beams buckle in the correct direction, not downward and not sideways; and the SU-8 epoxy insulating connector works.

Electrostatic actuation

We were not able to actuate devices as predicted electrostatically. One actuator did move vertically under electrostatic actuation, but not with the expected mechanism.

Thermal actuation

We were able to actuate a thermal actuator (Figs. 1 and 2). Simplified versions of the actuators were fabricated without electrostatic elements. Current was run through the beams of these devices to heat them. The expansion of the beams moved the actuators. Buckling was observed at 8 mW, and displacements of as high as 9 µm were observed at 35 mW.

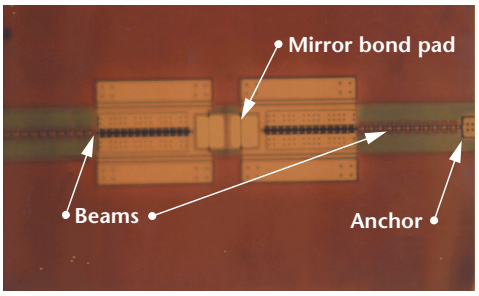

Figure 1. *Photograph of thermal actuator.*

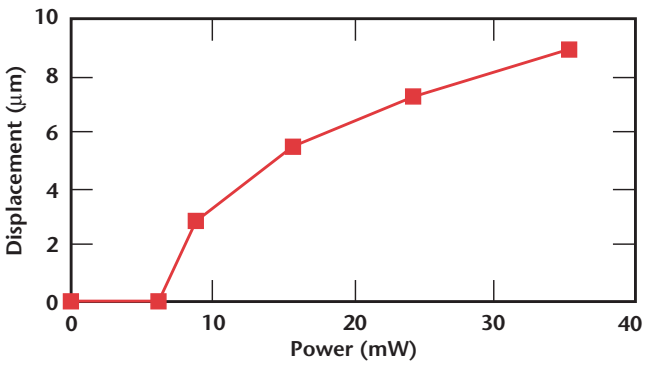

Figure 2. *Plot of thermal actuator displacement data.*

Water Security Microdevices

E. R. Cantwell

The goal of this project was to evaluate new concepts for a device to handle the near-real-time, continuous detection of biological materials in raw water. The acquisition and processing of samples in current technologies present a set of new problems, e.g., biofilms, filtration systems, and low concentrations that can affect human health, when conducted continuously in water. We have developed an in-house base of expertise, such that LLNL now has a credible team for attacking the main problem areas.

Design issues we have dealt with include:

1) continuous feed of water into the system;
2) low concentration of pathogens—the system must sample a large amount of water, and the samples must be concentrated to reduce detection time and increase accuracy;
3) distribution of beads—a bead-based system mitigates the effect of biofouling;
4) contamination threat scenarios.

A system was built to investigate the possibility of using magnetic beads (which would be antibody-coated) to capture pathogens in large volumes of water, then to filter it down to a manageable size. Our five-gallon tank represented an inlet from a lake. Magnetic beads were mixed throughout the volume using a stream of compressed air. We pumped the beads into a series of pipes ranging from 1.25-in. ID to 0.25-in. ID. Magnets were placed external to the pipe to collect the beads.

The hope was to provide enough magnetic force to move the beads to the side of the tube to fractionate the liquid, but invariably beads would accumulate, particularly in areas where discontinuities in the pipe caused eddy flows. The accumulated beads naturally focused the magnetic field, inducing further accumulation. Thus, this technique was more appropriate for capture and release methods of concentration even on this scale.

Magnetic beads are not necessarily attractive for DNA assays, so a large filter capture system was built for polystyrene bead capture. Filters do not return all beads, but they are inexpensive and be easily replaced.

A flow-through dielectrophoresis (DEP) device was being built. Good side-wall electrodes were difficult to fabricate. Experiments indicated that much higher voltage could be used than had been used previously, thereby reducing the restriction on channel width from 25 µm to nearly 500 µm. A larger channel will make the fabrication of side-wall electrodes easier. The advantage to DEP focusing is the elimination of beads.

This project has several sources of funding:

- Funding from the US Bureau of Reclamation to do water security studies of dams and reservoirs.
- New funding from the SFPUC to do the same sort of studies for San Francisco.
- Negotiations between LLNL and LA Metropolitan Water for laboratory methods for detecting biological WMD materials.
- Chem-Bio Nonproliferation Program (CBNP) proposals to DoD that are pending. CBNP is also looking at extending the Advanced Particle Detection System capability to water by adding a new "front-end" that will do extractions from raw water. This work would be dependent on next year's funding, which is unknown at this date.
- New technology-base proposal based on discussions and meetings with the Joint Services Water Monitoring program at Edgewood Chemical and Biological Center, part of the Army's Aberdeen Proving Ground in Maryland.

Although we did not achieve our goal of demonstrating a prototype device, all involved acknowledge that the problems we propose to solve are significant and that we have a head start over many others doing research in this area.

This work has also served to convince NAI and Energy & Environment that water security is an arena in which LLNL can make a difference. NAI has cosponsored several high level speakers to give talks on water security and biological detection, and has verbally supported a technology-base proposal that is an outgrowth of this work. Energy & Environment is nearing the point of announcing their Water "Grand Challenge," and again, water security is likely to play a significant role in this plan, in part due to input on technology from the investigators in this project.

Portable Bioanalysis Instrument with Integrated Sample Preparation and Detection

P. Krulevitch, M. Bennett, J. Dzenitis

We are designing microfabricated systems for preparing biological samples for immunological and genetic assays. We investigated alternative miniature and robust detection strategies that can be integrated with our sample preparation modules.

While sample preparation is one element of a portable bioanalysis instrument, new detection methods must also be designed. The accepted techniques – flow cytometry and the polymerase chain reaction (PCR) – suffer from several drawbacks that prevent miniaturization and portability.

Flow cytometers, which are large, delicate, and alignment-sensitive, use large volumes of sheathing fluid to precisely position particles for individual confocal detection. Instrumentation for PCR-based DNA amplification and detection can be miniaturized, but automated sample handling and the ability to run multiplexed assays remain elusive.

In this project, we investigated alternative miniature and robust detection strategies that can be integrated with our sample preparation modules to create portable bio-detection instrumentation for counter biowarfare and biomedical applications. M. Bennett, from LLNL's Biology and Biotechnology Research Program, worked closely with our microfabrication group to quantify the effectiveness of sample preparation and detection methods.

We investigated the use of microchip-based capillary electrophoresis (CE) for DNA sequence detection. Real-time fluorescence monitoring of PCR, the current approach used by LLNL for rapid, DNA-based biodetection in the field, is limited in its ability to screen for multiple agents simultaneously.

In our work, PCR is used to amplify specific sequences of interest if they are present, and CE is then used to detect and identify the amplicons by size. This approach lends itself to both multiplexing and miniaturization. We ran multiplexed PCR with new fluorescently labeled primers and demonstrated amplification of different bacterial bio-warfare surrogates by running standard agarose gels. To demonstrate our ability to run this assay in a capillary/microchannel format, we performed separations using a commercial CE sequencer (ABI Prism 310) and saw that we could identify the amplicons in the resulting fluorescent electropherogram (see figure).

Recently, we have been working with a microchip-based CE platform that, with the incorporation of compact optics, electronics, power, and packaging, has the potential for miniaturization. We have been successful in showing signal differences between a singleplex PCR solution with and without amplification, and are working toward a demonstration of multiplex detection and identification.

DNA purification and concentration using microfabricated chips was investigated as a sample-preparation front-end for microchip capillary electrophoresis. *Erwinia herbicola* DNA samples were mixed with a chaotropic salt solution (pH 5.3), which lysed the bacterial cells, and the resulting solution was applied to the DNA extraction chip. This solution contained both the nucleic acids in which we were interested, along with detritus from the lysing process.The components of the lysing solution that were trapped on the purification chip were washed with 70% EtOH and air-dried. Ten mM Tris (pH 8.5) was applied, the devices were warmed to 72 °C, and this concentrated, purified sample was eluted as single 20-μl drops. This procedure was established elsewhere, to separate, purify, and concentrate the nucleic acids as preparation for PCR. Real time PCR was then performed to determine capture and concentration efficiency. Results showed a 12-fold concentration using the chip-based pre-concentration. A design for a miniature, automated instrument for performing the DNA concentration and purification process was submitted for funding to the DOE Chem-Bio Nonproliferation Program. The work performed through this project seeded several new efforts aimed at portable bio-detection instrumentation. Our concept for a fieldable microfluidic system for nanoparticle-based bioassays was submitted to the National Cancer Institute. Our proposal to develop a multiplex portable bioanalysis instrument for detecting biological warfare agents was accepted as a new LDRD ER FY03 project. We submitted a FY03 proposal with Sandia National Laboratory to DOE for the BioBriefcase, a portable bioagent detector.

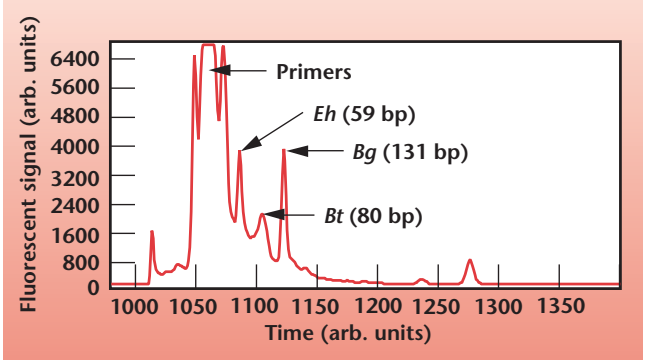

Electropherogram of a PCR solution, showing identification of three pathogen surrogates (Erwinia herbicola (Eh), Bacillus thuringiensis (Bt), and Bacillus globigii (Bg)).

Three-Dimensional Microlithography System (3D-MLS)

V. Malba, A. F. Bernhardt, L. Evans

We have initiated the upgrade of an existing Laser Pantography system by installing new motion control hardware and software, and interconnecting them with an existing set of precision stages.

A decade ago, LLNL's Microelectronics Program developed a unique quasi-3-D laser direct writing tool, called Laser Pantography, to fabricate metal interconnects on multichip modules. The program also developed a suite of processes for deposition, etching, and lithographic patterning of 3-D surfaces. In addition to the multichip modules for which the system was created, this tool and the associated processes allowed the program to make unique millimeter- and sub-millimeter-scale parts such as RF inductors, diamond anvils with electrode structures, NMR microcoils, micromotor stators, and magnetic relays.

The Laser Pantography tool had fundamental limitations, however, and because of the original mulitchip module application and limitations in the CAD/CAM systems of the time, the configuration could not support out-of-plane patterns more complicated than straight lines of fixed length parallel to the z-axis. Also, the workstation was out-of-date, using an operating system no longer supported.

Another limitation was that motors could not be started at exactly the same time. This meant that diagonal lines in the x-y plane, to use a simple example, were executed as stair steps. A modern motor control system would allow simultaneous movement of multiple stages so that smooth diagonals, ovals, and other shapes could be drawn.

The limitations have been addressed in this TechBase project.

We have begun the assembly of a modern, fully 3-D, sub-μm-accuracy motion system driven by a commercial CAD/CAM package. This 3-D Microlithography System (3D MLS) functions as a five-axis milling machine with a focused laser as the "cutting tool."

With improvements in the optical system, the "cut size" can be 1 µm. The upgrade of the 3D MLS will involve the replacement of the original custom hardware and software with a standard motion control hardware package, together with commercially available 3-D CAD/CAM software, which is licensed to LLNL. The new software will output standard G-code, which the new hardware will be able to execute in the same fashion as a five-axis CNC milling machine.

A true 3-D Microlithography System will be the final product. It will be a unique capability, and is expected to generate considerable interest and funding. It will dramatically increase the 3-D patterning capability of the present system, making it more applicable to surfaces and structures, which cannot now be patterned. As technology demonstrations, we will pattern helices on < 400-µm-diameter cylindrical surfaces (for NMR and MRI applications) and simple periodic structures on spherical or elliptical surfaces of radius of order 1 mm (for NIF physics targets).

In FY-02 we installed new motion-control hardware, including a Pentium computer, a Delta Tau microprocessor control card (PMAC card), motor amplifiers and motor controllers for up to eight degrees of freedom. A 3-D, CAD/CAM package has been installed, and initial handshaking software linking it to the motion control hardware is in place. X, y and z translation stages (existing equipment) have been installed and wired. Requirements for high-precision theta motion in x and z axes have been ascertained, and stages with sufficient speed and precision have been identified for purchase. A high-power UV argon-ion laser was procured internally and is being refurbished. An optical design emphasizing a small focal spot, which can be expanded for rapid patterning of large areas, has been completed, and the required components identified. Advances in all-quartz microscope objectives now permit deep sub-µm resolution at the UV wavelengths we use.

In the coming year we will complete the motion system with two rotation stages. We will also complete a system motion mapping capability for obtaining high-accuracy motion and we will characterize system performance. We will assemble a new optical system (objectives, tube lenses) designed for versatility as well as minimum feature size under various motions.

A kinematic mounting scheme is envisioned for smaller parts and for rigid parts. This scheme will be our focus in the third year of the TechBase project.

Gallium-Arsenide Cutting Techniques

G. Cooper, G. Jacobson, S. Oberhelman, M. Shirk, T. Hauck, N. Raley

High-voltage components, including photovoltaic circuits, invariably have to contend with electrical leakage and arcing through gases, along surfaces, and through solids. Recent test results on arrays of photocells fabricated as monolithic, integrated circuits have revealed the presence of undesirable currents flowing through the solid substrate from areas of high potential to areas of low potential. The devices were designed and fabricated with special layers between the photocells and the underlying substrate to reduce or prevent such currents from flowing in the substrate. The goal of this project was to investigate techniques to isolate the high- and low-potential areas of the array from each other while parallel work is done to analyze the mechanisms of the current leakage and identify integrated solutions.

One of the problems inherent in the design of high-efficiency photocells is the substrate requirement. Gallium arsenide (GaAs) is the semiconductor of choice for producing the most electrical power from a given optical collection area and fixed illumination. Unfortunately, as a substrate, GaAs is not a good insulator.

One technique to keep electrical charges from flowing through the substrate is to physically partition the substrate into isolated islands. Because there will be many small islands produced in a high-voltage array, individual handling of each island should be avoided.

The isolation concept examined by this work is to permanently bond the GaAs substrate (upon which the photovoltaic array is fabricated) to an appropriate insulating substrate. GaAs material is removed between the islands all the way down to the insulating substrate. The islands thus become electrically isolated from each other by the channels, but the array may still be handled as a single component.

Two existing processes at LLNL were examined for functionality, repeatability, and simplicity: saw cutting and femtosecond (fs) laser ablation. The common issues are: minimal achievable width of cut, lateral extent of collateral damage, redeposition of material on wafer surface, mechanical retention of separated islands, cracking, and complete removal of the GaAs material between islands.

Samples for each technique were prepared by adhesively bonding 20-mm -x-20-mm pieces of 350-µm-thick GaAs to 1-mm-thick pieces of glass. Permabond 910 cyanoacrylate was used for the initial tests because of past favorable experience and ease of handling.

Sawing, using an older model semiconductor wafer saw that has been adapted for use with hazardous materials, has demonstrated promising results. Of the available blades, the 0.8-mil thickness with 4- to 6-µm grit appears to produce a cut of 90-µm width, including minimal chipping (Fig. 1).

Paradoxically, the 0.6-mm-width blade produces more chipping and a more extended damage width. Parallel cuts at a pitch of 500 µm did result in debonding of the GaAs island between the cuts. This was probably a result of mechanical vibrations and the crystalline nature of the Permabond adhesive. Samples were prepared using an alternative UV curing adhesive, but have not yet been cut with the wafer saw.

Removing material with a fs pulsed laser has also produced favorable results. The laser used for these experiments produces 150-fs-width pulses at an energy between 25 µJ and 250 µJ per pulse, and a repetition rate of 1000 pulses/s at a wavelength of 820 nm. The beam is focused to a spot size of 45-µm diameter on the GaAs surface inside of a vacuum chamber. The beam is rastered back and forth across the channel that is to be removed between the islands, removing a thin layer of GaAs with each pass. Figure 2 shows a magnified view of an 80-µm-wide channel using optimized cutting parameters. Complete removal of the GaAs in the channel has been achieved with minimal redeposition. We have not seen any debonding of GaAs between channels using this technique.

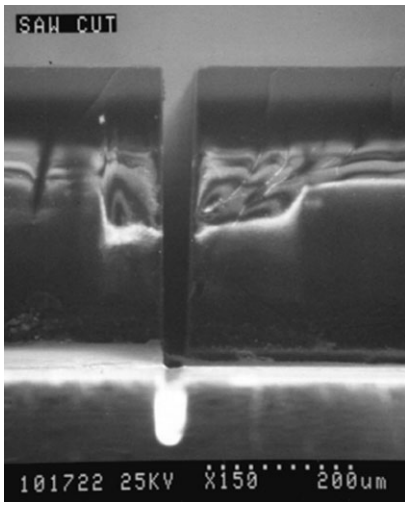

Figure 1. *SEM micrograph of profile of saw-cut channel through GaAs substrate into glass plate below.*

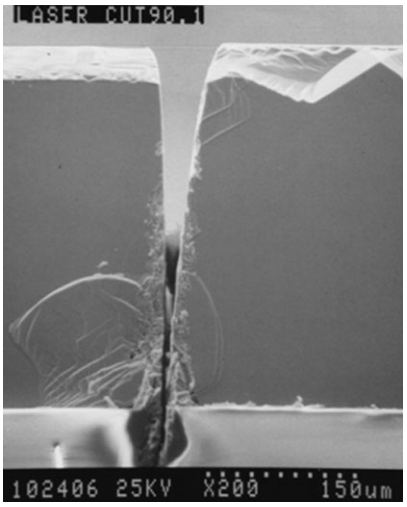

Figure 2. *SEM micrograph of profile of laser-cut channel through GaAs substrate into glass plate below.*

Nucleic Acid Sample Preparation Methods

K. Ness, S. Lehew

The objective of this work is to demonstrate rapid and effective extraction and concentration of DNA from solution using a micromachined high-surface-area silicon chip.

In our approach (Fig. 1) we replace the glass beads in the traditional "Boom" purification method with an array of silicon micro-pillars. The MEMS-based DNA pillar chip structure offers a high surface area (~25-fold increase); a low liquid volume (~2 μl); integrated thermal control; and reproducible fluid flow fields to provide efficient capture and release of DNA in a flow-through system.

Results show the DNA pillar chip is able to concentrate and purify DNA in about 10 min.

Figure 2 displays the results from real-time PCR used to quantify the DNA pillar chip performance. Over 1000-fold increase in concentration and removal of PCR inhibitors from the sample are seen with the pillar chip.

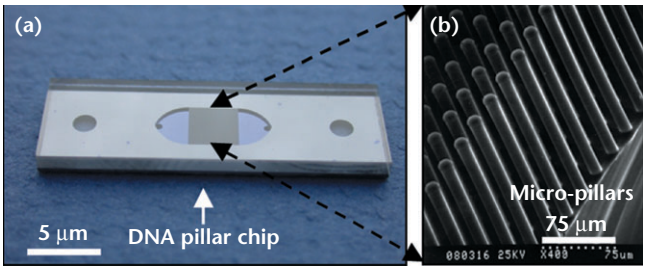

Figure 1. *(a) DNA pillar chip: array of 30,000 micro-pillars (gray region in center of chip); (b) SEM of micro-pillars (diameter x height : 5 µm x 225 µm).*

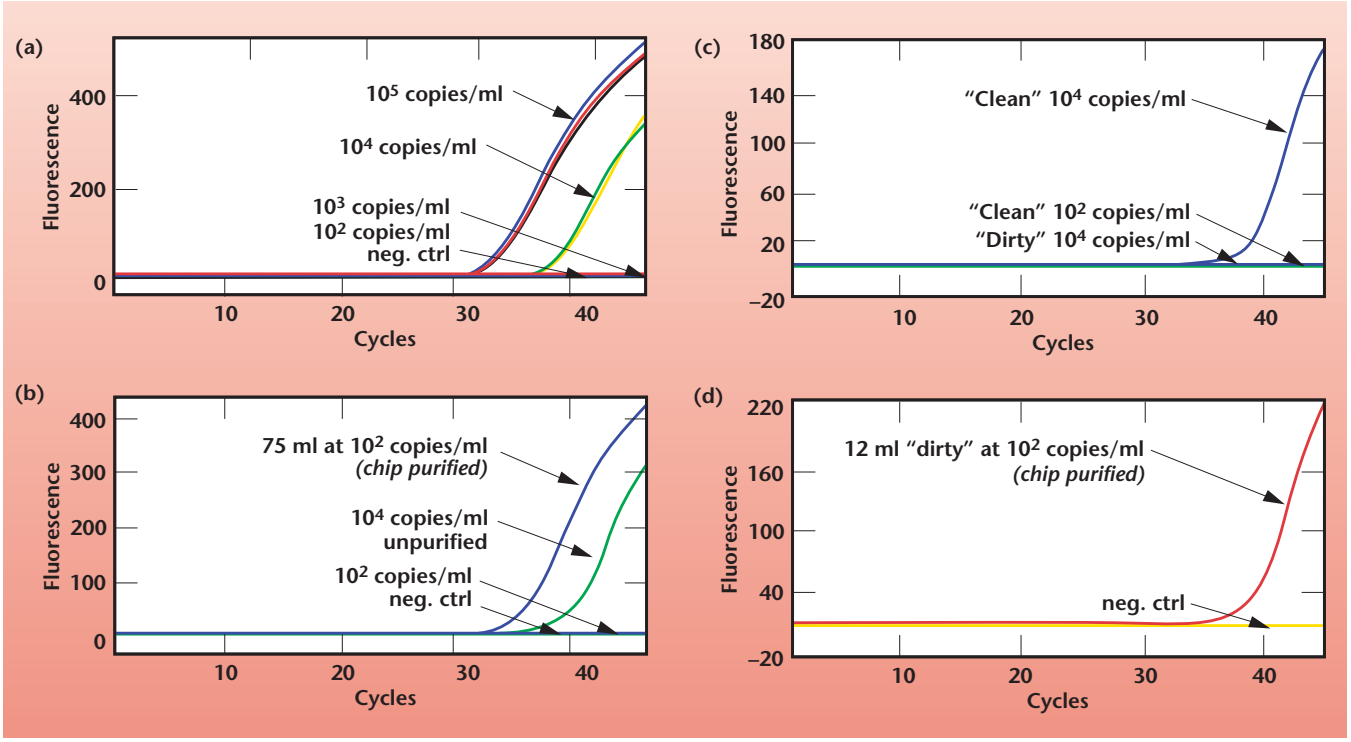

Figure 2. *(a) Standard taqman curves for Francisella tularensis: starting samples 10^2 – 10^5 DNA copies/ml; (b) 1000-fold concentration: 10^2 DNA copies/ml concentrated to 10^5 DNA copies/ml using large volumes (75 ml); (c) PCR inhibition studies demonstrating "dirty" water sample is inhibitory in nature at a concentration of 10^4 DNA copies/ml; (d) extraction of DNA from "dirty" water sample showing purification using the DNA pillar chip.*

Miniature Aerosol Collector

D. Masquelier

The objective of our experiments was to evaluate the physical particle collection efficiency of our prototype aerosol collector. The design was evaluated at a slightly larger scale than the ultimate construction, but it allowed the concept to be thoroughly explored and any challenges to be examined.

The first step in any system for detection and characterization of biological agents is a sample collector. This can take on the simple form of a cotton swab for solid surfaces, or as in the case of airborne pathogens, an aerosol sample collector to collect and concentrate airborne particulate onto a filter medium, or into a liquid sample volume for subsequent preparation and analysis.

An aerosol sampler is the most appropriate for continuous monitoring scenarios, where repeated swabbing of settled particles is impractical. Most commercial samplers now available for field use are large, power-consuming, and produce collected sample into large volumes of liquid, typically >30 mL. Emerging miniature detection systems analyze much smaller sample volumes, typically <250 µL. When using the currently available air samplers, the sample volume must be "sub-sampled," effectively diluting the sample, resulting in a loss of sensitivity of detection.

This project explored a new concept to collect particulate at a relatively high air-flow rate, and yet designed so that the resultant delivered liquid volume would be only 200 µL or less. This would address the problem of dilution because of sub-sampling. The size, weight, and low-power specifications of this aerosol sampler would ultimately need to closely match the current state of the art in pathogen detection systems, which would greatly ease the deployment in remote locations.

We have tested an alpha prototype of a working collector. Figure 1 shows the assembled collector "piggy-backed" onto a modified vacuum cleaner that served as an ideal test-bed fixture and an airflow source.

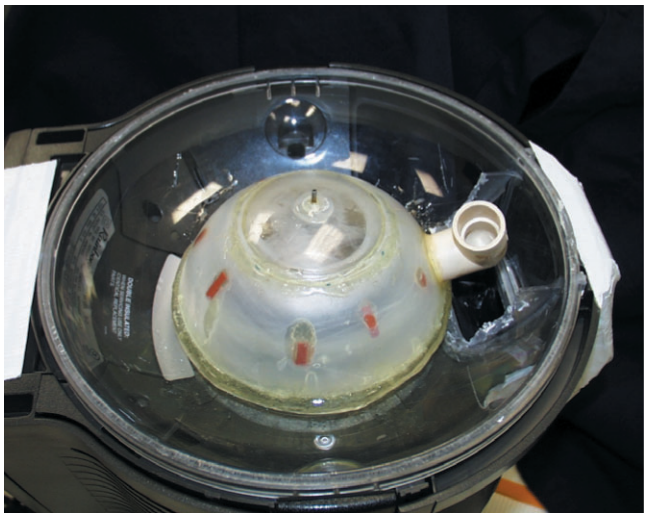

Figure 1. *Prototype of a working collector.*

The test system for the determination of the particle collection efficiency is shown schematically in Fig. 2. In several of the experiments an optical particle counter was used in parallel to the Aerosizer (not shown). Using the particle size distribution data measured upstream and downstream of the collector, the collection efficiency was determined by:

Overall Collection Efficiency = $(1 - C_{DOWN}/C_{UP}) \times 100\%$

Typical experimental results (Fig. 3) measured collection efficiencies between 35 to >95% for particulate sizes between 0.5 to 1.5 µm into liquid volumes of 2 mL, at airflow rates up to 275 L/min.

A "path forward" plan has been initiated to continue this effort and scale down to the final dimensions. A patent application has been submitted based on this work.

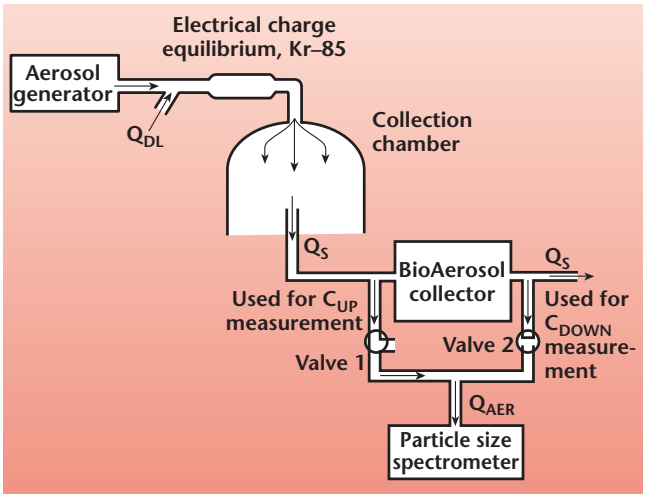

Figure 2. *Test system for the determination of the particle collection efficiency.*

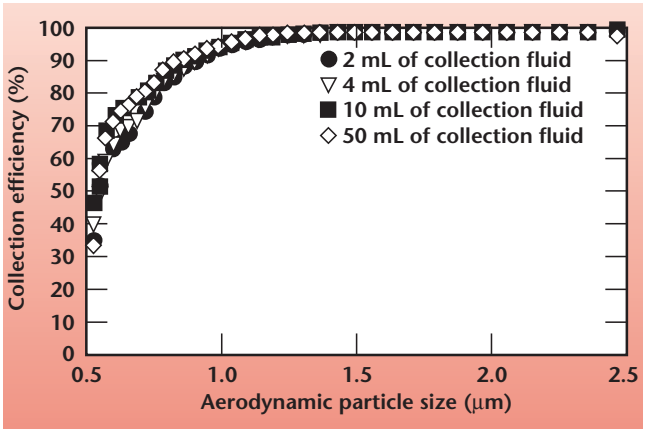

Figure 3. *Overall collection efficiency when collecting polydispersed oleic acid particles at 275 L/min.*

Center for Nondestructive Characterization

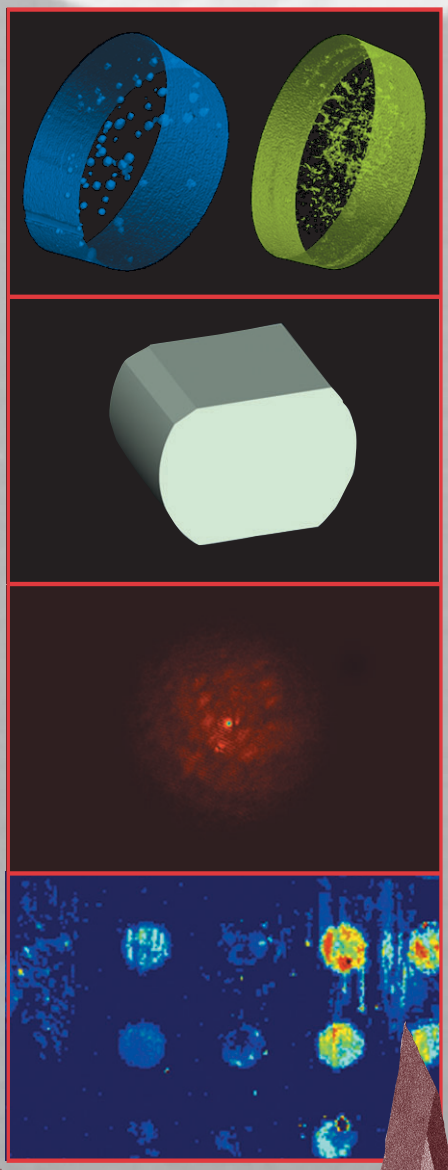

Feldkamp X-Ray Tomographic Reconstruction Algorithm on a Distributed Computer System

H. Jones, D. Barker, M. Kartz, P. Roberson, P. Schaich, Y.-M. Wang

A parallel Feldkamp tomographic reconstruction code is needed at LLNL to reconstruct CT volumes of unprecedented scale, varying from 2k x 2k x 2k to 8k x 8k x 8k (32 GB to 2048 GB). This follows the trend in CT detector technology that ranges from 3k x 2k (current) to 8k x 8k pixels (near future). This implementation encompasses a small segment of a much larger infrastructure requirement to deal with enormous NDE volume data sets, including postprocessing and visualization. This project was successful at developing a foundation for the methodology and techniques used to port an existing code into a parallel execution framework.

A portion of this project evaluated the efficacy of porting and running parallel Feldkamp on existing LLNL ASCI computer resources, while maintaining the design philosophy of low memory footprint, limited internode communication bandwidth, automated resource discovery, a worst-case execution time of 24 h maintained across problem sizes, and *in-situ* postprocessing analysis.

An existing LLNL NDE cone-beam tomographic code was modified to port easily to many parallel architectures, including Linux-PC, Compaq Clusters (GPS and TC2K), and ASCI Blue. Internode communications are MPI-based. Code additions include Node/Memory resource discovery, modified File I/O to accommodate NFS or GFS (networked file systems), distributed reconstruction volume and I/O, and a communication mechanism to interchange projections (the input data set).

The first phase was concerned with feasibility studies on parallelizing the Feldkamp (fkrecl) and Convolution Back Projection (CBP) NDE codes. A small PC-based cluster was put together for the initial implementation.

The second phase was to design for low memory footprint and port to LLNL ASCI machines. In addition to the Linux NDE cluster and GPS, the algorithm was successfully exercised on 100 nodes of ASCI TC2K (see figure).

The formula for the Feldkamp, Davis, & Kress (FDK) algorithm may be analyzed for scalability and used to predict execution times as the problem's size and/or number of processors is varied.

The parallel Feldkamp project was successfully implemented and demonstrated to run on a variety of architectures using up to 100 processors. An expanded version of this report includes details on porting issues, example usage on various platforms, and implementation.

Next, the communications scaling should be analyzed when the execution environment involves thousands of processors. *In-situ* postprocessing of the reconstruction volume should also be considered. The inner loop memory access patterns should be analyzed at all levels of the processor memory hierarchy. Also, before a large production effort, a sensitivity analysis should be done on the core numerics over a range of cone angles, sensor characteristics, and acquisition geometry, to better understand the limitations of the algorithm.

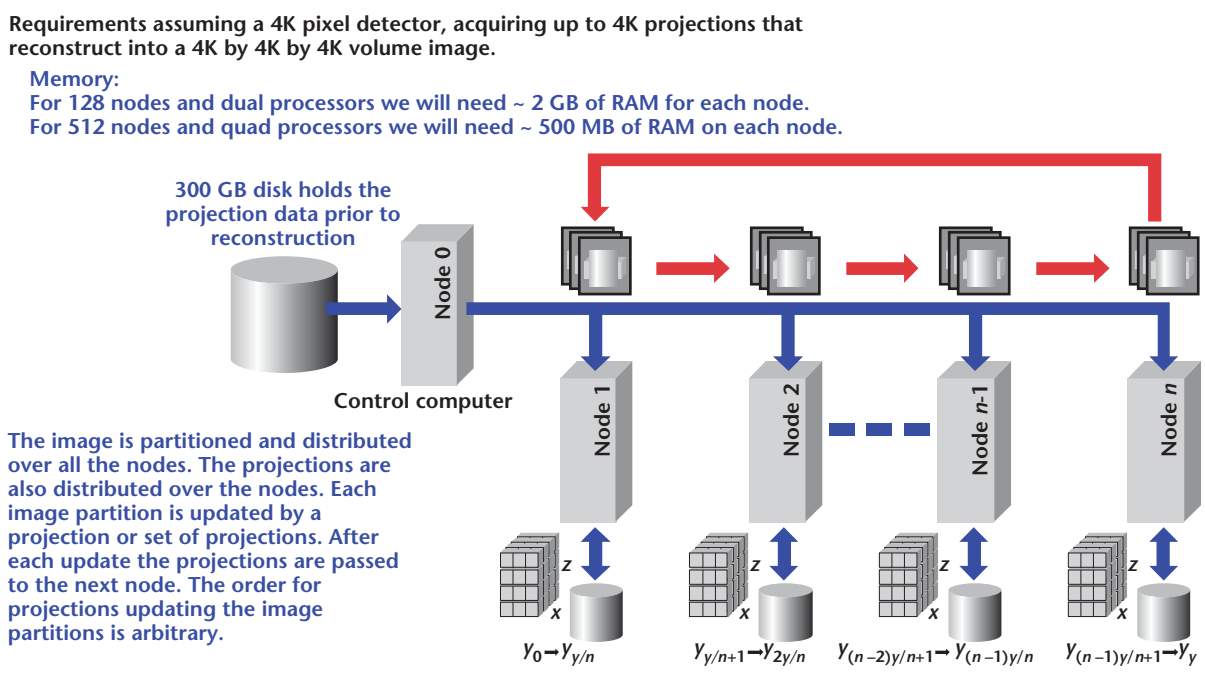

Diagram illustrating data partitioning and flow during reconstruction.

Three-Dimensional Rendering of High-Frequency Ultrasonic Data

G. Thomas, S. Benson

This project is evaluating techniques to render ultrasonic nondestructive evaluation data in three dimensions, thus greatly increasing our ability to interpret data.

Traditional ultrasonic imaging converts amplitude-time information into a 2-D image by time-gating the data and color-coding the amplitude of the signal in the gate. Unfortunately, this approach throws away the depth information. We are capturing all the information in the ultrasonic waveform and processing that information to generate a 3-D image.

Once the image is rendered, it can be manipulated to best display the internal structure of a component. Thus, 3-D rendering of ultrasonic images greatly increases our ability to interpret the data. Our customers gain a better understanding of the results when viewed in three dimensions. Also, our ability to characterize components in three dimensions will support modeling of the parts.

There are two main tasks involved in rendering ultrasonic data in three dimensions. One task is to capture the full ultrasonic data set and store the data in the computer. The other main task is processing the data to render the 3-D image.

Our progress to date includes specifying and acquiring a software package that renders data in three dimensions. We selected a software package called Terra Recon, which generates 3-D images and manipulates the images to improve visualization of internal structure. We learned to operate the software first on a set of x-ray computed tomography data, and then on a set of model-generated ultrasonic data. We do not have real ultrasonic data sets yet.

We are presently configuring the electronics and writing software to acquire real ultrasonic data. Capturing the full ultrasonic waveform entails assembling the instrumentation and writing the computer drivers to digitize the signals. These signals must be correlated to the scanner position at the time of digitization. Once the ultrasonic data has been stored, computer programs convert the large data set of full waveforms into a volumetric display. These conversion codes need to be written.

This display can be manipulated to best show defects and other characteristics of the inspected components. These tasks will be completed next year.

The final product will be a technology to capture and render ultrasonic data so that 3-D characterization can be realized. This information can be incorporated into modeling codes to predict component performance based on as-built characteristics.

Application of Photothermal NDE to Large-Scale Optics

R. Huber, D. Chinn, C. Stolz

A photothermal system built during FY01 was modified to allow faster data acquisition.

The major modifications to the photothermal system involved changing from a camera with slow readout to one with a faster readout, and the specification and incorporation of a long-working-distance microscope lens. The camera readout has been reduced from around 40 s to less than 8 s, a considerable decrease. The new lens allows a field of view ranging from around 200 µm to several mm. Also, major modifications were made to the control software to allow for the new camera, and to complete scans.

The major difficulties encountered during this work dealt with finding and mitigating the various sources of noise in the images. Primary among these noises were fringes that did not subtract out in the images. Several sources for these fringes were found, including two glass covers on the CCD camera.

Another problem is associated with the probe laser that is used to produce the images. Tiny variations in intensity and pointing stability become significant since we are operating with short exposures and very small field of view. Also, the mounting of the probe laser and lens/camera combination was found to give problems—any motion of these components can produce errors, because this technique uses image subtraction. If there is motion between the images to be subtracted, this will add to the noise in the final images and possibly obscure the data.

Even though there were numerous difficulties encountered during the course of the year, significant progress was made and the current system is up and running. The figure shows a bright spot associated with an absorber on a BK7 glass sample. This particular image has tremendous signal-to-noise, but suffers somewhat from the fringes mentioned above.

There is still room for improvement to make this system robust and more sensitive. We are looking into the possibility of removing the cover over the CCD chip to help remove more fringes. However, this will need to be done in a clean room, as the dust in the lab is significant. Also, continued improvements in laser technology may provide a far superior laser that could be used as the probe laser. The system currently works with optics up to 15.24 cm on a side. The system will be modified to work with full-sized (40 cm) optics.

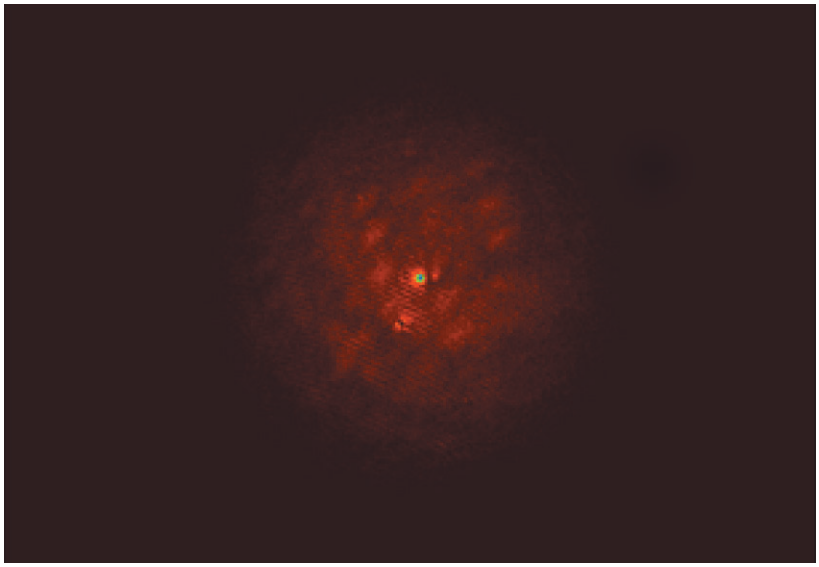

Photothermal image of defect on coated BK7 glass. Field of view is approximately 3 mm X 2 mm.

Time Reversal in a Layered Medium

D. H. Chambers, B. L. Guidry, A. Meyer

We are using a time-reversal array to detect voids between two layers of materials. We have determined the sensitivity of the spectrum of eigenvalues and eigenvectors to the presence of a 4.75-mm-diameter hemispherical bump on the underside of an aluminum slab.

The array is positioned on the surface of a layered material so that acoustic pulses propagate in a direction roughly normal to the layers. These pulses are reflected from both the layer interface and small voids in the interface. The reflected pulses are time-reversed and sent back into the material. This process is iterated until it converges into an eigenstate of the time-reversal operator associated with either a void or the interface.

The eigenstates associated with the interface can be understood in terms of interactions between the array and its image in the interface. We look at the problem of detecting eigenstates associated with voids in the presence of the interface eigenstates.

The figure shows the spectrum of eigenvalues for an aluminum slab with and without a 4.75-mm-diameter hemispherical bump on the underside. There is a slight increase in the magnitude of the first three eigenvalues and a larger decrease in eigenvalues 6, 7, and 8.

A simplified analytical model predicts the increase of low order eigenvalues, but does not do as well for eigenvalues 6, 7, and 8. Though not shown here, the eigenvectors are more sensitive to the presence of the bump than the spectrum of eigenvalues, for both modeling and experiment.

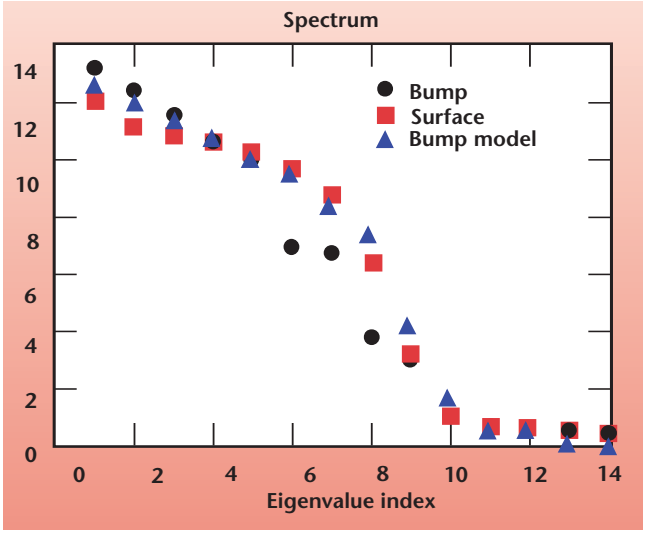

Spectrum of eigenvalues for an aluminum slab with and without a 4.75-mm-diameter hemispherical bump on the underside.

Implementation of a Cone-Beam Reconstruction Algorithm

Y.-M. Wang, P. Roberson

The objective of this project was to evaluate and implement an efficient cone-beam reconstruction algorithm that is capable of reconstructing the full detector view of an object, without distortion of image due to the cone-beam effects.

A CCAT system for a large variety of objects has been developed at the Center for Nondestructive Characterization. CCAT is a micro-focus x-ray source coupled to an amorphous silicon flat-panel detector, used to acquire digital radiography (DR) and CT data. The CCAT system has a large detector area and a small source-to-detector distance, creating an extremely high cone angle from the x-ray source.

CCAT will require the implementation of a cone-beam reconstruction algorithm if we want to take advantage of the full detector area without distortion caused by the large cone angle. The CCAT system will require an exact 3-D reconstruction algorithm capable of reconstructing a large cone angle of 15° to 20°. Exact cone-beam algorithms are relatively new and are only recently maturing to the point where they are becoming a viable solution.

There are a number of these algorithms in existence today, including one that is being developed at LLNL, called LCONE_CCG. The practical obstacle for applying an exact reconstruction algorithm in the CCAT system is the computational complexity of the algorithm, which is on the order of N^5 in most of the cases.

During the past year, an intensive review has been conducted on a variety of reconstruction algorithms for the cone-beam configurations. The emphasis has been concentrated on the practical approximation algorithms that can be implemented in our CCAT system.

With the consideration of the computational complexity and implementation of the potential algorithms, we finally came to a conclusion that the best choice is an algorithm that is incorporated with the use of the Feldkamp algorithm and has scan geometry compatible with our CCAT system.

One reason for the use of the Feldkamp algorithm as an intermediate stage is that we have invested a considerable resource in the implementation of the algorithm to our Linux cluster. We have also made the parallel version available in both the local Linux cluster and LLNL's supercomputers (see report by H. Jones, *et al.*, in this document).

Finally, one algorithm that satisfies our requirement is Lin's algorithm. The reconstruction scheme can be summarized as follows:

1) apply Feldkamp to the circular scan data, obtaining an image in Fourier space;
2) apply Feldkamp to the linear scan data, obtaining an image in Fourier Space;
3) patch in the missing parts of data in the Feldkamp reconstruction of the circular scan with the relevant pieces from the Feldkamp reconstruction of the linear scan in Fourier space;
4) use the inverse Fourier transform to obtain the final image in the image space.

As we can see from the above procedure, the center part of the algorithm is the data patch in Fourier space. We might have difficulties in the implementation of the algorithm; however, we concluded that the risk could be mitigated with a careful selection of smoothing technique in the data patch process.

Meanwhile, examples given in a reference paper demonstrated that the algorithm gives reasonable reconstruction for an 18° cone-beam scanner. Therefore, we are confident that we should be able to implement it for our CCAT system with a reasonable effort.

We have finished the identification of the algorithm for our CCAT system. The feasibility has been confirmed with our current Feldkamp capability. The implementation of a cone-beam reconstruction algorithm for CCAT will provide the opportunity to use the CCAT system to its full potential. This will open up a wealth of new opportunities for programmatic work for NDE. Meanwhile, our current cone-beam reconstruction algorithm (Feldkamp) can only reconstruct approximately 20% of the detector area on CCAT without considerable distortion. It is imperative for us to obtain a full cone-beam reconstruction capability in NDE. We think that we should proceed to the implementation of the algorithm in the next fiscal year.

Quantitative NDE for Ceramic Processing Defects

D. Chinn, C. Logan

Our objective is to understand the response of a suite of NDE methods to known flaws in ceramics. The overall approach is to apply NDE methods to intentionally-flawed ceramic specimens of Al_2O_3 and BeO. Dimensional inspection, density measurements, swipe analysis (for BeO), film radiography, and candling are complete. Ultrasonic characterization is underway.

We selected Brush Wellman to make the specimens for our analysis, and approached them with a list of potential defect types compiled from past experience and internal consultations. They manufactured four defect types—inclusion, unsintered agglomerate, microcracks-thermal, and delamination—in two ceramics, Al_2O_3 and BeO. They also made blanks for recreating (at LLNL) a type of machining damage observed several years ago.

We have 24 specimens (15 flawed) made of each material. Specimen geometry is shown in Fig. 1. This geometry provides orientation cues for most cross-sectional views and offers two sets of parallel surfaces for ultrasonic velocity measurements. All as-received specimens were below the DOE release limits for BeO surface contamination. While measurable contamination was observed on about half the specimens, there was no statistically significant difference between BeO and Al_2O_3 specimens.

We explored a potential alternative to water immersion for ultrasound—a pulsed Nd:YAG laser was used to generate ultrasound, detected on the opposite side by an air-coupled transducer. Figure 2 shows a typical waveform from the air-coupled receiver.

We found these specimens too thick and the ceramic too intensely scattering for our usual candling method to work. The machining damage blanks are thinner, 7 mm, and light does pass through. These specimens contain no defects at present. We measured light transmission as a function of wavelength in a standard spectrophotometer for one specimen of each ceramic type.

Al_2O_3 transmission is insufficient to measure, but we observed structure in the light transmission of BeO.

Film radiography is complete for all specimens. It appears that in every case where we intended to have a defect, it can be discerned on one or the other of two radiographic views. Figure 3 shows an unsintered agglomerate in one Al_2O_3 specimen.

One unexpected result is evident in radiographs of specimens with inclusions. It appears that Mo inclusions strongly affected the sintering process in the BeO. Much work remains to completely characterize this, but the radiographs reveal a large volume of low x-ray opacity centered on the Mo inclusions.

We are exploring the feasibility of microwave imaging, with the University of Missouri-Rolla. X-ray CT, dye penetrant, optical coherence tomography, IR, and ultrasound will be completed at LLNL in FY03.

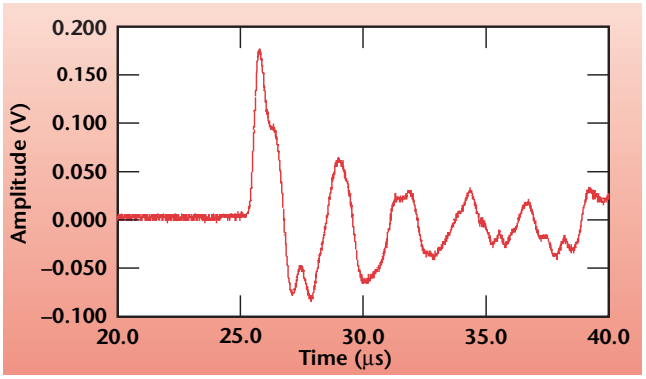

Figure 2. *Ultrasonic waveform detected in non-contacting transmission through a ceramic specimen.*

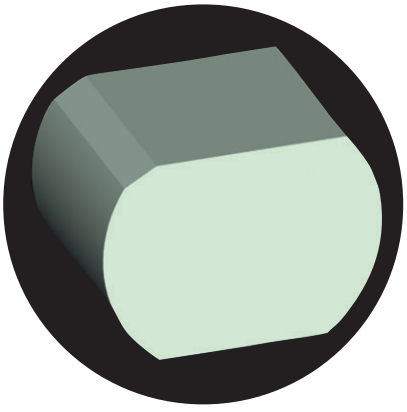

Figure 1. *Ceramic specimen geometry. Distance between each pair of parallel surfaces is 22 mm.*

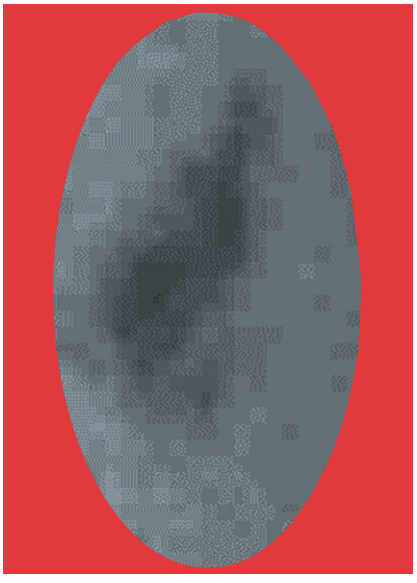

Figure 3. *Portion of a film radiograph revealing an unsintered agglomerate.*

Developments in Sonic IR NDE

W. O. Miller

Sonic IR shows promise as a new NDE technique that can detect flaws, such as tightly closed cracks, that are difficult to detect with other methods. This project is extending the reliability and reach of this technology, and also providing this capability at LLNL.

IR NDE methods have several unique advantages, including noninvasive and non-contact inspection, portability, simplicity and relatively low cost. IR NDE is well-suited for evaluating certain material characteristics and flaw types, including temperature, thermal properties, closed cracks, and buried pockets.

Sonic IR works by dynamically exciting the part being tested with an acoustic probe that is in physical contact with the part. Any resulting differential motion across a crack face creates heat by friction, and a traditional IR camera images the transient temperature rise at the crack (Fig. 1). The camera can image a large area, so scanning is not required. We have found that the method is generally applicable to a wide variety of materials and flaw types.

Our FY02 efforts have focused on enhancing and improving this technology, with emphasis on hardware integration, image processing, computer modeling, and basic analysis of the process physics.

We have constructed a Sonic IR test facility centered around a state-of-the-art IR camera with a high frame rate to capture short transients, and an industrial 30-kHz welder as the acoustic source.

The following accomplishments are also noteworthy.

Flaw quantification

This signal processing method is able to extract and quantify flaw features such as crack length and depth. It relies on comparing the IR data to exact analytical results for prototypical flaws, using the flaw geometry as fitting parameters. A preliminary software version has been encoded which successfully extracts crack geometry.

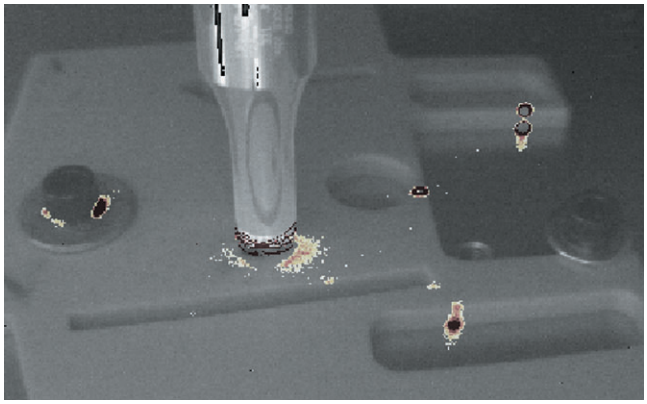

Figure 1. *Sonic IR image showing damage locations (black/orange/white areas) on a machined aluminum oxide plate. The acoustic probe is in the image center.*

Image synthesis

This signal processing method fits the raw image data into a mathematically precise series expression, creating a synthesized image. The series expression allows exact mathematical manipulation for image enhancement, which increases the detection range of the method (*e.g.*, deeper flaws can be detected). We now have a preliminary software version which exemplifies all these features (Fig. 2).

Inspection limits

The current effort on this task is to analytically and numerically predict the frictional heating of a generic crack subject to a cyclic acoustic load. When this is coupled with a conduction model for heat diffusion, then the inspection limits can be found. The analytical effort is nearly complete.

Damage limits

Experience has shown that Sonic IR can damage brittle parts with existing flaws. This effort attempts to define the damage threshold by considering established theory for fatigue crack propagation using the Paris equation. The results indicate that only relatively large existing cracks are at risk.

Future directions

The goal for FY03 is a deployable capability. Further enhancements to the method will be evaluated, including a virtual model of the process physics, and a study of optional acoustic sources. Finally, extensive applications of the method will be made to construct a valuable experience base.

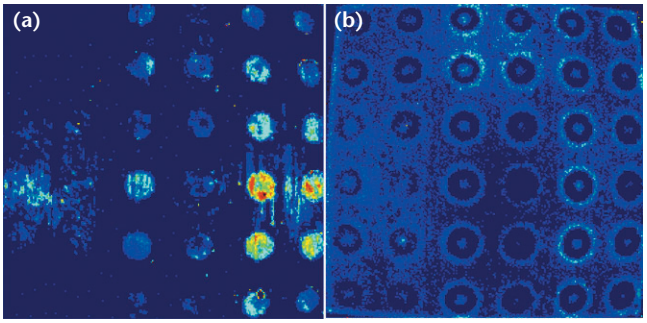

Figure 2. *Example of image synthesis: (a) raw IR image of plate with holes at various depths; (b) synthesized image with time-derivative processing.*

Evaluating CMOS-Based X-Ray Detectors

D. Schneberk, D. Rikard, H. E. Martz, Jr.

The introduction of Complementary Metal-Oxide Semiconductor (CMOS)-based x-ray detectors has generated considerable interest as a low-cost high-performance alternative to amorphous-silicon (Am-Si) or amorphous-selenium (Am-Se) panels. We have evaluated three different types of CMOS imagers.

For Am-Si or Am-Se panels, available pixel sizes are 127 to 400 µm and 139 µm, respectively. CMOS panels support pixel sizes down to 50 µm. In addition, CMOS panels benefit from the large manufacturing expertise in configuring silicon-based devices.

While the current arrays are 2 and 4 in. square, we think CMOS x-ray detectors in 8-in.-square to 12-in.-square formats with the same small pixel size are on the horizon. At least three different projects at LLNL could benefit from large-format small-pixel-size detectors: high-magnification micro-focus DR and CT of HE detonators; DR/CT imaging of high explosives, simulants, and false alarm items; and DR/CT of weapons components.

We evaluated three different types of CMOS imagers: a RAD-ICON 1-k-x-1-k CMOS panel with a LANEX FINE scintillator; a similar RAD-ICON 1-k-x-1-k panel with a 20-ml lead screen; and, a HAMAMATSU 2.2-k-x-2.2-k (4.5-in.-x-4.5-in.) panel that includes columnar CsI as the scintillator bonded to the CMOS array. A similar set of radiographic objects was imaged on the three different detectors to evaluate the sensitivity, linearity, persistence, and image fidelity. All three of the detectors included spatial resolution down to 8 lp/mm, as measured with a line-pair gauge. The RAD-ICON panel with the LANEX FINE had the best spatial resolution of the three, showing the most modulation at 8 lp/mm. However, the RAD-ICON panels showed the most persistence (latent image from a previous exposure). Some of the objects were radiographically opaque at low energy, and for the RAD-ICON panels this pattern became part of the background image for every subsequent image.

This effect was less for the HAMAMATSU panel. To illustrate some of the promise of larger format CMOS arrays we imaged a 20-lp/mm line-pair gauge with a micro-focal source, magnifying the small section of the gauge onto the HAMAMATSU panel. Figure 1 contains an image of this configuration.

In addition to standards objects, we radiographed HE simulants, HE false-alarm items and HE detonators. Using resources from other projects, we are presently configuring the HAMAMATSU panel for use in the KCAT micro-focal cabinet as the detector for this CT system.

The CMOS panel with the lead screen provided a different means for imaging at high energy. The mechanism with the lead screen is different: with this detector we are measuring the electron output from the lead screen, not the photon output from a scintillator. Tests conducted here have shown this detector to have every bit of the spatial resolution as with the scintillators, but an intrinsic resistance to low energy x rays.

We routinely perform DR and CT with a 9-MV Linac for scanning dense objects and assemblies. One difficulty in this imaging is the preponderance of low-energy scatter. Both the LANEX-FINE and CSI scintillators are made for medical sources and are particularly sensitive to low-energy x rays. Most of these lower-energy x rays carry very little information about the object, and are the result of scatter interactions from the fixturing in the beam path.

Figure 2 includes an image of the 1-in. steel step-wedge acquired at 450 kV using the Pb-Screen CMOS detector. Analysis of this image shows the detector preferentially records the higher energy content of the spectrum with no loss in spatial resolution. We are currently exploring the possibility of configuring larger versions of the Pb-Screen panel with both RAD-ICON and HAMAMATSU.

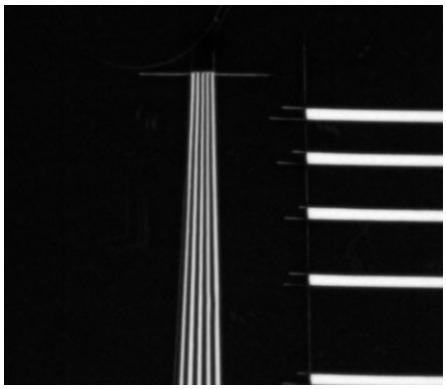

Figure 1. *Image of the end of a 20-lp/mm line-pair gauge.*

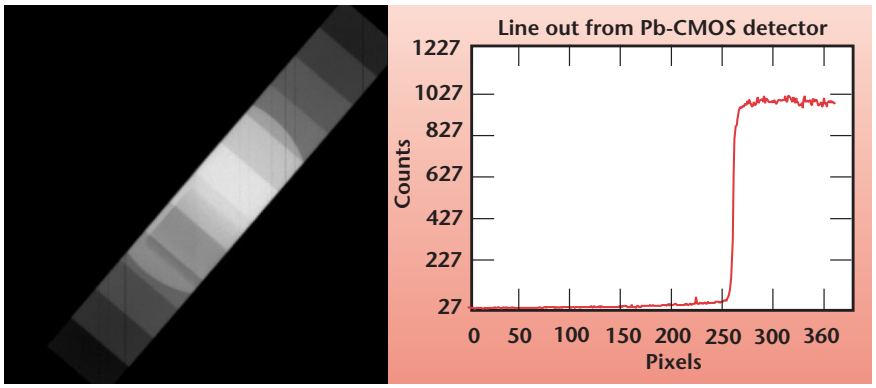

Figure 2. *Image of steel step-wedge and line-out through the wedge from a Lead Screen RAD-ICON CMOS panel.*

Synchrotron Microtomography at ALS

K. Dolan, T. Smith, D. Haupt, D. Schneberk, J. Kinney

A microtomography system is being designed and fabricated for nondestructive microstructural characterization and internal dimensioning at small length scales.

The objective of this project was to design and install an x-ray microtomography system for the dedicated CT beam line at the Advanced Light Source (ALS) facility at LBNL. The microtomography system is intended to provide nondestructive characterization of microstructure, and internal dimensioning of samples and components at small length scales. The microtomography system consists of translation and rotational stages; a lens-coupled camera-based imaging system; and data acquisition and control software. It was designed to obtain spatial resolution as small as 1 to 2 µm, with parallel beam geometry at x-ray energies in the range 4 to 140 keV.

During the past year, the data acquisition software was rewritten to reduce electronic overhead involved with camera readout and stage motion; a new structure for supporting, housing, and aligning the imaging detector (camera and scintillator) was designed, built, and tested; image tiling software was developed to handle samples of larger diameter than the field of view; and a number of application results were obtained to test and demonstrate system capability with the system fielded at the Stanford Synchrotron Radiation Laboratory (SSRL).

To take full advantage of the high brightness of the synchrotron source, the data acquisition software was significantly modified by using onboard features of the camera, resulting in a data acquisition process that is fully asynchronous. With these modifications, the acquisition software, which remains compatible with our existing laboratory capabilities, is no longer the rate-limiting step in data acquisition. Extensive modifications were also made to the camera and scintillator mounting designs to improve alignment and to ease the alignment process.

Imaging specimens of importance to LLNL programs (high explosives, shock spallation, and laser targets specimens) provided an important test of the new system design. High-explosive samples were imaged with microtomography for the first time allowing particle and boundary phases of the explosive to be separated and analyzed (Fig. 1).

High quality 3-D images of the microstructure of shock spallation samples were obtained which show both void morphology and particle size distribution (Fig. 2). A new tiling algorithm that enables imaging of large diameter specimens at high spatial resolution was designed and tested on aerogel witness plates being used in the debris-shield mitigation program for protecting laser optics. Laser-ruled targets were imaged and reconstructed in 3-D to determine the as-machined rule pattern periodicity and groove depths.

Among problems that have benefited from synchrotron tomography, and are in urgent need of the greater precision this beam line will allow, are 3-omega damage studies, shock spallation studies, high-energy-density target characterization, and high-explosive aging.

We anticipate that the full capabilities of the system will be demonstrated at ALS in February 2003. Significant improvements in image resolution and contrast and extended capabilities are expected since the beam divergence and beam intensity at ALS are both improved by nearly a factor of 10 compared to SSRL; x-ray energies extend to nearly a factor of 5 higher; and new contrast mechanisms, such as phase contrast, can be explored.

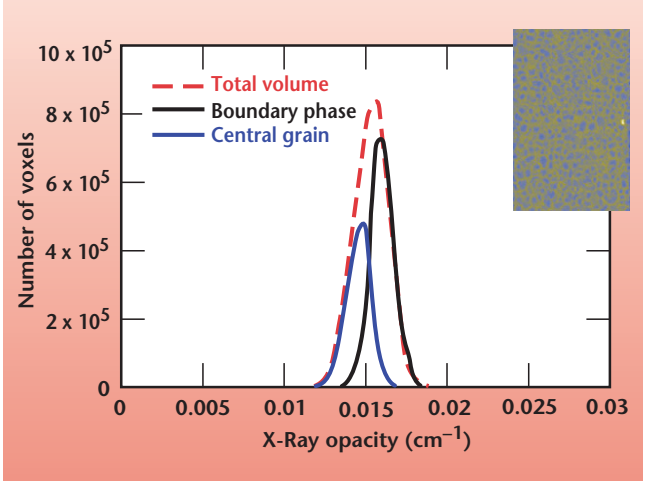

Figure 1. *Tomographic image of a cylinder of LX17 high explosive obtained at SSRL.*

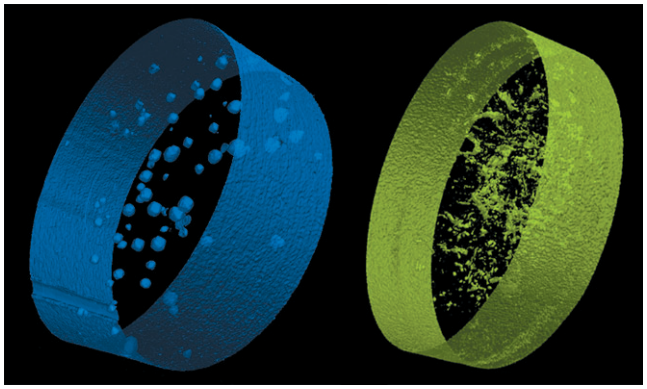

Figure 2. *High-quality images of the microstructure in shock spallation experiments, from synchrotron microtomography. Image on the left is a 3-D representation of the internal void structure in a single crystal aluminum cylinder that was shocked in the LLNL gas gun facility. On the right is the corresponding image from a polycrystalline specimen.*

Center for Precision Engineering

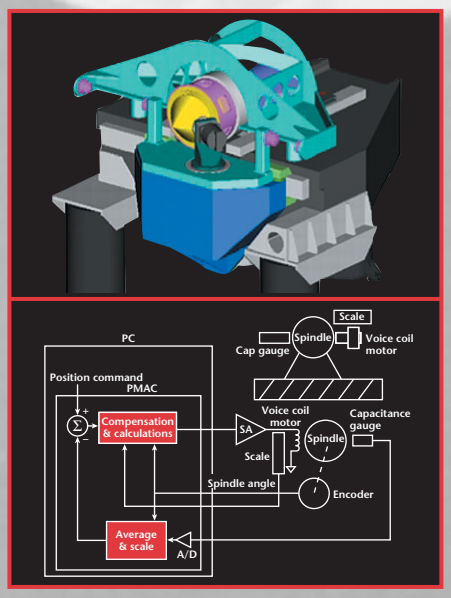

Active Vibration Isolation of an Unbalanced Machine Spindle

D. J. Hopkins, P. Geraghty

Proper design and application of controls, sensors, and metrology technologies have enabled precision turning machines to achieve nanometer positioning. However, at this level of resolution, vibration sources can become a limiting factor on the ability to achieve this level of positioning. One of the largest sources of vibration in a turning machine is an unbalanced rotating spindle. The purpose of this project is to design a system that can be used to actively cancel unbalanced spindle forces.

An unbalanced spindle creates a rotating force vector with a once per revolution period. The cause and size of this force vector may be a function of the spindle, the part, the part fixturing, the part setup, and the spindle speed. In addition, certain spindle speeds coupled with the size of the unbalance force vector can contain other harmonics that may excite machine structural resonances. The magnitude of the unbalanced force vector increases as the square of the spindle speed.

We have designed a system that can be used to actively cancel spindle unbalance forces, specifically, to attenuate the spindle housing vibration using an active vibration control process to prevent the unbalance forces from disturbing the rest of the machine systems, *e.g.*, the slide servo system or the machine metrology frame.

The displacement induced by the unbalance force is held to nanometer levels regardless of the spindle speed or changes in the part contour, and adapts in real time to changes in unbalance forces.

The ideal solution is to cancel the unbalance forces at the source or rotor of the spindle. This is difficult, since the rotor must hold the part and any apparatus that would be used to cancel the rotor unbalance. Our approach is to cancel the vibration forces that radiate from the spindle housing so that these forces do not induce motion into sensitive machine systems.

Unbalance forces in a precision machine can impart energy into the machine base, and provides a forcing function to the machine slides or the machine metrology frame, and can cause undesirable slide motion. This motion can be rejected to some extent by the control system loop gain, but the loop gain decreases with increasing frequency. This is exactly opposite of what is desired, since the unbalanced spindle forces increase with spindle speed (frequency), compounding the problem. Force disturbance of the metrology frame can cause non-ridge body motion of the frame and distort the measured tool position. Eliminating or canceling the spindle unbalance force reduces these error sources.

The basic concept of the system is to measure the force-induced spindle-housing motion and exactly cancel this motion with a controlled moving inertial mass. Essentially, the spindle housing motion is measured with a displacement sensor referenced to the machine base. This measurement, along with the spindle angle (measured with an encoder) is fed to a controller running a specific algorithm. The algorithm computes the required signal, and the controller actuates a voice coil motor, canceling the original force-induced motion. The motor is mounted on the opposite side of the spindle housing, directly in line with the displacement sensor. The voice coil motor reacts against the moving inertial mass and not against a reference structure. The amount of force that can be developed to cancel the unbalanced spindle force is a function of frequency (spindle speed), the amount of mass the voice coil is moving, and the range of voice coil travel.

During this past year, the system shown in the figure has been assembled and implemented. The system is designed to cancel a single-sensed point of force-induced motion. The plan for next year is to extend this control to cancel a plane, and then two planes, for two-plane spindle balancing. The control algorithm is potentially patentable and is sensitive only to the fundamental signal of force-induced motion.

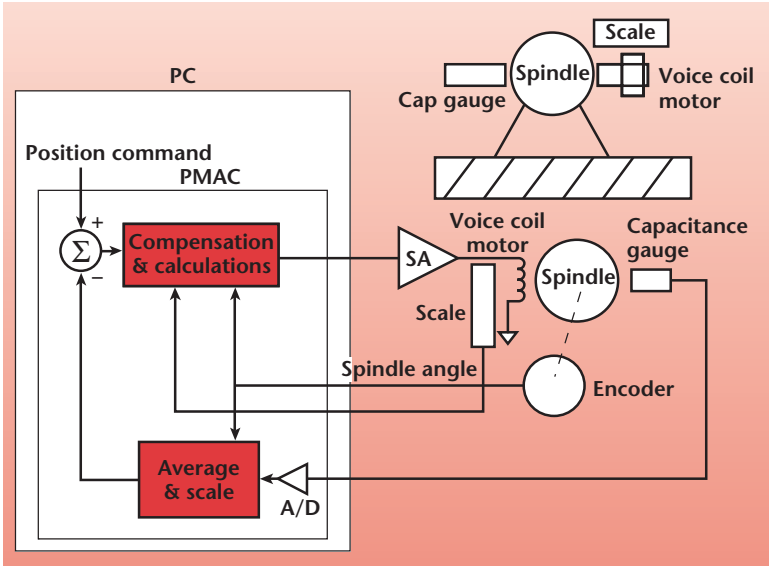

Control system block diagram and simple sketch of the physical system.

Ultra-Precision Machine Spindle Using Porous Ceramic Bearings

P. Geraghty, K. Carlisle, L. Hale

Air-bearing spindles have typically been employed for ultra-precision machine applications, due to the low asynchronous error motion and the high rotational accuracies achievable. Traditional oil-fluid-film bearings have not been able to match the accuracies of air bearings, but they have the advantage of higher stiffness and improved dampening capabilities. With the advent of new oil-fluid-film porous ceramic bearing materials, we may now be able to have the best of both worlds: the accuracy of an air bearing with the high stiffness and improved dampening capabilities of a traditional oil-fluid-film bearing.

Fluid-film and air-film bearings have been used for machine spindles whenever precision motion requirements exceed the capabilities of traditional contact bearings. For example, in the 1970s, "T"- based lathe spindles used contact (ball or roller) bearing technology. A quantum leap in spindle accuracy was achieved when these spindles were replaced with porous graphite air-bearing spindles.

In the late 1970s and early 1980s, LLNL led in the field of high-precision diamond-turning machining, using porous graphite air-bearing spindles. Machines such as DTM #1, DTM #2, DTM #3, and LODTM all pushed the field of precision diamond turning to higher and higher levels of accuracy. Though 20 years old, these machines still operate at the limits of current machine accuracies.

LLNL is now designing the next-generation machine tool. Precision Optic Grinder and Lathe (POGAL) is the next machine that will push the limits of accuracy farther still. POGAL is required to have spindle accuracies of less than 50 nm in both axial and radial directions.

In addition to the precision requirements of POGAL, there is also an increasing demand for larger parts requiring diamond turning that is reaching the load capacity of air-bearing spindles. Precision grinding of hard optics, a capability of POGAL, is also on the increase, requiring greater stiffness and damping from our machine spindles.

This all leads to the use of hydrostatic oil-film bearings. When compared to air bearings, hydrostatic oil bearings have higher stiffness, higher load capacity, and better damping characteristics. The problem is conventional oil-film-bearing spindles have not been able to match the accuracies achievable with air-bearing spindles.

The materials science laboratory at Cranfield University, UK, has developed and commercialized the production of a porous ceramic bearing material, which is now readily available. It is hoped that with this new ceramic material, we may now be able to get the accuracy of an air-bearing spindle with the high stiffness and improved dampening capabilities of a traditional oil-fluid-film-bearing spindle.

As part of the initial phase of this project, we are collaborating with staff at Cranfield Precision, UK, to design an ultra-precision machine spindle using this new material. This spindle has been designed to meet the requirements of POGAL.

This is a two-year project. The goals of this first year were to: 1) design a porous-ceramic-bearing spindle that meets the requirements of POGAL; 2) prepare a complete engineering package, including assembly drawings, detail drawings, tooling drawings, and engineering analysis; and 3) generate a mathematical model to predict the performance of the spindle.

We have achieved all three goals. Additionally, the long lead-time material was ordered and received, in preparation for spindle fabrication next year.

The spindle will be built and tested next year.

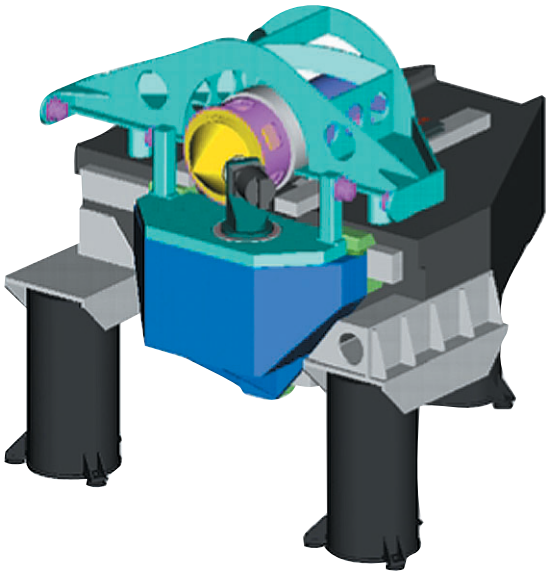

Conceptual drawing of the new POGAL machine, the next-generation machine tool being designed at LLNL.

Other Technologies

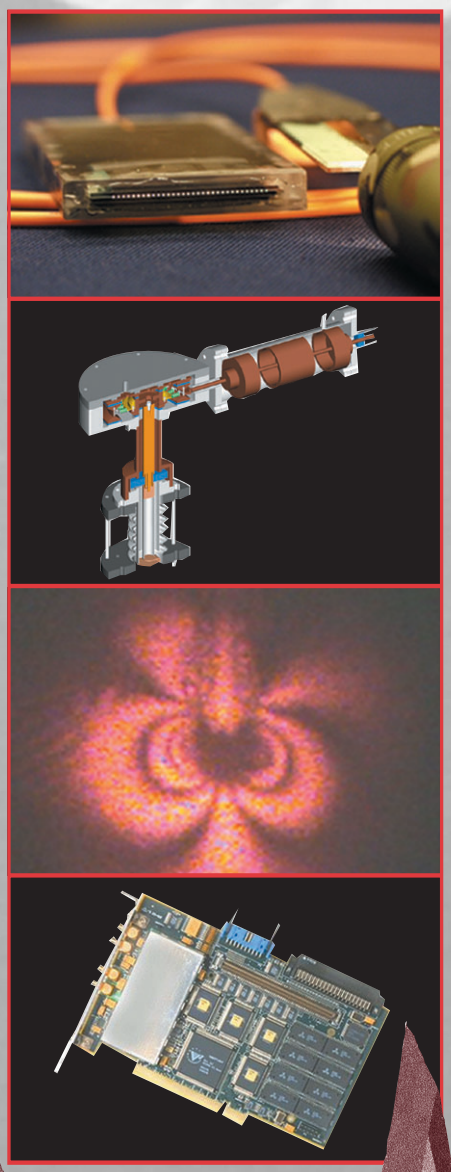

General-Purpose Digital Signal Recovery

G. W. Johnson, C. Kecy, K. Nelson

Modulation and demodulation of RF and base-band signals can now be implemented quickly and cost-effectively by purely digital means. Numerous computer interface boards and high-level graphical programming tools are commercially available that enable rapid prototyping of digital signal processing (DSP) systems. This project focused on a market survey, an example project, and the creation of a tutorial course to update LLNL engineers on this important new capability.

Signal generation (modulation), detection (demodulation), and control system implementation by digital means are now commonplace, driven by mass markets such as digital audio and wireless communications. Such systems are extremely flexible, stable, and cost-effective when compared to their analog counterparts.

This has resulted in an explosion of hardware and software tools suited to LLNL's scientific applications, such as precision measurement of amplitude, frequency, and phase, as well as signal synthesis and detection using arbitrarily complex modulation schemes.

The latest plug-in computer interface boards for these applications have impressive specifications and are quite affordable, obviating the need for custom hardware development in most cases. More importantly, the latest generation of high-level graphical programming languages (such as Matlab/Simulink, LabVIEW, and HyperSignal RIDE) drastically reduce learning curves and development times (see figure).

We began our educational project by surveying the relevant hardware and software market, then built a database of products and specifications, and acquired boards and software. We then applied those tools to an immediate problem of interest: precision microwave phase measurement for a metrology project. That project served as a demonstration of the possible approaches to a specific problem, contrasting traditional methods (analog and/or low-level software) with the new high-level, general-purpose DSP approach.

The original phase measurement system contained a microwave-modulated optical beam. This beam, after hitting a target, was detected, and the microwave signal processed to retrieve the phase, or distance, information. The method used was IQ demodulation, requiring a local oscillator signal and a measurement signal. This required the use of many analog RF components, such as an IQ demodulator, low-pass filter, and several splitters and amplifiers. All of these analog components added in an unknown amount of phase noise and drift, thus reducing the accuracy of the overall system. The goal was to design a digital IQ demodulation system to reduce phase noise by replacing many of the analog RF components.

Hardware and software were chosen based on speed, performance, and cost. The signal of interest was 10 MHz, so a high-speed acquisition board was required. A 65-MHz A/D board (ICS-652) was purchased. We used Mathwork's Matlab as the implementing software, and simulations were also performed in LabVIEW.

The local oscillator and measurement signals were digitized immediately after being down-converted from 8 GHz. An algorithm was then applied to the digitized signals. This algorithm performed the same functions as the original analog components. The phase information was then directly available with no further data collection.

Advantages of this system included ease and speed of implementation, flexibility in changing the code, and fewer analog components to manage thermally. The original analog RF components contributed approximately 1 mrad of phase noise to the measurement system. The measured phase noise from the substituted digital system was reduced to 600 nrad, an order of magnitude improvement.

We have prepared a half-day training seminar which will also be available on the web.

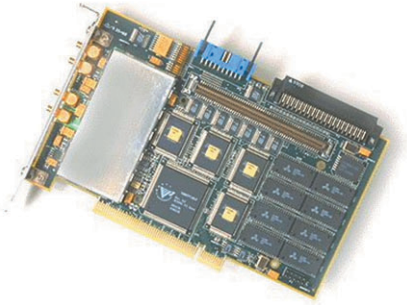

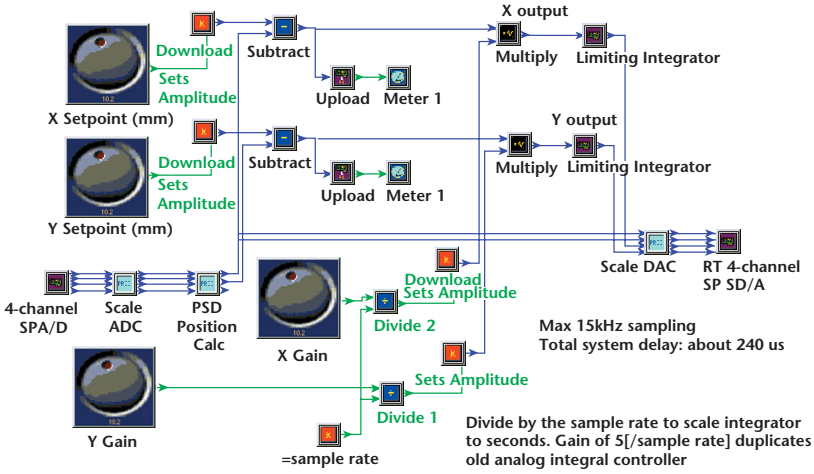

High-performance data acquisition board (left), combined with graphical programming software (right), enabling rapid prototyping of complex signal recovery algorithms.

System Architecture for High-Speed Transient Diagnostics

G. Le Sage, K. Hagans, B. Tran, T. Strand; E. Daykin, G. Perryman, P. Parker, R. Eichholz (Bechtel, Nev)

We have applied new system architecture to modernizing a Fabry-Perot (F-P) velocimeter.

There are special needs in terms of channel count, transient record length, dynamic range, and resolution that are specific to the diagnostics for nuclear stockpile measurements. We made a plan to integrate modern large channel-count digital technology with a multi-channel photomultiplier tube (PMT) and a fiber-optic array to supplement or replace the function of an optical streak camera in a specific laboratory application, the F-P velocimeter. For µs record lengths, and ns resolution, modern inexpensive digitizers controlled by fast PCs provide a new alternative that was not available a decade ago.

This type of diagnostic is well-suited to transient diagnosis of fast-moving surfaces driven by explosive forces. Up to now, streak cameras backed with film have been the standard transient recording device for this diagnostic.

Our device will provide up to 100 spatial channels, temporal resolution of 10 ns, and a record length of 10 µs. These 100 channels will record a portion of the overall spatial field that contains all the information necessary to diagnose velocity. Creation of this new device is motivated by cost, durability, and simplicity. Our proposed device will have the footprint of a desktop PC, in addition to a small chassis containing electronics and a PMT.

We focused on a commercial PMT with a linear array of anodes, each coupled to an optical fiber, which are fused together at one end to provide the array input that spans the image plane of the incident light. The PMT outputs are quantized and passed to an array of 100 digitizer channels controlled by a PC. The 100 separate digital records are processed and recombined to produce an image.

Progress in FY02 included system testing to identify the best digital architecture, selection of the appropriate PMT sensor, design and fabrication of the fiber-optic array, and progress toward the design of the discriminator (quantizer) that feeds the digital recording system. A basic schematic of the digital system is shown in Fig. 1.

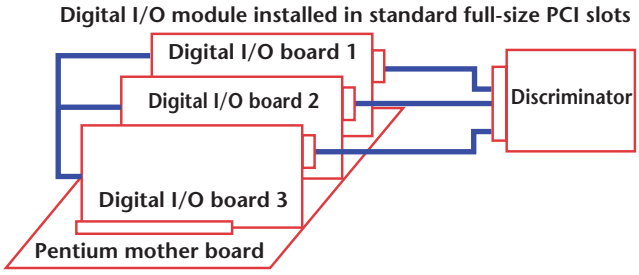

Figure 1. *Digital recording system architecture.*

The fiber-optic array or bundle is used to collect light at the image plane of the F-P interferometer output, and to distribute the light to the separate PMT channels. The plane of the array input corresponds to the normal location of the streak camera input window. The fiber connection gives great flexibility in terms of placing the input arbitrarily with respect to the location of the PMT and the rest of the system. Alignment of the fiber array input end is all that will be required. The completed fiber array is shown in Fig. 2.

The output of the fiber-optic array (Fig. 3) is matched to the spacing of the PMT anodes. The PMT can be placed remotely, and housed in the same chassis as the discriminator electronics.

The key challenge for the continuation of this project is fielding of an integrated instrument, and demonstration that the collected data matches the quality of a streak camera. Our device will hopefully be the first in a continuing line of new diagnostics that fully use modern technology to benefit the LLNL Stockpile Stewardship mission.

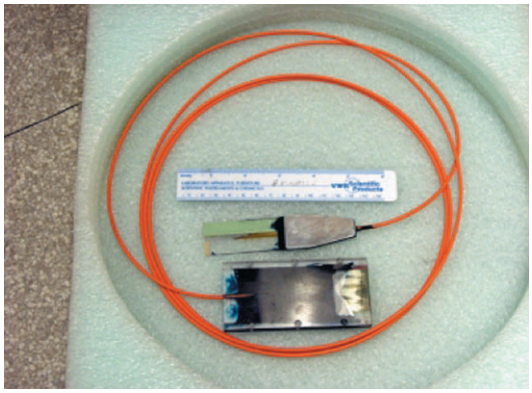

Figure 2. *Completed fiber optic array.*

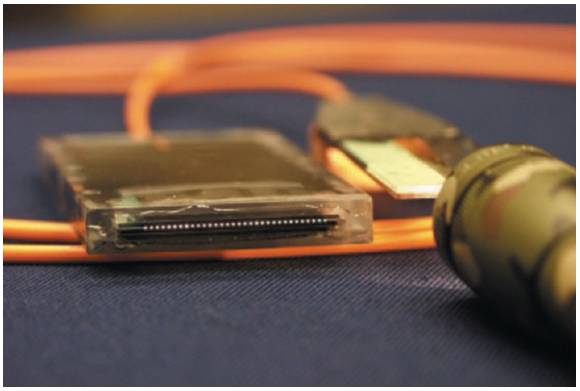

Figure 3. *Fiber optic array output plane.*

Next-Generation Fast Tuner for the Rare Isotope Ion Accelerator

B. Rusnak, S. Shen, M. Roeben

Superconducting RF accelerating cavities have been used for over 30 years to accelerate particle species from electrons, to heavy ions, up to uranium. We are designing an operational electromagnetic fast tuner that would advance the present state of the art.

In heavy-ion superconducting accelerators, where a large range of elemental ions are accelerated, beam currents are typically low, which makes these machines susceptible to detuning, resulting from mechanical vibrations collectively called microphonics. To mitigate these effects, an electromagnetic circuit that fast-switches the load impedance for reactive power stored in a transmission line can be coupled to a cavity to compensate the original detuning. Technology-base funds were used for an operational electromagnetic fast tuner that would advance the present state of the art.

By pursuing design concepts that used either an over-designed RF system, or a smaller, better-matched RF system that used fast tuners, we were able to show that using the fast tuner would reduce the installed RF power by 65 to 75% on a major nuclear physics accelerator, which would reduce the installed RF system costs by 35%, an appreciable savings at 6 to 16 $M.

Advancing the design for the fast tuner beyond the state of the art that is currently operational at the ATLAS heavy-ion accelerator at Argonne National Laboratory required increasing the reactive power handling capability and operational frequency of the device. Due to the extent that each phase extrapolated the technology, the development process at that point was divided into two phases, both based on the distributed-element transmission line concept shown in the figure.

In the first phase, we aim to establish the feasibility of the transmission line design to increase power handling by 50% and frequency by 350%. The second phase would take the concept up a factor of 10 in power and a factor of 8 in frequency over what is available today.

The distributed-element design was created to allow the capacitive-dominated impedance state at the end of the coaxial transmission line to change at 25 kHz. The design shown in the figure combines the essential elements for fast-tuning the cavity-tuner system.

After the tuner was mechanically designed, electromagnetic and RF modeling was done to fine-tune the design to operate properly at the desired frequencies. We used Microwave Studio, a state-of-the-art 3-D electromagnetic modeling design code. An example of the modeling work is the distributed-element low-pass RF filter that allows the 25-kHz signal to reach the PIN diodes while keeping the main RF frequency of 345 MHz from being transmitted out.

If this design proves workable, it will be of interest to researchers in high-gradient, lightly-beam-loaded superconducting cavities, since it would give them a design option for making their RF system designs more robust and cost effective.

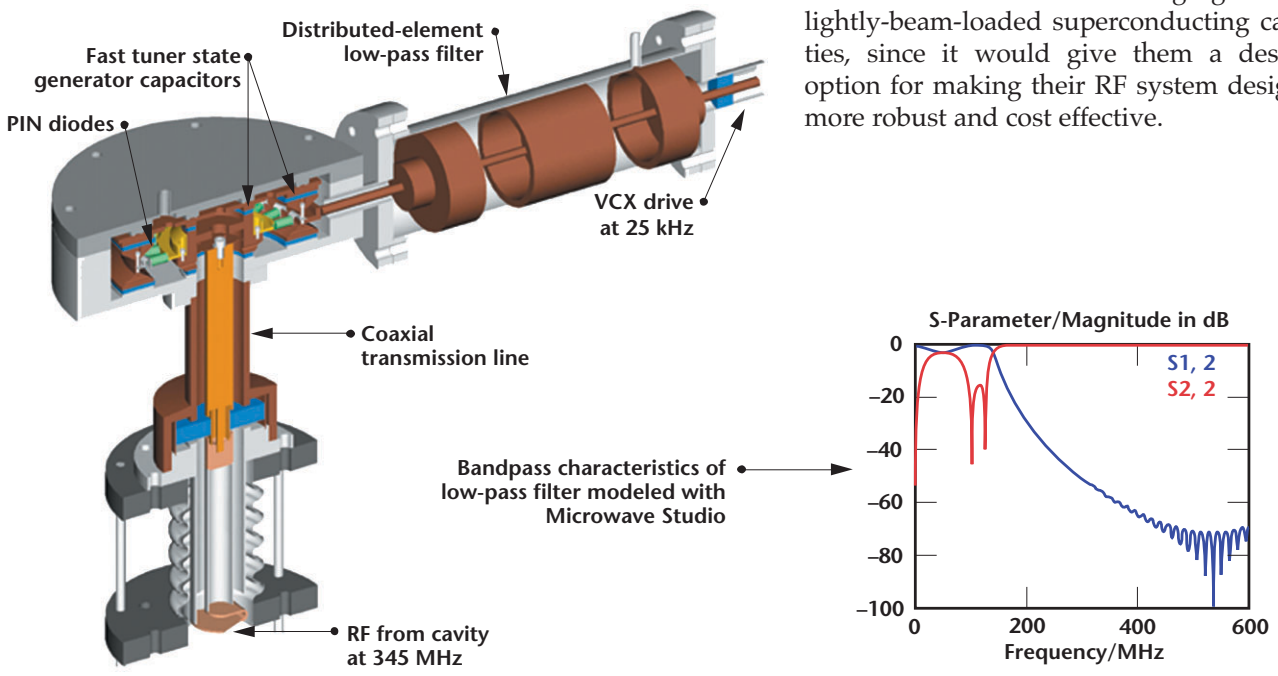

Mechanical design of fast-tuner assembly; coaxial transmission line with magnetic field coupling loop; and low-pass filter, with bandpass characteristics of the filter as modeled.

Nitrogen Augmentation Combustion Systems

L. E. Fischer, K. O'Brien, B. Anderson, K. Wilson, D. Flowers, A. Lamont

A consortium of industry and University partners has been formed to further LLNL's Staged Combustion with Nitrogen-Enriched Air (SCNEA) technology for coal and natural-gas-fired boilers.

Stationary combustion sources account for 50% of the NOx emissions in the US. The markets for stationary power include electrical power generation, industrial processes, and peaking back-up power systems. The fuels used in these processes consist of coal, natural gas, and fuel oil. One of the greatest market opportunities exists in the generation of electrical power using coal and natural-gas-fired boilers. Another major opportunity exists in the processing and transmission of natural gas by natural-gas-fired reciprocating engines.

Coal is one of most commonly used fuels for stationary power generation throughout the nation and world, yet it suffers from high emissions. Increased energy demands are placing extreme pressure on existing power plant facilities.

Source emission control has become a major focus for large diesel and natural-gas-fueled drivers. National Air Quality Standards are especially expected to address issues with fine particulates, *e. g.*, PM2.5 and PM10, and ozone precursors such as NOx and VOCs. Natural-gas-fired reciprocating engines are commonly used for peak power, distributed power, and the recovery, transmission, and processing of natural gas, and are under pressure to reduce NOx emissions.

Reduced NOx emissions to meet EPA guidelines for 2007-2008 can be achieved only through the use of secondary processes such as Selective Catalytic Reduction (SCR). This is extremely costly, introduces catalyst disposal issues, and is difficult to retrofit.

A process is needed that enables coal-burning facilities and natural-gas-fired reciprocating engines to achieve the NOx emission requirements, yet is cost-effective, maintains efficiencies, and can be readily deployed with existing equipment (*i. e.*, easily retrofit).

Preliminary economic studies performed by Virginia Polytechnical Institute indicate that coupling the nitrogen enrichment membrane technology with LLNL's SCNEA technology would be more cost-effective than existing approaches.

Discussions with McDermott Technologies Inc. (MTI, a division of Babcock and Wilcox), Brigham Young University, and the University of Utah have determined that boilers currently equipped with Overfired Air (OFA) could be easily retrofit to use SCNEA. Over 80% of industrial boilers use OFA.

An experimental project plan has been written in conjunction with MTI, University of Utah, Stanford University, Virginia Polytechnical Institute, and Ohio State University. This plan accounts for the heterogeneous kinetics of combustion of coal, as compared to the gas-phase reactions typically observed with natural gas or fuel oil.

A consortium of industry and University partners has been formed to further the SCNEA technology for coal and natural-gas-fired boilers. MTI and American Electric Power (AEP) have indicated interest in assisting in evaluating the use of SCNEA for the reduction of emissions by boilers in electrical power generating facilities. Stanford University, Virginia Polytechnical Institute, University of Utah, and Brigham Young University (leading coal research facilities) have reviewed the technology and are anxious to evaluate SCNEA. Preliminary experimental testing at Ohio State University indicated promise, in that a combination of nitrogen enrichment and staged combustion reduced NOx emissions relative to staged combustion without the use of nitrogen enrichment. LLNL and its partners have been encouraged to submit for funding to explore the use of SCNEA with coal.

Dynamic Fracture Mechanics Experiments

S. DeTeresa, C. Syn, R. Riddle, R. Becker

The goal of this project is to bring state-of-the-art experimental capabilities to LLNL for full-field, real-time studies of dynamic fracture, to be used in support of Laboratory needs for advanced computer simulations of material behavior. This capability will provide measurement of dynamic fracture toughness, crack velocity, and fracture mode transitions. Additionally, if a high-speed IR camera can be procured, the same experiment can be used to measure the temperature distribution ahead of a dynamically propagating crack.

Our approach is to build an experimental capability based on the dynamic fracture experiments developed at Cal Tech. A schematic of one version of this experiment is shown in Fig. 1. Another component of this project is to hire an engineer with expertise in designing and conducting dynamic fracture experiments.

During the first year of this project we have made progress on several fronts: we have established a working relationship with staff at Cal Tech to support our efforts and to evaluate candidates for the new hire; and we have made significant progress in several aspects of the experimental capability.

The 2.5-in. gas-gun facility has undergone several modifications and upgrades that will allow us to eventually conduct dynamic fracture experiments on the hazardous materials of interest to the programs. The safety note has been signed, and pressure-supply system modification and testing are nearly complete. Power lines for the laser illumination and containment vessel vacuum systems have been installed. A new vacuum pump and HEPA filtration system has been purchased and will be installed early in FY03. Several of the consumable items such as steel projectiles and surrogate steel fracture specimens have been fabricated. A 20-W laser was obtained and will be installed in the gas-gun facility after it is fitted with a Pockels cell and a pulser for controlling beam pulse intervals and durations.

The preferred instrument for the diagnostics is a high-speed framing camera, and two can be borrowed for short-term proof-of-concept experiments. However, a dedicated imaging system is needed, and a request will be submitted to the FY03 capital equipment list.

Since our experiments will be conducted in a containment vessel, a means to provide "soft-catch" of both the projectile and the fracture specimen is needed to protect the windows on the vessel and to preserve the condition of the dynamically fractured specimen for post-test evaluation. This soft-catch system has been designed and is nearly fabricated.

In addition to the effort to bring the 2.5-in. gas gun to operating status, we have been working concurrently on building the laser diagnostics capability using quasi-static fracture tests. All of the diagnostic optics, other than the high-speed camera, were either purchased or fabricated during FY02. Related holding and positioning parts and optical tables and benches were also procured. Both the caustic and coherent gradient sensing (CGS) techniques, which are capable of measuring fracture processes even at supersonic velocities, have been demonstrated in quasi-static fracture tests of polymethylmethacrylate (PMMA).

An example of the CGS technique applied to crack initiation and growth in a notched three-point bend specimen is shown in Fig. 2. The fringe pattern is due to the in-plane gradients of out-of-plane displacement, and from this information strain and stress fields can be calculated to determine fracture toughness values.

Our goal at the end of the next fiscal year is to demonstrate the full capability on the fracture of a nonhazardous material.

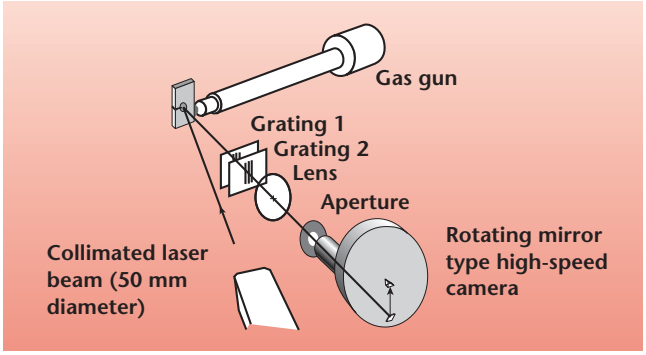

Figure 1. *Schematic of dynamic fracture experiment.*

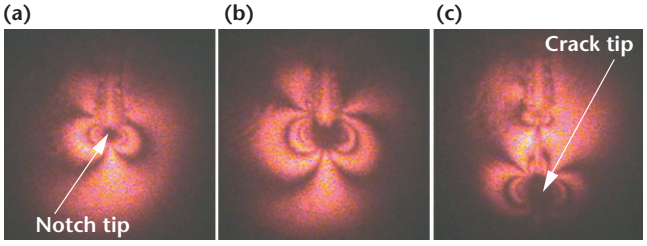

Figure 2. *CGS measurement of initiation and propagation of statically-driven crack through PMMA notched-beam specimen. Interference fringes show stress build-up at the notch tip in (a) and (b). Crack generated at the notch tip has moved downward in (c).*

Author Index

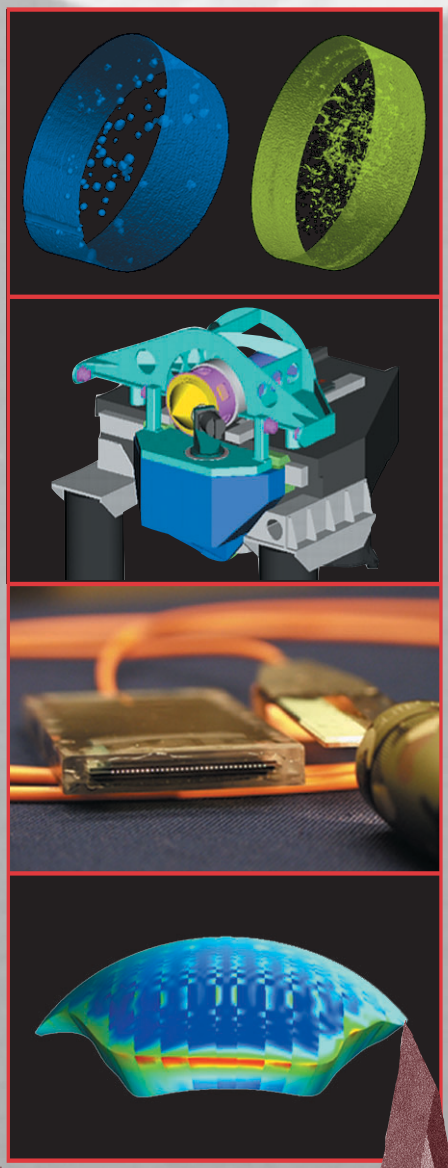

Author Index

Author Index (continued)

Manuscript Date March 2003
Distribution Category UC-42

This work was performed under the auspices of the U.S. Department of Energy by the University of California, Lawrence Livermore National Laboratory under Contract W–7405–Eng–48.
ENG-02-0143-AD

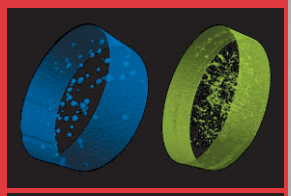

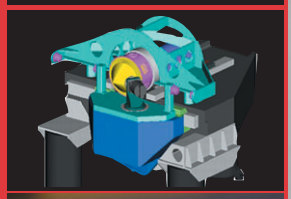

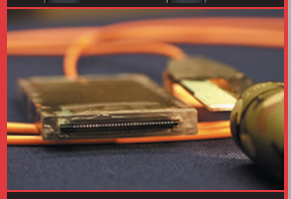

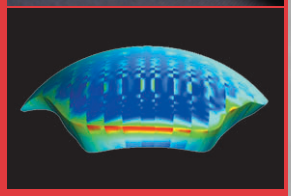

ENGINEERING

Lawrence Livermore National Laboratory
University of California
P.O. Box 808, L-124
Livermore, California 94551

http://www_eng.llnl.gov/